Spring 5-5-2023

Durability of Large-scale 3d Printed Materials for Transportation Infrastructure

Felipe Saavedra
University of Maine, felipe.saavedra@maine.edu

DURABILITY OF LARGE-SCALE 3D PRINTED MATERIALS FOR TRANSPORTATION INFRASTRUCTURE

By

Felipe Saavedra

B.S., Universidad de Concepción

A THESIS

Submitted in Partial Fulfillment of the

Requirements for the Degree of

Master of Science

(in Civil Engineering)

The Graduate School

The University of Maine

May 2023

Advisory Committee:

Roberto A. Lopez-Anido, Professor, Dept. of Civil and Environmental Eng., Advisor

Keith A. Berube, Associate Professor, Mechanical Engineering Technology

Sunil Bhandari, Assistant Research Professor, Dept. of Civil and Environmental Eng.

DURABILITY OF LARGE-SCALE 3D PRINTED MATERIALS FOR TRANSPORTATION INFRASTRUCTURE

By Felipe Saavedra

Thesis Advisor: Dr. Roberto A. Lopez-Anido

An Abstract of the Thesis Presented
in Partial Fulfillment of the Requirements for the
Degree of Master of Science
(in Civil Engineering)
May 2023

Large-format extrusion-based polymer Additive Manufacturing (AM) or 3D printing has been used for transportation infrastructure applications, including culvert outlet diffusers and precast concrete formwork. This research assesses thermoplastic composite material system durability and dimensional stability under different environmental exposure conditions. Accelerated exposure in the laboratory was conducted for moisture absorption, freeze-thaw cycles, and ultraviolet (UV) weathering. Specifically, this thesis investigates the use of bio-based renewable polymer composites for transportation infrastructure applications by correlating accelerated laboratory durability tests with site-specific environmental durability for selected applications.

The thesis compares the performance of bio-based composite materials, wood fiber/ polylactic acid (WF/PLA), wood fiber/amorphous polylactic acid (WF/aPLA), and synthetic materials, carbon Fiber/ acrylonitrile butadiene styrene (CF/ABS). The material's durability is evaluated using visual and quantitative surface analysis methods, dimensional stability, and retention of mechanical properties after accelerated exposure. The surface analysis methods implemented are

contact angle measurement and surface roughness measurement. The representative mechanical properties selected are flexural strength and flexural modulus.

Standard test methods for mechanical performance and durability assessment were adapted and implemented for large-format extrusion-based 3D printed materials to account for print toolpath and bead size. The performance of semicrystalline and amorphous PLA polymer systems was evaluated and compared to determine the feasibility of these bio-based materials for 3D printed applications in transportation infrastructure. Non-contact full-field digital image correlation with the GOM ARAMIS system measured strains and displacements in the flexure tests. The durability assessment is based on the retention of mechanical properties, surface analysis, and dimensional stability of exposed specimens relative to baseline specimens.

ACKNOWLEDGEMENTS

I would like to thank in the first place my advisor for selecting me as one of his graduate students and giving me the opportunity to take the next step in my career. Also, I would like to thank my committee member for their help during my studies.

Thanks to all my friends and family for helping and supporting me throughout these two and a half years. Especially to my parents; even though they were so far away from me, I always felt their support.

Last but not least important, I would like to thank a younger Felipe for overcoming one of the hardest moments in his path, finding the strength and will to pursue his dreams.

This work was supported in part by funding from the Transportation Infrastructure Durability Center with the U.S. Department of Transportation's University Transportation Centers Program under Grant 69A3551847101.

TABLE OF CONTENTS

LIST OF TABLES

LIST OF FIGURES

CHAPTER 1

INTRODUCTION

1.1 Additive manufacturing

In recent years, additive manufacturing (AM) has increased significantly to produce functional products. This trend has increased the need for quality assurance of AM-produced products in terms of overall mechanical properties and their structural durability in-service loading [1]. As defined by ASTM International[2] additive manufacturing is the process of joining materials to make parts from 3D model data, usually layer upon layer, as opposed to subtractive manufacturing and formative manufacturing methodologies. In the literature, the term “additive manufacturing” is used as exchangeable with the term “3D printing” [3]. The additive manufacturing process adopted to obtain the necessary materials in this research work is material extrusion, in which the material is selectively dispensed through a nozzle or orifice.

In AM, a computer aided design (CAD) solid modeling program is used to model the geometry of the component. This model then undergoes the slicing process, which is the process of dividing the 3D model into layers, and generating the deposition path, to determine how each layer of material should be deposited (tool path). Following the receipt of the slicing file by the printer, the material is deposited using a procedure that involves layering the material; when one layer cools and resolidifies, the next layer is deposited until the part is finished. Once the part is finished, it usually requires post-processing involving cleaning and machining [4-7].

The AM feedstock for large-scale 3D printing is compounded pellets. The pellets are dried prior to extrusion, then they are fed into the extrusion equipment and heated to the processing temperature, at which the polymer can be extruded via the machine's nozzle. A thermocouple is placed in the nozzle to record the temperature. An example of this technology is the Ingersoll MasterPrint at the University of Maine, which has a single screw extrusion unit. The single-screw extrusion machine has a cylindrical barrel that continuosly pushes the filled polymer through a constant profile die [8]. The MasterPrint extrusion system is designed to work for a wide range of polymers and supports processing temperatures from 100°C to 500°C. The nozzle has a diameter of 12.7 mm.

The polymer materials for AM methods need to meet certain requirements such as rheological properties (viscosity), thermal properties (crystallinity, conductivity of heat, heat capacity) and mechanical properties (elastic modulus and strain at yield) to be printable at a constant flow rate [4, 9].

1.2 Adoption of large-scale AM for civil infrastructure applications

Examples of applications of large-scale additive manufacturing in civil infrastructure are: diffusers for the rehabilitation of highway culverts [10], formworks for a precast concrete pier cap of a highway bridge [11], formworks for window openings for a precast concrete parking garage wall system [12], formworks for casting precast concrete ballast retainers for railroad bridges [13], and a biobased additively manufactured house [14].

1.2.1 Large-scale 3D printed forms for precast concrete structures

Formworks are the single most significant cost component in constructing a concrete structure [15]; this raises the interest in new alternatives to replace the typical formworks used in the industry that are generally made of timber or steel. Large-Scale 3D printing technologies offer an option, using thermoplastics as raw materials like PLA (polylactic acid)/ wood composites or ABS (acrylonitrile butadiene styrene)/ carbon fiber composites. These formworks can be disposable, functional, structural, and permanent. Peters [16] studied the potential and advantages of flexible formwork for precast concrete architectural applications, showing that it can be implemented immediately in the construction industry since it improves an already-known technique and material. Bhandari et al. [11] studied the use of PLA/ wood filler blend as raw material for an extrusion-based additive manufactured formwork for a precast concrete pier cap, with 16.5 m (643.5 in) in length, 1.22 m (48 in) in width, and 1.34 (53 in) in height. The estimated cost was higher than conventional wooden formwork, but if the part to be cast has a complex geometry, and the extrusion rate can be increased effectively, the price of the 3D printed formwork could be competitive with the conventional one.

Bhandari et al.[12] also studied the use of biodegradable polymer composites wood-fiber polylactic acid (WF-PLA) and wood-fiber amorphous polylactic acid (WF-aPLA), along with a conventional polymer composite – carbon fiber acrylonitrile butadiene styrene (CF-ABS) for precast concrete formwork. This work showed that combining large-scale 3D printing with CNC machining could effectively manufacture complex forms for concrete casting operations. The design of a continuous extrusion toolpath is required to minimize the number of seams in the

formwork. It also addresses postprocessing repair methods that can be used to correct manufacturing defects.

In Germany [17], the stairs of the Aufbaubank were constructed using customized formwork sections manufactured with highly accurate, high-quality 3D-printed shells. The results in timesaving and quality of concrete finishing were considerable.

1.2.2 Large-scale 3D printed diffusers for highway culvert rehabilitation

Monitoring underground infrastructure like highway culverts is a challenging task, requiring estimation of the service life of assets, risk analysis of failures, and their impacts on the quality of life [18]. Variations in structural characteristics, environmental exposure, and wide geospatial distribution of these infrastructure assets, accompanied by strict budget restrictions, pose significant challenges for transportation agency officials [19]. Bhandari et al. [10] explored rehabilitation of highway culvert using large-scale 3D-printed thermoplastic polymer composite culvert diffusers. The diffuser was printed in segments that were assembled using adhesives. The results showed considerable reductions in manufacturing costs and time using large-scale 3D printing technology.

1.2.3 Biobased additively manufactured housing

The University of Maine and Oak Ridge National Laboratory collaborated to design and manufacture a biobased additively manufactured home, as (BioHome3D) [20].
The BioHome3D uses additive manufacturing to print each module of the house to later be assembled on site. The modules consider walls, floors and roofs, all made of biobased 3D printed

materials. The advantage of using AM in this type of application is that it can be scaled to any size of house since it can be developed in modules [14].

1.3 Advantages and limitations of large-scale AM

Material extrusion additive manufacturing techniques advantages are : Multi material printing, versatile and easy to customize, widespread use, scalable and capability to build fully functional parts [21-23]. These advantages are still present at the large-scale, although new obstacles and challenges also exist. Important technical considerations for large-scale polymer extrusion AM are: weight of the part, adjusting temperature between layers, part distorsion (warping) [24], maximum dimensions of parts, mechanical properties for short-fiber reinforced composites (non continuous fiber), cycle-time compared to conventional manufacturing methods, surface roughness of the as-printed part may require machining, and maximum operating temperature.

1.4 Durability

Some key differences between thermoplastic composite materials manufactured with 3D printing compared to conventional manufacturing methods (e.g., injection molding) are the layered structure of the material (deposited beads) with relatively weak interfaces and the presence of voids. The nature of the material structure in 3D printing makes the material more susceptible to moisture absorption and water ingress, which affects durability.

From the structural point of view durability can be defined as the ability of a building structure to remain fit for the design purpose during its service life [25]. Specifically, the durability of a material or structure is summarized as “its ability to resist cracking, oxidation, chemical

degradation, delamination, wear, and/or effects of foreign object damage for a specified period, under the appropriate load conditions, under specified environmental conditions" [26].

Large-scale 3D printed parts for exterior use are exposed to freeze-thaw cycles, moisture, and ultraviolet radiation (UV). This exposure affects the durability of the part in service, therefore it is necessary to understand the types of exposure that degrade the material. Once the exposures are identified, it is possible to simutale in a laboratory environmental durability by conducting accelerated testing. Accelerated testing uses several test techniques to cut the lifespan of products or speed the performance degradation of such products. Such testing seeks to generate data that can be promptly and accurately modeled and analyzed, yield desired information on product life or performance under regular use. Such tests can be translated into savings in time and money if we compare them with typical conditioning on-site [27].

Structural design specifications consider durability of the material. The American Association of State Highway and Transportation Officials (AASHTO) specifications for the design of bonded FRP systems for repair [28] addresses durability using extreme values (minimum or maximum) for the end use. For example, for moisture content equilibrium the AASHTO specicifications state that the average value shall not be greater than two percent. The ASCE standard for pultruded FRP structures [29] recommends minimum requirements for hardness, glass transition temperature and maximum moisture content equilibrium. In addition, the ASCE standard specifies adjustment factors for end use that account for sustained in-service moisture and temperature.

The durability of wood plastic composites (WPC) has been studied for various exposures [30], like solar radiation, temperature, and moisture, being separated into two broad categories: structural durability and aesthetic durability. Both categories are important since, from the structural durability point of view, WPC need to withstand service loads while at the same time maintaining the required aesthetic during their service life.

Stark et al. [31] studied the outdoor durability of WPC made of high-density polyethylene (HDPE) with 50% wood flour, comparing extruded, compression-molded, and injection-molded WPC. For moisture, hydroxyl groups on wood or other lignocellulosic materials are primarily responsible for water absorption. As the wood particle absorbs moisture, it swells, producing stresses in the WPC matrix and creating microcracks. Swelling also creates stress in the wood particles. Once the material is dried, there is no adhesion at the matrix and wood particle interface, creating voids that water will penetrate at a later exposure, affecting its durability.

WPC has also been studied for a ten-year field study [32]. Stakes made of polypropylene (PP) with 49-52% wood flour were inserted in the ground to evaluate decay, termite ratings, surface weathering, biological colonization, and dimensional changes. In addition, flexural tests were conducted to evaluate the flexural properties after ten years, showing a decrease or no change depending on the composite formulation. The formulation of the WPC was relevant, showing that WPCs with a greater amount of coupling agent and colorant showed no significant difference in flexural strength between the control and weathered stakes. The findings of the field study showed that the durability of the WPC would be affected, this highlights how important accelerated tests are when a longer time frame, such as ten years, is not possible.

When reviewing in the literature for what has been done do address durability of large-scale 3D printed polymer materials, Grassi et al. [33] studied the durability of a large-scale 3D printed facade for desert climates. Samples and prototypes were exposed to accelerated aging of cycles of UV and condensation. The polymer materials used in this study showed a high sensitivity to UV rays in terms of color change and shape.

ASTM international in D4762-18 [34], addresses environmental conditioning and resistance test methods for plastics, polymer matrix composite materials, sandwich construction structures, glass fiber reinforced structures and chemical agents. However this standards do not fit to the materials used in this research work. There is on going research and developments from F42 committee on additive manufacturing, D20 committee on plastics, and D30 committee on composite materials from ASTM international, but no guidelines or standards yet to follow when evaluating the durability of polymer composite materials produced by large-scale AM; this demonstrates a lack of understanding of this type of materials.

Understanding durability is crucial since it guides the design of the structure, the formulation of the material, and its implementation. Analyzing the durability of a material helps to identify the desired characteristics according to the environmental constraints to which it will be subjected during expected service life [35]. In addition, studying durability could help to identify areas for improvement in the additive manufacturing process, such as optimizing printing parameters and extrusion temperatures.

1.5 Research objectives

This research focuses on evaluating the durability of polymer composites (WF/PLA, WF/aPLA, and CF/ABS) manufactured using large-scale 3D printing for transportation infrastructure applications. The accelerated testing conducted includes moisture immersion, freeze-thaw cycling and simulated weathering based on UV and condensation cycles. These tests involve the use of lab equipment such as ovens to achieve the necessary temperature for water immersion, environmental test chambers (ESPEC chambers) to simulate temperatures for freezing and thawing cycles, and QUV weathering machines to simulate daylight irradiance with UV lamps and condensation cycles. To address the objectives, the formulated the research questions:

1. Characterize the effects of environmental exposure on the mechanical properties of 3D-printed polymer composite materials.
2. Implement material property retention factors to account for environmental exposure in the structural design of 3D-printed polymer composites.

1.6 Research questions

1. How does moisture absorption affect the hygro-mechanical response on large-scaled 3D printed materials?
2. Are flexural modulus and flexural strength dependent on specimen dimensions?
3. Are flexural modulus and flexural strength dependent on the printing directions?
4. Are there any differences in the hygro-mechanical response between machined and as-printed test specimens?
5. How to select 3D printed materials based on site environmental conditions?

1.7 Organization of thesis chapters

The thesis chapters are organized as follows:

1. The first chapter introduces the thesis and explains concepts necessary to understand the topic, what has been done in the field, and what this research work covers.
2. The second chapter discusses the research methods for this research work, including flexure tests and environmental conditioning.
3. The third chapter discusses the materials used, how they were manufactured, sample preparation and characteristics, and a discussion on the baseline material properties.
4. The fourth chapter shows the moisture absorption results on the different materials and the findings compared to baseline properties.
5. The fifth chapter shows the results from freeze-thaw cycling on the different materials and the findings compared to baseline properties.
6. The sixth chapter shows the results from simulated weathering based on UV and condensation cycles for carbin fiber acrylonitrile butadiene styrene CF/ABS and the findings compared to baseline properties.
7. The seventh chapter introduces the concept of the property retention factor due to environmental conditions.
8. The eighth chapter shows the results and findings from a finite element analysis model of the highway culvert diffuser.
9. The ninth chapter presents the conclusion and recommendations of this research work.

CHAPTER 2

RESEARCH METHODS

2.1 Introduction

This chapter presents and discusses the standards used for the environmental conditionings implemented in this research work and the standard used for testing large-scale 3D printed materials. This chapter also discusses deviations for each standard to adapt them for a large-scale format.

For determining flexural moduli and strengths, the ASTM standard test method used is D7264M – 21 [36]; for moisture absorption, the standard used is D5529-14 [37]; for freeze-thaw cycling, the standard used is D7031-11 [38]; for simulated weathering based on ultraviolet (UV) and condensation cycles, the standard used is G154 – 16 [39].

2.2 Flexure test

Flexure test was selected due to its simplicity, flexural material properties were calculated as performance indicators, the flexure test method D7264 was adopted for this research work.

2.2.1 ASTM D7264 standard

ASTM D7264 [36] test method is described as a bar of rectangular cross-section, supported as a beam, deflected at a constant rate. The procedure used corresponds to Procedure B of the standard.

- Procedure B: The bar rests on two supports and is loaded at two points (employing two loading noses), each at an equal distance from the adjacent support point. The distance between the loading noses (the load span) is one-half of the support span.

One of the advantages of using D7264 Procedure B is that four-point bending is a test configuration in which the central region of the beam is subjected to pure bending without shear. This avoids accounting for the effects that shear might have on the specimen. Figure 2.1 illustrates the loading diagram for this procedure. The testing speed was computed according to test method D6272 – 17 [40] since the specimen dimensions vary significantly from the standard sizes; this is explained in Section 2.2.2.

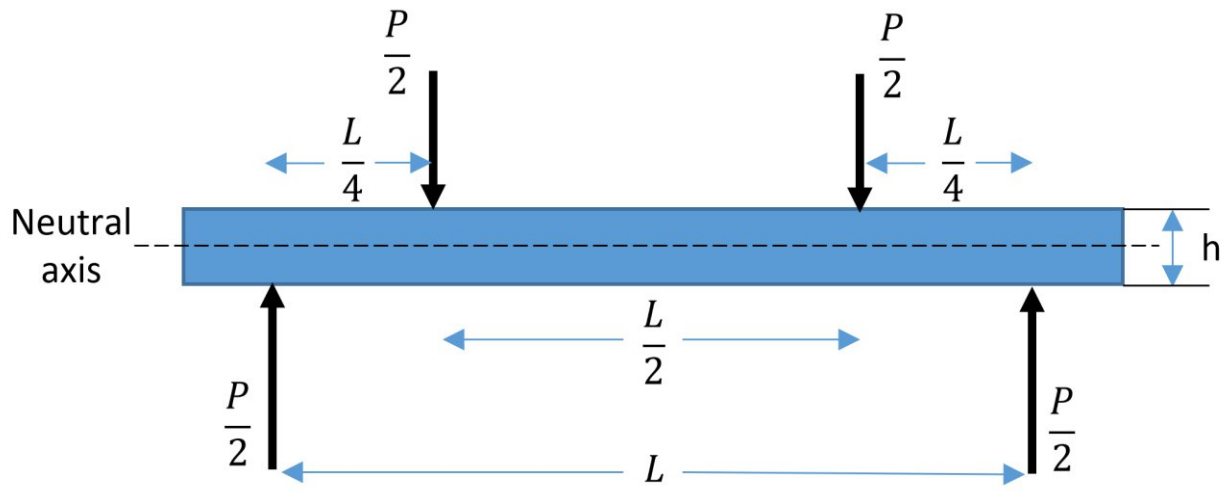

Figure 2.1: Loading diagram adapted from ASTM Standard D7264 -21 [36]

2.2.2 ASTM D7264 standard modification

This test method determines the flexural properties (including strength, stiffness, and load/deflection behavior) of polymer matrix composite materials under defined conditions. This

test method is under the jurisdiction of ASTM Committee D30 on Composite Materials and is the direct responsibility of Subcommittee D30.04 on Lamina and Laminate Test Methods.
The support span-to-thickness ratio adopted was 16:1, which is an option in D7264. The support span-to-thickness ratio selected is the same specified in ASTM D790 [41]. This support span-to-thickness ratio of 1:16 was applied to all the specimens regardless of the printing direction considered.
A deviation in the specimen dimensions was necessary to adapt D7264 to large-scale 3D printed materials. The thickness and width adopted for the 3D printed specimens correspond to the orientation of the bead dimensions; as opposed to the standard specimen thickness of 4 mm (0.16 in), and the standard specimen width of 13 mm (0.5 in).

2.2.3 Four-point bending specimen geometry

The specimen geometry depends on the printing direction and dimensions of the plates or forms obtained, considering bead width and layer height as the main parameters to define the specimen dimensions. Detailed explanations of the plates and forms and how the specimens were obtained are presented in Section 3.2.

2.2.4 Prediction of strength properties

An ARAMIS 3D-Digital Image Correlation (DIC) system from GOM mbh, Braunschweig, Germany was used to record full-field strains on the test specimen surface during testing. Compared to conventional strain sensors, DIC allows a larger specimen area to be monitored during testing without requiring physical contact with the specimen. This is advantageous for large-scale 3D printed materials where size and placement can influence test results or when it is

not possible to place instrumentation due to constraints with test fixtures. The specimens were prepared for the DIC measurement system by applying a speckled grayscale pattern of paint to the side of the specimen or by putting uncoded white single-point markers of 0.8 mm diameter, as shown in Figure 2.2 and Figure 2.3, respectively. This allowed full-field strain measurement to be recorded for the entire observed area of the beam during testing.

ASTM test standard D7264 was used to conduct the flexural test. The specimens were tested in four-point flexure with a ¼-point load configuration, as shown in Figure 2.1 at a span-to-thickness ratio of 16-to-1. The flexure tests were performed on a 100 kN servo-hydraulic load frame from Instron, Norwood, MA, equipped with side-loading hydraulic grips at a temperature of 23°C±2°C and 50±5% relative humidity in an environmentally controlled test lab at the Advanced Structures and Composites Center at the University of Maine in Orono, Maine. The specimens were tested in displacement control at a crosshead rate according to ASTM D6272.

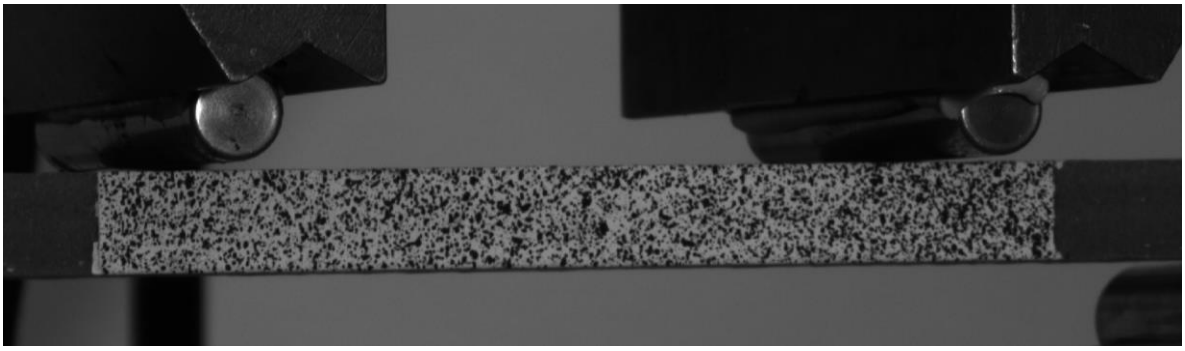

Figure 2.2: Central span of specimen loaded in four-poing bending with grayscale speckle pattern

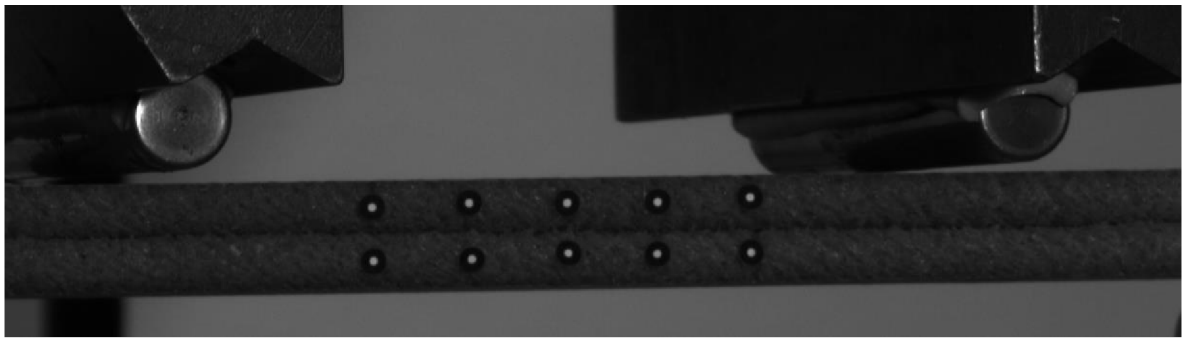

Figure 2.3: Central span of specimen loaded in four-poing bending with white single-point markers with 0.8 mm diameter.

Strains were measured at a specific distance, z, from the neutral axis. Figure 2.4 and Figure 2.5 show the distance z considered to calculate flexural strength and flexural tangent modulus of elasticity (referred to as flexural modulus) for specimens with speckle patterns and with point markers. These figures only show the z-distance for the tension side of the specimen. The same procedure was adopted to measure strains in the compression side of the specimen.

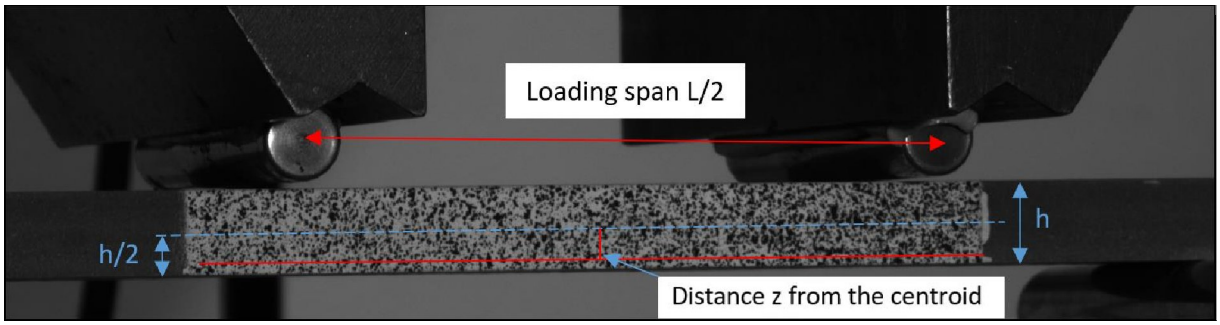

Figure 2.4: Distance z considered to calculate stresses in specimens with speckle patterns

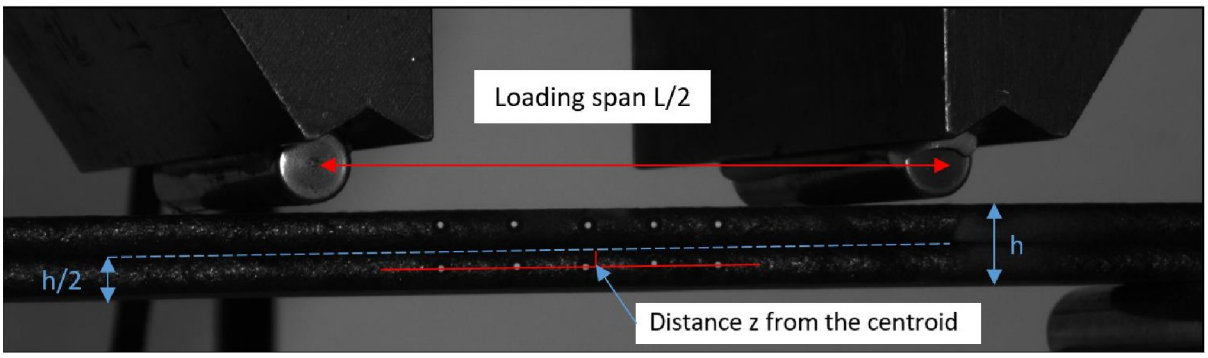

Figure 2.5: Distance z considered to estimate stresses in specimens with uncoded point markers.

The following variables are defined and implemented in Figure 2.6 showing tension and compression strains at the mid point of a large-scale 3D printed specimens subjected to four point bending loads.

$\varepsilon_{c\,max}$	=	Maximum compression strain on the outer top fiber of the specimen
$\varepsilon_{t\,max}$	=	Maximum tension strain on the outer top or bottom fiber of the specimen
ε_{x2}	=	Compression strain measured at a distance of z
ε_{x1}	=	Tension strain measured at a distance of z
z_{na}	=	neutral axis
h	=	height of the specimen

With the variables defined, the following procedure was used to obtain flexural strength and flexural modulus:

- Using GOM Correlate tension and compression strains ε_{x2} and ε_{x1} are obtained at a distance of z.
- With tension and compression strains and considering Bernoulli-Euler beam theory (any section of a beam that was perpendicular to the neutral axis before the beam deforms will remain perpendicular to the neutral axis after the beam deforms). Strain are assumed linear as a function of its distance from the neutral axis. Then the location of the neutral axis can be calculated.
- With the neutral axis, the maximum strain $\varepsilon_{t\,max}$ on the tension side of the specimen is calculated according to Equation 1.

$$\varepsilon_{t\,max} = \frac{\varepsilon_{x1}\left(\frac{h}{2} + z_{na}\right)}{-z_1} \tag{1}$$

- Considering the stress calculation for a simply supported beam subjected to a four-point bending configuration (Figure 2.1). Stresses are calculated according to Equation 2.

$$\sigma(z) = \frac{3}{2}\frac{PL\left(\frac{h}{2} + z_{na}\right)}{bh^3} \tag{2}$$

- With stresses, Stress v/s Strain curves are obtained.
- Flexural modulus is the slope of the linear fit (using all data points between 0.001 and 0.003 strains according to ASTM D7264) of the Stress v/s Strain curve.
- Flexural strength corresponds to the maximum stress of the Stress v/s Strain curve.

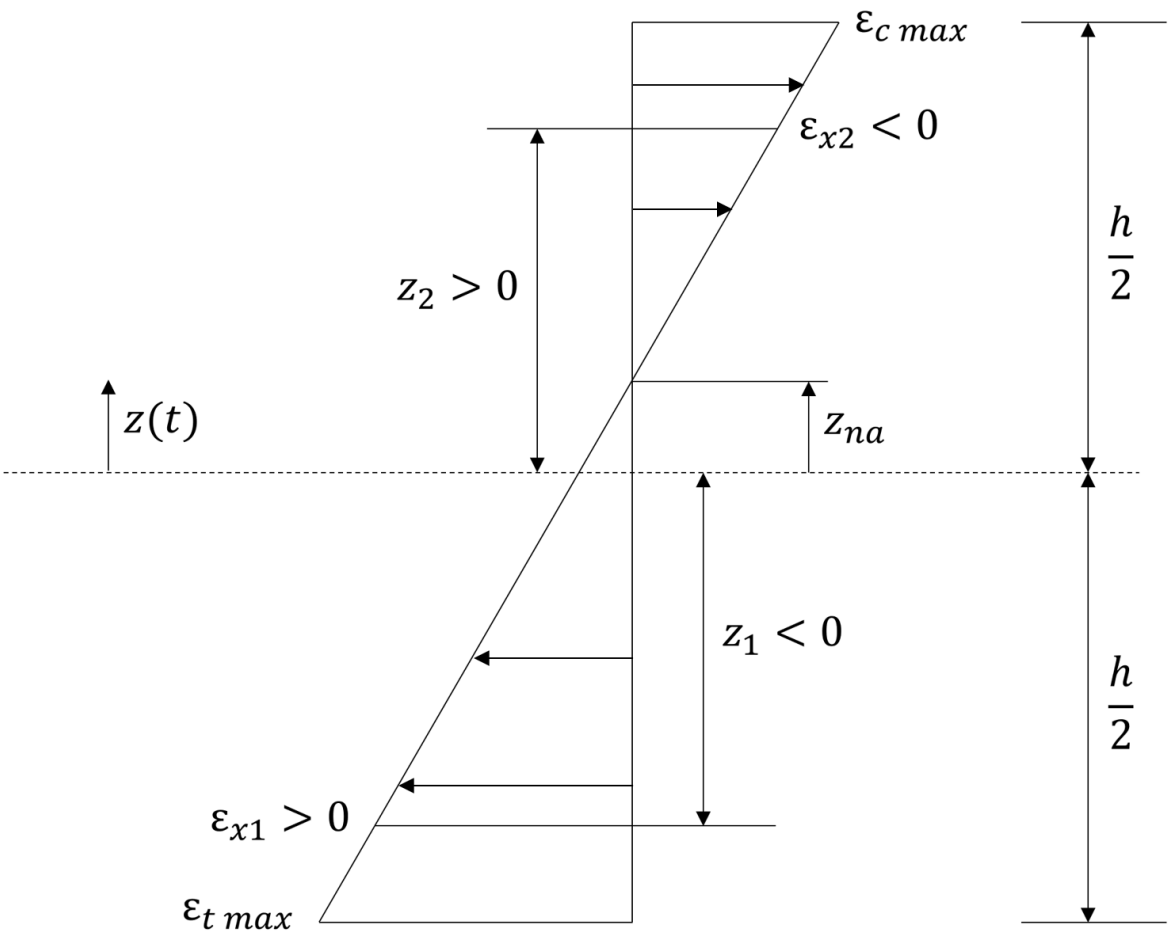

Figure 2.6: Tension and compression strains at the mid point of a large-scale 3D printed specimens subjected to four point bending loads.

2.3 Moisture absorption

2.3.1 ASTM D5229 standard description

Water absorption was conducted following the ASTM D5229-14 Standard Test Method for Moisture Absorption Properties and Equilibrium Conditioning of Polymer Matrix Composite Materials [37]. This test method covers a procedure for determining moisture absorption or desorption properties in the through-the-thickness direction for single-phase Fickian solid materials in flat or curved panels. This gravimetric test method monitors the change over time to the average moisture content of a material specimen by measuring the total mass change of coupons exposed on two sides to a specific environment.

The following procedure for moisture absorption was adopted:

- The selected temperature for oven-dry and water absorption was 40°C (below the glass transition temperature (Tg) of WF/PLA 60°C, being the lowest Tg of the three materials).
- Oven-dry specimens: Specimens were oven-dried at 40°C until there is less than 1% change in mass.
- Specimens were immersed in distilled water at 40 °C after oven-drying, and the conditioning time was 81 days.
- Moisture content was calculated according to the ASTM D5229 standard.
- Sorption curves were generated according to the ASTM D5229 standard.

2.3.2 ASTM D5229 standard modification

The following deviations are considered for moisture absorption:

- The conditioning time adopted, 81 days, was based on lab equipment availability. Moisture equilibrium content was not achieved during the conditioning time.
- The specimens were conditioned under water immersion at 40°C.
- The number of specimen replicates was selected based on material availability.

2.4 Freeze-thaw cycling

Freeze-thaw cycling was conducted following the ASTM D7031-11 Standard Guide for Evaluating Mechanical and Physical Properties of Wood Plastic Composite Products [38]. This standard states that a minimum of three specimens shall be subjected to the cycle described below to determine the effect of freeze-thaw exposure. The test specimens shall be prepared using the whole cross-section of the as-manufactured product whenever possible.

2.4.1 ASTM D7031 standard description

The cycles are:

- Test specimens shall be submerged underwater (using weights to hold them down, if necessary) for 24h.
- The specimens shall then be placed in a freezer at -20°F (-29°C) for 24h.
- After being frozen, the specimens shall be returned to room temperature for 24h. This process comprises one hygrothermal cycle.
- The above procedure shall be repeated two more times for a total of three cycles of water submersion, freezing, and thawing. After three freeze-thaw cycles, the specimens shall be allowed to return to room temperature, followed by flexure testing.

2.4.2 Freeze-thaw cycling standard modification

The following deviation is considered for freeze-thaw cycling:

- After three freeze-thaw cycles, the specimens were returned to room temperature and stored in sealed plastic bags prior to testing in flexure. The storage time depended on testing equipment availability.

2.5 Simulated weathering based on ultraviolet (UV) and condensation cycles

2.5.1 ASTM G154 standard description

Simulated weathering based on UV radiation and condensation cycles was conducted according to ASTM Standard G154 – 16[39]. The adopted cycle corresponds to Cycle 3, which considers eight hours of UV exposure at 70° C and four hours of condensation at 50° C.
Specimens were exposed for 2000 h, approximately 84 days. Surface roughness and contact angle measurements were measured after 500 h, 957 h, and 2000 h. This environmental conditioning was applied only to CF/ABS specimens since there was interest in assessing the weathearability of this material for transportation applications.

2.5.2 Surface roughness

Surface roughness was measured using a Mitutoyo SJ-210 Portable Surface Roughness Tester. It is a portable measuring instrument that measures surface roughness. The device must be placed on top of the material's surface, and the retractable detector moves longitudinally and takes a measurement. Figure 2.7 illustrates how the machine works.

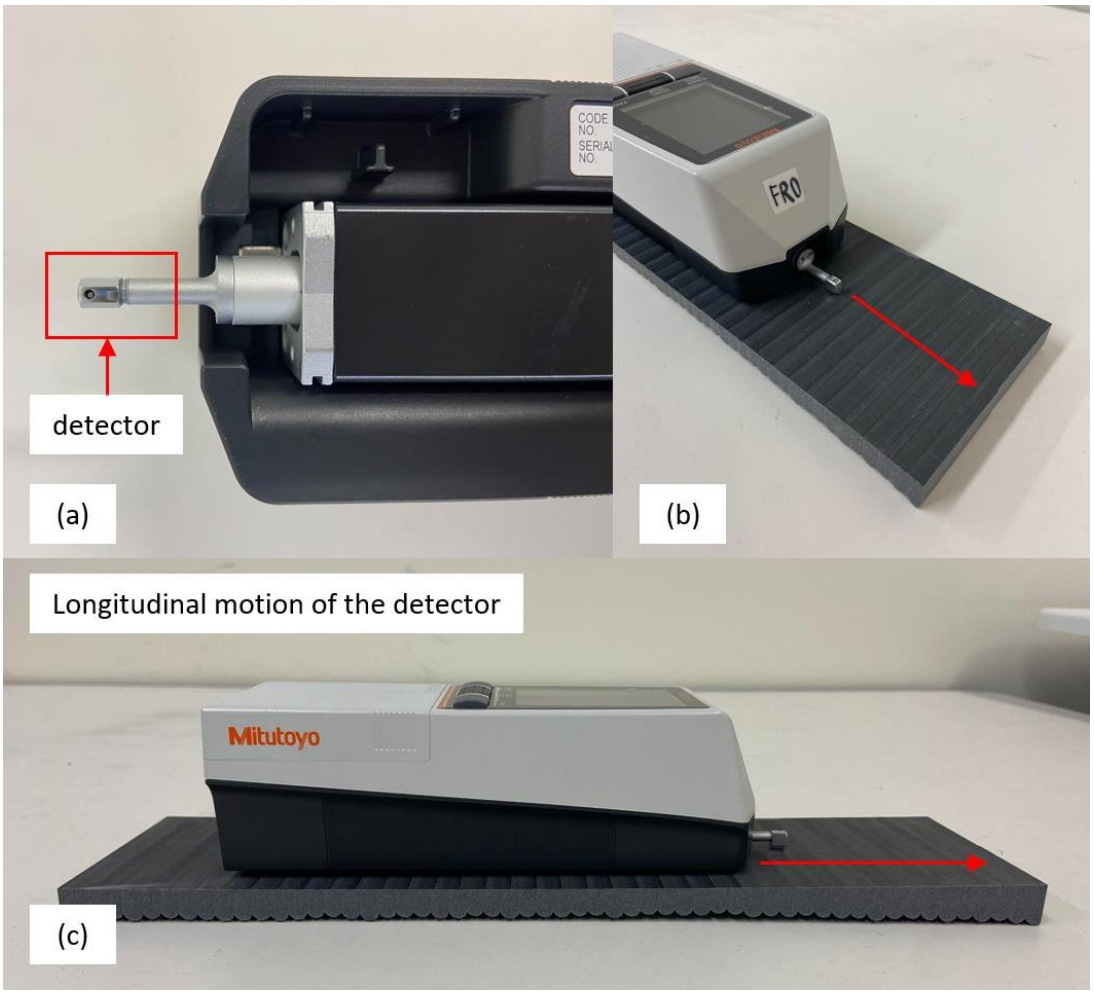

Figure 2.7: Mitutoyo SJ-210 Portable Surface Roughness Tester, (a) detector, (b) and (c) longitudinal motion of the detector on the specimen.

Surface roughness is a series of microscopic “peaks and valleys” across a surface, calculated by measuring the average surface height and depth. This equipment reports Ra, which is defined as the arithmetic average of the absolute values of the profile height deviations from the mean line recorded within the evaluation length.

Seven measurements per conditioning time (500 h, 957 h, and 2000 h) were taken for each specimen at a standard laboratory atmosphere with a temperature of 23 ± 2 °C and relative humidity of 50 ± 10%. Measurements were taken only on machined specimens.

2.5.3 Contact angle

The contact angle is measured using a KRÜSS Mobile Surface Analyzer MSA-One-Click SFE shown in Figure 2.8 (a). To take a measurement, the equipment needs to be placed on top of the surface of the specimen; once it is activated, it places a drop of water (polar liquid) and a drop of diiodomethane (non-polar liquid). It has a camera that measures the contact angle of the two mentioned liquids, as shown in Figure 2.8 (b) and Figure 2.9.

Machined specimens were first conditioned for 24 h in a standard laboratory atmosphere with a temperature of 23 ± 2 °C and relative humidity of 50 ± 10%. Then contact angle was measured, and specimens were conditioned under the exposure cycle for 500h, 957 h, and 2000 h. Multiple areas and multiple measurements were taken per specimen.

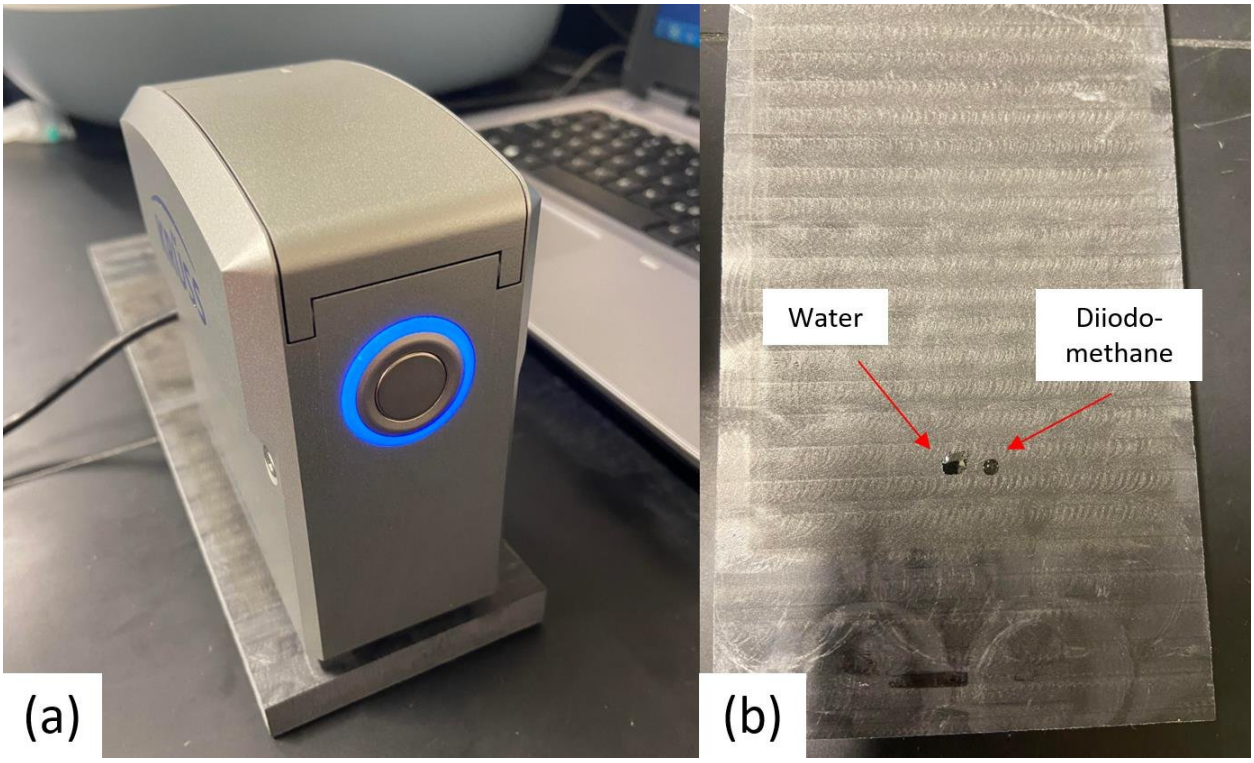

Figure 2.8: (a) KRÜSS Mobile Surface Analyzer MSA-One-Click SFE and (b) Drops of water and diiodomethane on a CF/ABS specimen

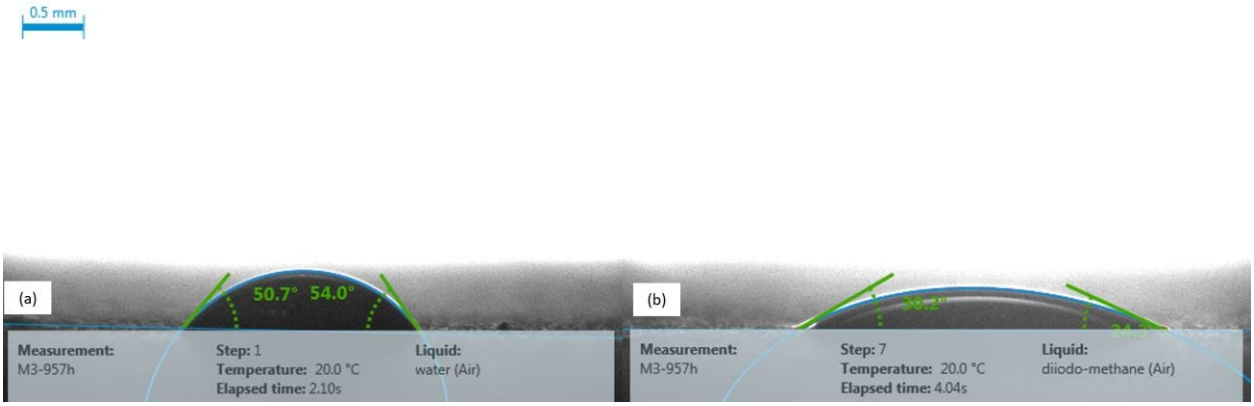

Figure 2.9: Example of how equipment measures contact angle on (a) water and (b) diiodomethane

2.6 Large-scale 3D printing methods

Two different large-scale 3D printing machines were used to extrude the plates and forms used:

- MasterPrint 3x manufactured by Ingersoll Machine Tools. This machine has a printing volume of 18.3 m. (60 ft) length by 6.7 m. (22 ft) wide by 3.3 m. (10.8 ft) height. This machine supports multiple heads including: a) extruder with a maximum throughput of 150 lb (68 kg) per hour, b) extruder with a capacity of 500 lb (227 kg) per hour, c) integrated CNC 5-axis head for subtractive manufacturing methods, including cutting, surface finishing, and part geometry finishing, and d) Automated Fiber Placement (AFP) unit.
- BAAM 100 – Alpha Size 2, Big Area Additive Manufacturing, manufacturted by Cincinnati Inc,. The machine has a printing volume of 3.6 m. (11.8 ft) length by 1.7 m. (5.6 ft) wide by 1.8 m. (5.9 ft) height. The machine has one extruder with a maximum throughput of 40-80 lb (18-36 kg) per hour. Its features include a heated build chamber, pellet extruder, and a 5-axis machine head.

CHAPTER 3

MATERIALS AND MANUFACTURING

3.1 Introduction

This chapter discusses and shows how specimens were obtained for each material, as well as the results for flexural strength and flexural modulus for the baseline specimens. Baseline specimens are used to make a comparison with the specimens under environmental conditions.

Plates and forms were previously printed for other projects; information regarding each plate and material is provided in Table 3.1 and shown in Figure 3.1- Figure 3.3, for the WF/PLA, WF/aPLA and CF/ABS, respectively.

Table 3.1: Plates and forms information for large-scale 3D printed materials

Raw Material	Plate/Form Thickness (in)	Project	Printing Date	Bead Width (in)	Layer Height (in)	Nozzle Used
WF/PLA plate	1.0	Highway Culvert Diffuser	10/20/20	0.5	0.2	90° - ID 0.4 in
WF/PLA plate	1.5	Window Frame – Unistress	04/16/21 04/19/21	0.75	0.2	90° - ID 0.4 in
WF/PLA form	1.6	Window Frame – Unistress	04/13/21	0.75	0.2	90° - ID 0.4 in

Table 3.1 continued

Raw Material	Plate/Form Thickness (in)	Project	Printing Date	Bead Width (in)	Layer Height (in)	Nozzle Used
WF/aPLA plate	1.5	Window Frame – Unistress	11/20/21	0.75	0.2	90° - ID 0.4 in
WF/aPLA plate	1.5	Recycling/ Hexagon	03/31/22	0.75	0.2	90° - ID 0.4 in
WF/aPLA form	1.5	Window Frame – Unistress	11/20/21	0.75	0.2	90° - ID 0.4 in
CF/ABS plate	1.5	Window Frame – Unistress	09/07/21	0.75	0.2	90° - ID 0.4 in

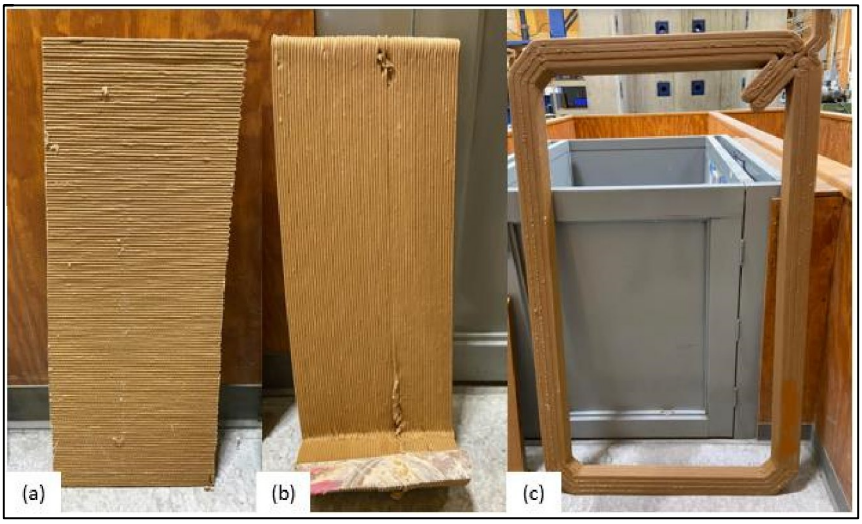

Figure 3.1: WF/PLA material (a) 1.0 in thick plate, (b) 1.5 in thick plate, and (c) 1.6 in thickness.

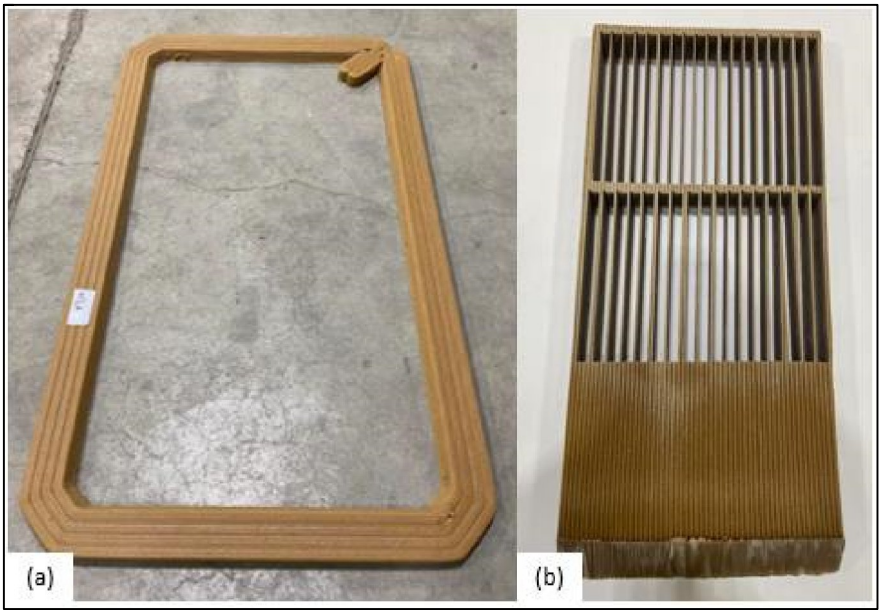

Figure 3.2: WF/aPLA material (a) 1.6 in thick form, and (b) 1.5 in thick plate after waterjet cut of specimens.

Figure 3.3: CF/ABS 1.5 in thick plate after waterjet cut of specimens.

3.2 Sample preparation

3.2.1 Specimen printing directions

The main printing directions for the large-scale 3D printed specimens are direction-1 longitudinal, direction-2 transverse, and direction-3 through-thickness. Figure 3.4 shows the mentioned printing directions.

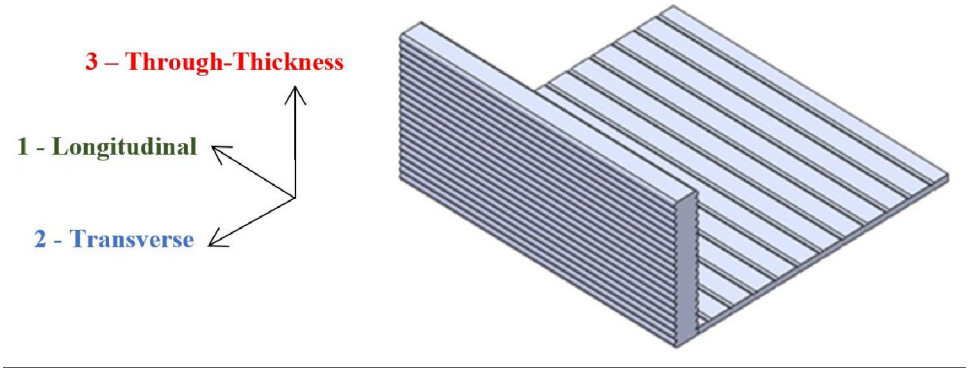

Figure 3.4: Printing directions considered for large-scale 3D printed specimens

3.2.2 Acronyms used for specimens

All the acronyms referring to material, printing direction, type of plate, and conditioning for specimens tested in flexure, are defined in Table 3.2. For example, if the denomination of a specimen is WF/PLA-LMP1.0, it can be broken down as:

- WF/PLA: The specimen is made of is WF/PLA.
- L: Its direction of interest is longitudinal, meaning it was cut in direction-1.
- M: The specimen was subjected to moisture absorption.
- P1.0: The specimen was cut from a plate of 1.0 in thickness.

Also, specimens with P1.0 and P1.5 are referred to as as-printed specimens of 1.0 in and 1.5 in width, respectively. If it's only mentioned as an as-printed specimen, it means that it is a specimen of 1.5 in width. Specimens with an F1.6 are referred to as machined specimens from 1.6 in thick forms.

Table 3.2: Acronyms used for specimens

Acronym	Definition
WF/PLA	Polylactic acid with wood filler
WF/aPLA	Amorphous polylactic acid with wood filler
CF/ABS	Acrylonitrile Butadiene Styrene reinforced with carbon fibers.
L	Longitudinal
T	Transverse or through thickness
P1.0	Specimen cut from a plate of 1.0-inch thickness
P1.5	Specimen cut from a plate of 1.5-inch thickness
F1.6	Specimen cut from a form of 1.6-inch thickness
M	Moisture absorption
F	Freeze-thaw cycling
B	Baseline

3.2.3 Specimen dimensions

Specimen dimensions were categorized into four main groups, and their width, height, and length are shown in Table 3.3. The first thing that was considered is that for specimens cut in direction-1, their 0.4 in height was selected to have two layers. In the case of specimens cut in direction-3, their 1.0 in height was considered to have two 0.5 in beads. Also, if the specimens were obtained from plates or forms, they can be as-printed or machined. The width and height considered as-printed rely on the printing direction in which it was cut. Width and height are the distance

between crests, as shown in Figure 3.5. Machined specimens are the specimens whose layers are not visible, as shown in Figure 3.6.

Table 3.3: Specimen dimensions

Groups	**Width b (in)**	**Height h (in)**	**Length L (in)**	**Crosshead rate (mm/min)**
L*P1.0	1.0	0.4	7.7	4.34
L*P1.5	1.5	0.4	7.7	4.34
T*P1.0	2.0	1.0	19.2	10.9
L*F1.6	1.5	0.4	8.0	4.34

*Specimen conditions: Baseline (B), Moisture (M), or Freeze-Thaw (F) specimen.

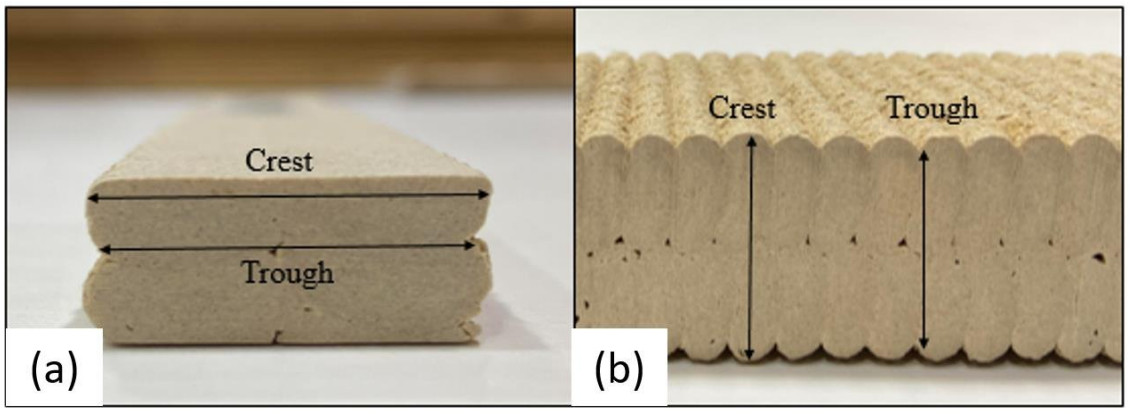

Figure 3.5: (a) As-printed specimen aligned in direction-1, (b) crest, and trough for specimen aligned in direction-3

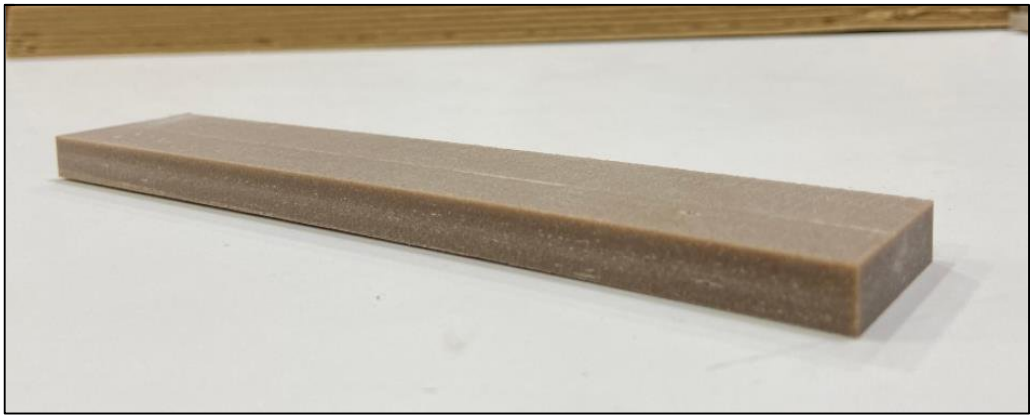

Figure 3.6: Machined specimens

Schematics of the specimen orientations are shown in Figure 3.7 and Figure 3.8 for the direction-1 and direction-3.

Figure 3.9, Figure 3.10, Figure 3.11 and Figure 3.12 illustrate the dimensions for each of these of groups LP1.0, LP1.5, TP1.0, LF1.6 respectively. This can be applied to any of the materials used in this study.

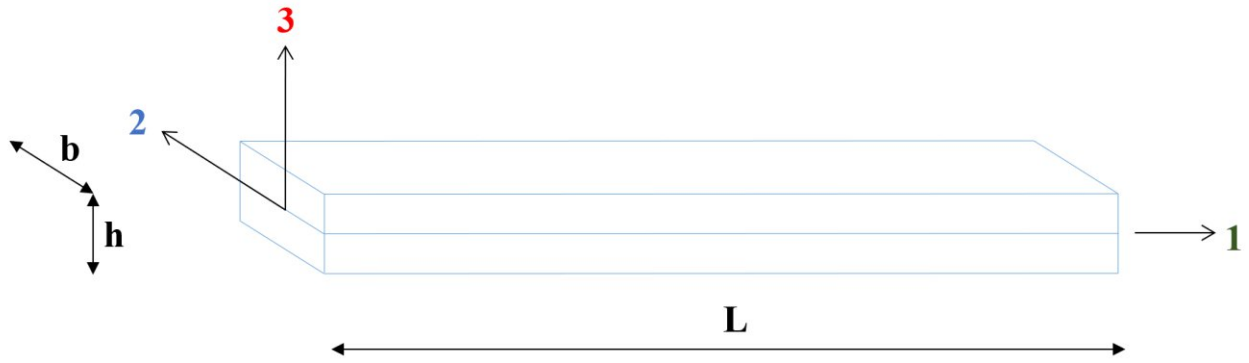

Figure 3.7: Prismatic specimen aligned in direction-1

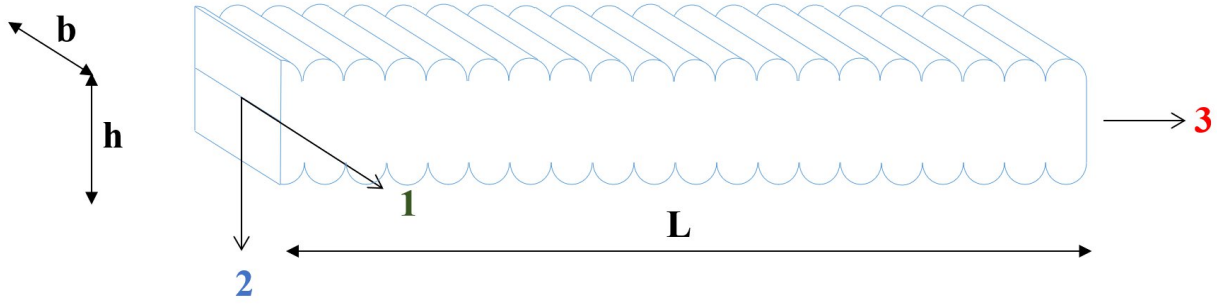

Figure 3.8: Prismatic specimen aligned in direction-3

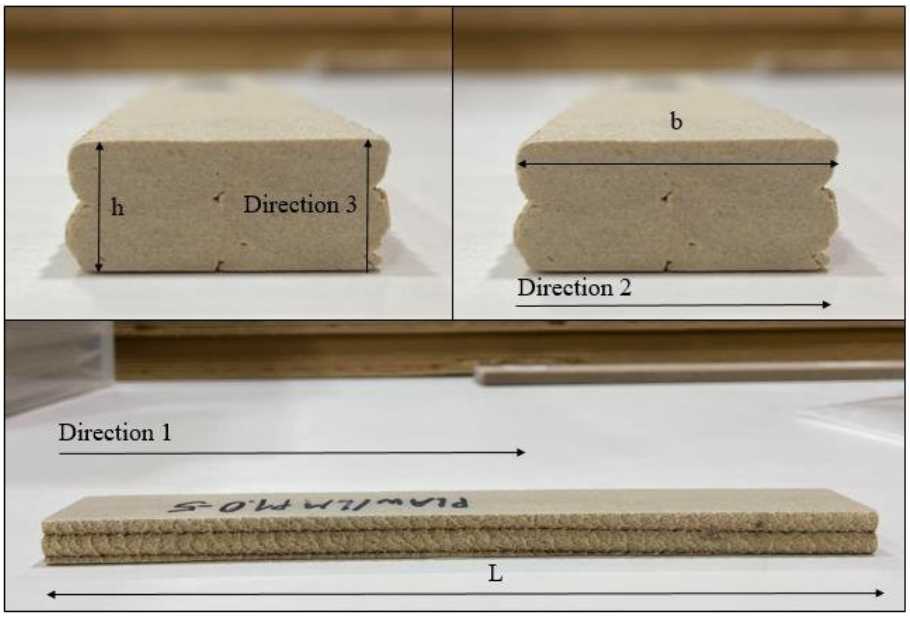

Figure 3.9: Dimensions and printing directions for set LP1.0 as-printed prismatic aligned in direction-1

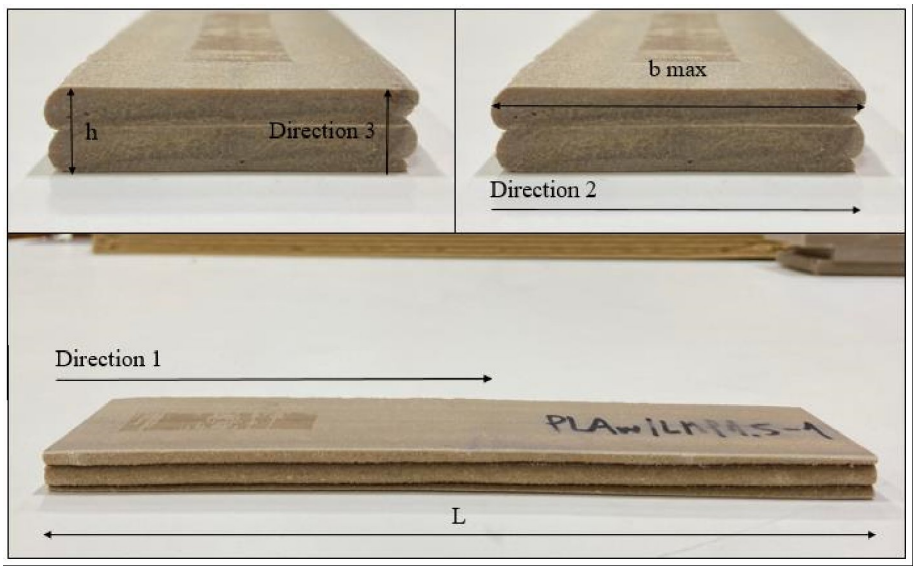

Figure 3.10: Dimensions and printing directions for set LP1.5 as-printed prismatic aligned in direction-1

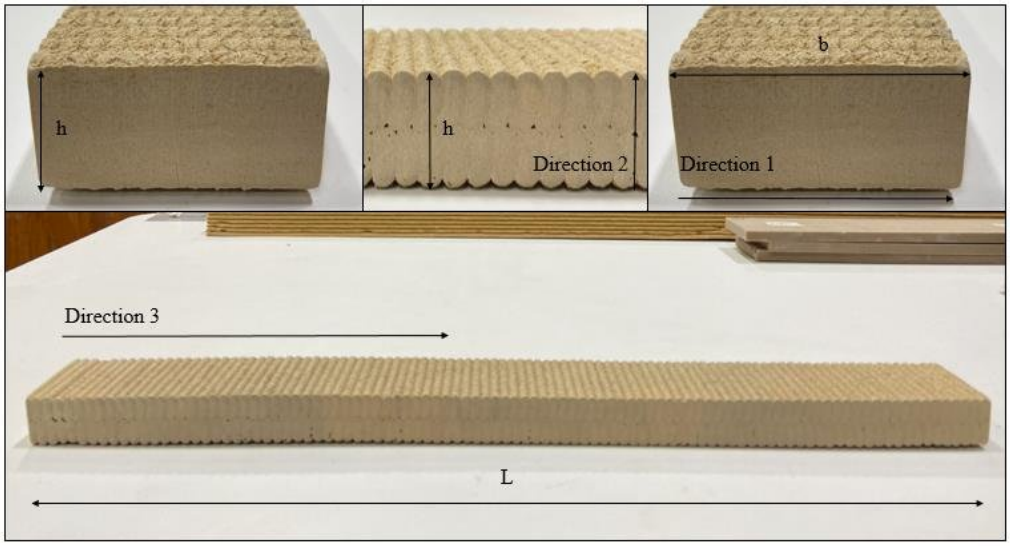

Figure 3.11: Dimensions and printing directions for set TP1.0 as-printed prismatic aligned in direction-3

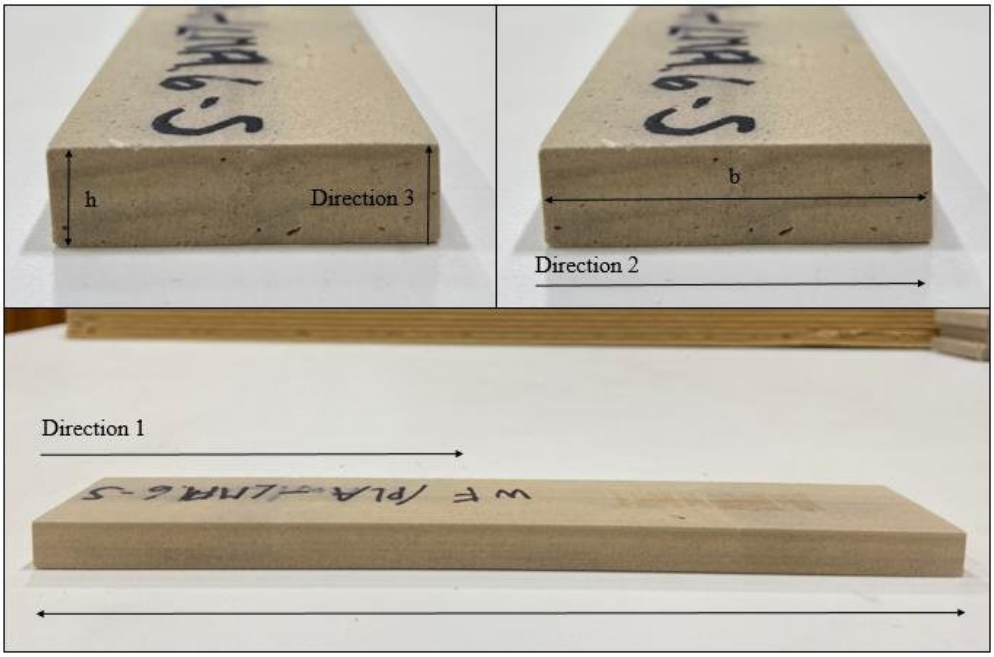

Figure 3.12: Dimensions and printing directions for set LF1.6 machined prismatic aligned in direction-1

3.2.4 Specimen dimensions for specimens under simulated weathering based on UV and condensation cycle.

Specimen dimensions were constrained by the size of the selected QUV machine fixtures, shown in Figure 3.13. It was decided to use the available ones to avoid purchasing or making new fixtures. Figure 3.14 shows the dimensions of the specimens; thickness is just a reference since it was not possible to get an even thickness. This is because the specimens had to be gripped in the CNC equipment on the side with beads, which made the machining difficult; beads do not have a uniform height, so the final thickness was between the range of 7.5 mm and 10.5 mm.

Specimens placed in the QUV machine are shown in Figure 3.15.

The CF/ABS specimens for this conditioning are: 5 as-printed, 5 machined and 5 baseline.

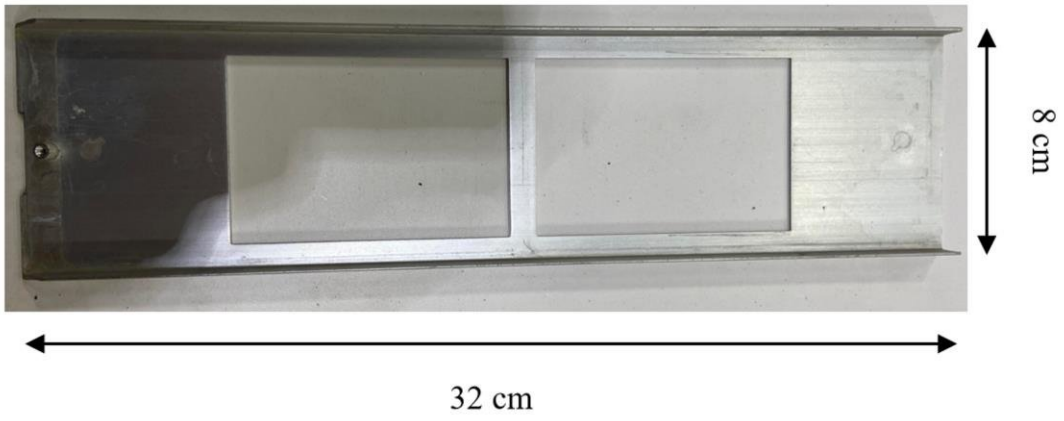

Figure 3.13: QUV Machine selected fixtures

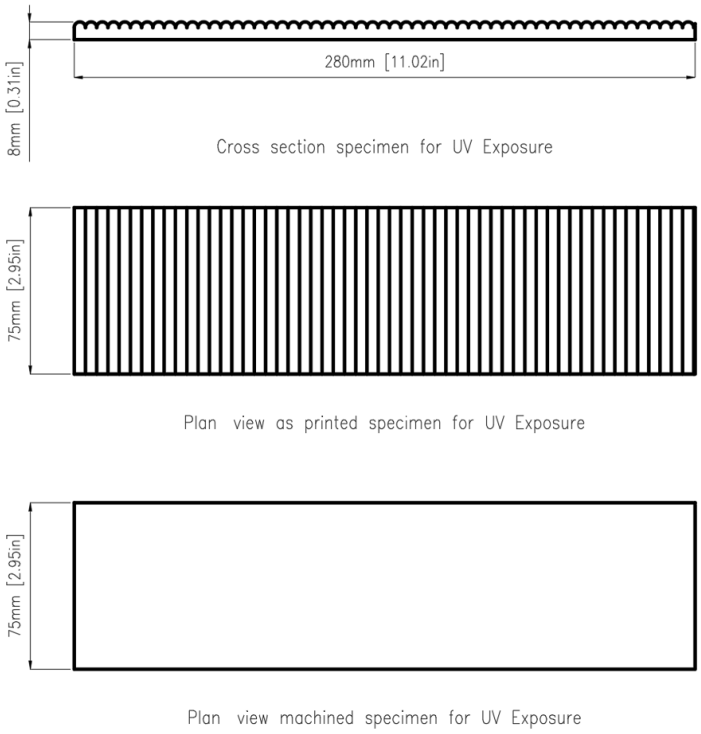

Figure 3.14: Specimens dimensions for UV exposure

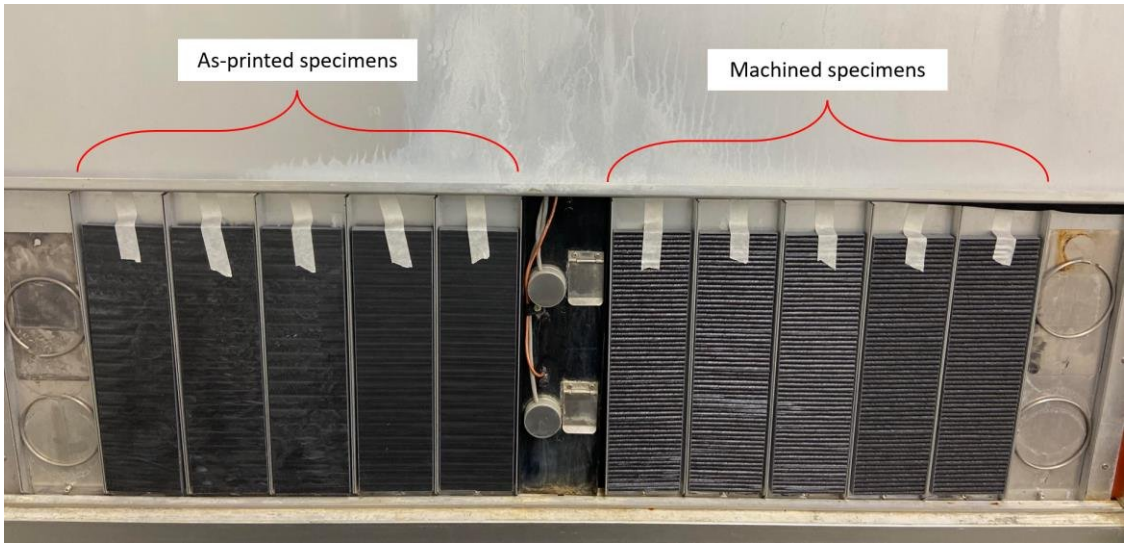

Figure 3.15: Specimens in the QUV machine.

3.3 Test matrix for baseline and conditioned specimens

The test matrix, with printing directions, the number of specimens, and dimensions, are provided in Table 3.4.

Table 3.4: Test matrix

Set	Direction	Height h (in)	Width b (in)	Length L (in)	# Of specimens
WF/PLA-LBP1.0	1	0.4	1.0	7.7	4
WF/PLA-LMP1.0	1	0.4	1.0	7.7	6
WF/PLA-LFP1.0	1	0.4	1.0	7.7	6
WF/PLA-LBP1.5	1	0.4	1.5	7.7	10
WF/PLA-LMP1.5	1	0.4	1.5	7.7	10
WF/PLA-LFP1.5	1	0.4	1.5	7.7	10
WF/PLA-LBF1.6	1	0.4	1.5	8.0	8
WF/PLA-LMF1.6	1	0.4	1.5	8.0	8
WF/PLA-LFF1.6	1	0.4	1.5	8.0	8
WF/PLA-TBP1.0	3	1.0	2.0	19.2	2
WF/PLA-TMP1.0	3	1.0	2.0	19.2	3
WF/PLA-TFP1.0	3	1.0	2.0	19.2	3
WF/aPLA-LBP1.5	1	0.4	1.5	7.7	10
WF/aPLA-LMP1.5	1	0.4	1.5	7.7	6
WF/aPLA-LFP1.5	1	0.4	1.5	7.7	10
WF/aPLA-LBF1.6	1	0.4	1.5	8.0	8
WF/aPLA-LMF1.6	1	0.4	1.5	8.0	6
WF/aPLA-LFF1.6	1	0.4	1.5	8.0	8
CF/ABS-LBP1.5	3	0.4	1.5	7.7	10
CF/ABS-LMP1.5	3	0.4	1.5	7.7	6
CF/ABS-LFP1.5	3	0.4	1.5	7.7	10

3.4 Flexure test results for baseline specimens

The flexural modulus was computed based on the flexural tangent modulus of elasticity. In this section, flexural material property tables have a parenthesis value corresponding to the coefficient of variation (CV). The number of specimens per set is also specified in the table. If a specimen had a non-desirable mode of failure due to incorrect placement or loading, then the flexural strength was not computed.

Flexure tests were conducted based on the load configuration shown in Figure 3.16 and Figure 3.17. Two beam orientations were considered: 1) material axis-1 aligned with the beam axis; and 2) material axis-3 aligned with the beam axis.

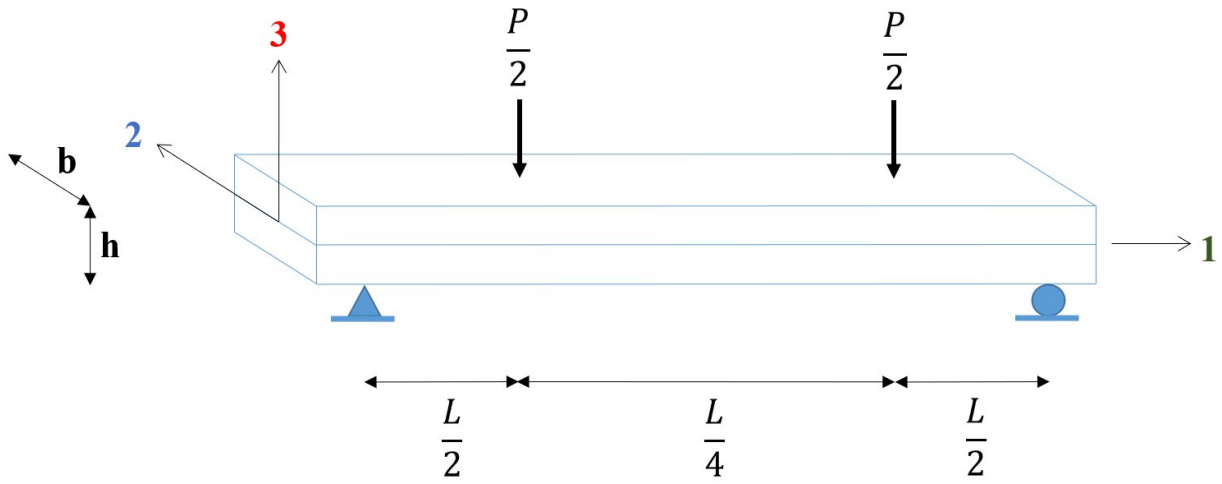

Figure 3.16: Beam specimen aligned in direction-1

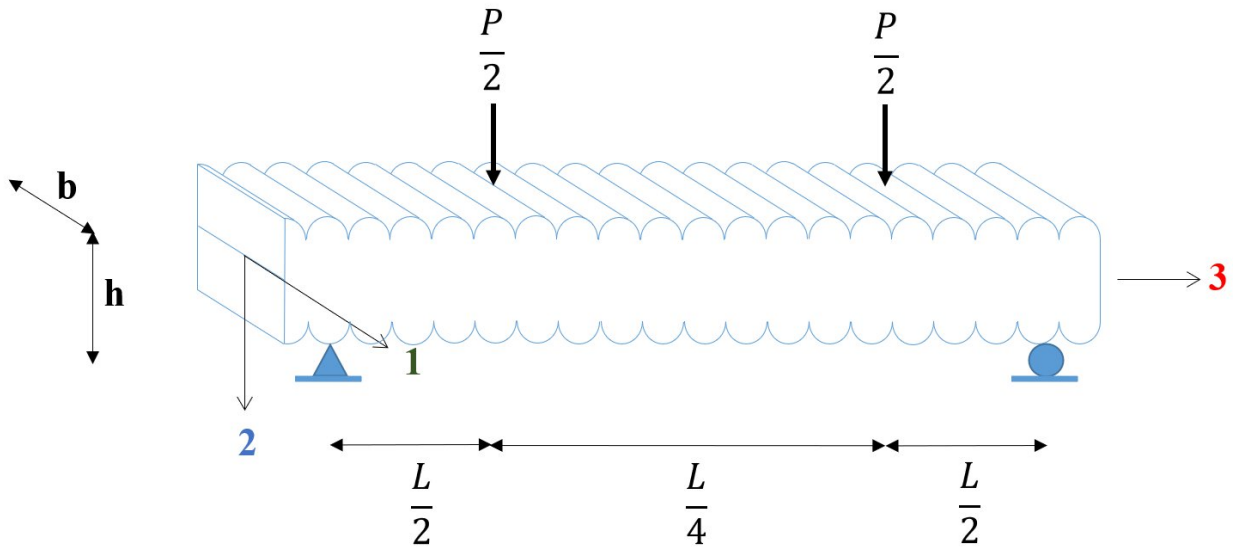

Figure 3.17: Beam specimen aligned in direction-3

3.4.1 Flexure test results for baseline WF/PLA sets

Table 3.5 shows the flexural strength and flexural modulus of WF/PLA baseline sets aligned in direction-1 a

Table 3.5: Flexural material properties for WF/PLA baseline sets aligned in direction-1

WF/PLA d-1 Specimen Set	**Flexural Results**	
	Strength ($F1_f$) MPa *(SpecQty/CV)*	**Modulus ($E1_f$)** GPa *(SpecQty/CV)*
WF/PLA-LBP1.5 *(as-printed)*	64.5 *(8/4.3%)*	4.2 *(10/8%)*
WF/PLA-LBP1.0 *(as-printed)*	64.4 *(3)*	4.27 *(4)*
WF/PLA-LBF1.6 *(machined)*	77.2 *(6/8.1%)*	5.15 *(6/7.2%)*

Table 3.6 shows the flexural strength and flexural modulus of WF/PLA baseline sets aligned in direction-3.

Table 3.6: Flexural material properties for WF/PLA baseline sets aligned in direction-3

WF/PLA d-3 Specimen Set	**Flexural Results**	
	Strength ($F3_f$) MPa *(SpecQty)*	**Modulus ($E3_f$)** GPa *(SpecQty)*
WF/PLA-TBP1.5 *(as-printed)*	26.9 *(2)*	3.30 *(2)*

Figure 3.18 to Figure 3.20 show the stress versus strain plots for WF/PLA-LBP1.5, WF/PLA-LBP1.0, WF/PLA-LBF1.6, and WF/PLA-TBP1.0 specimen sets, respectively.

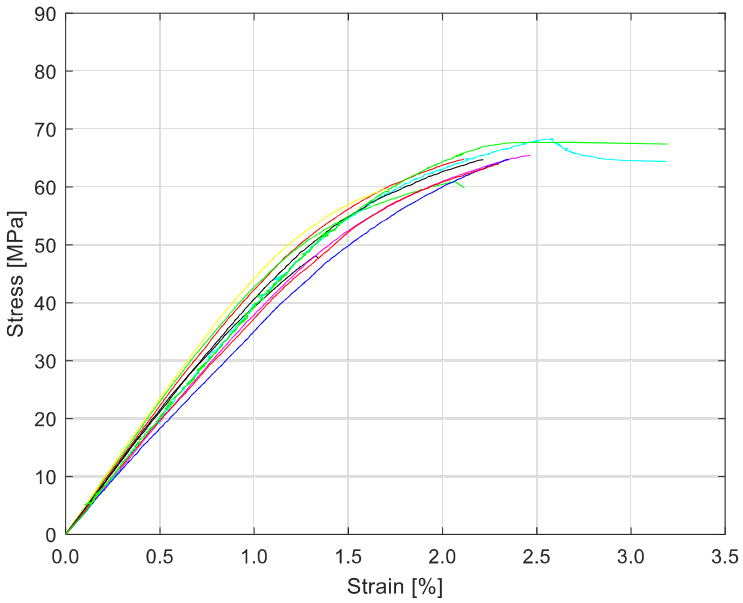

Figure 3.18: Stress versus strain curves for WF/PLA-LBP1.5 aligned in direction-1.

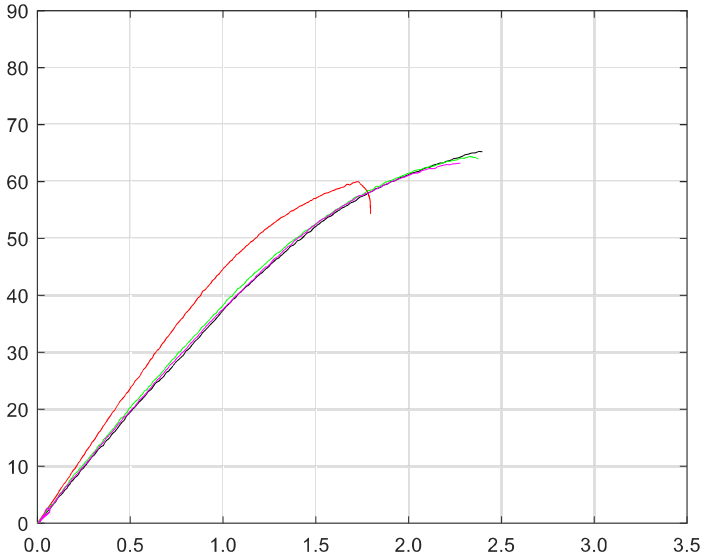

Figure 3.19: Stress versus strain curves for WF/PLA-LBP1.0 aligned in direction-1.

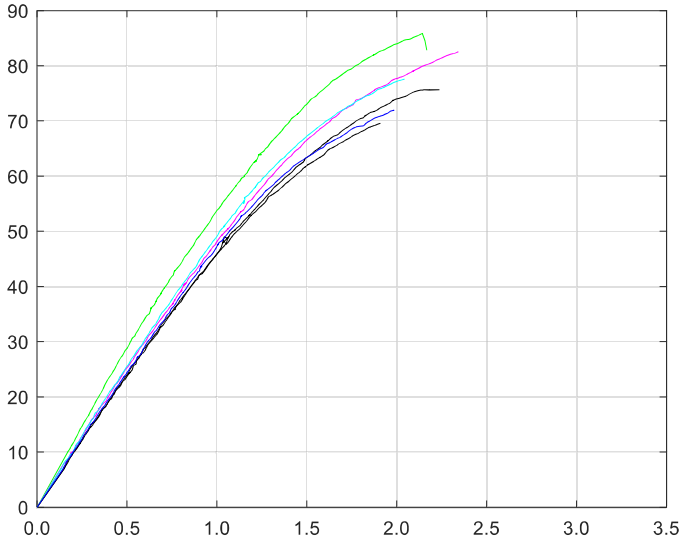

Figure 3.20: Stress versus strain curve for WF/PLA-LBF1.6 aligned in direction-1

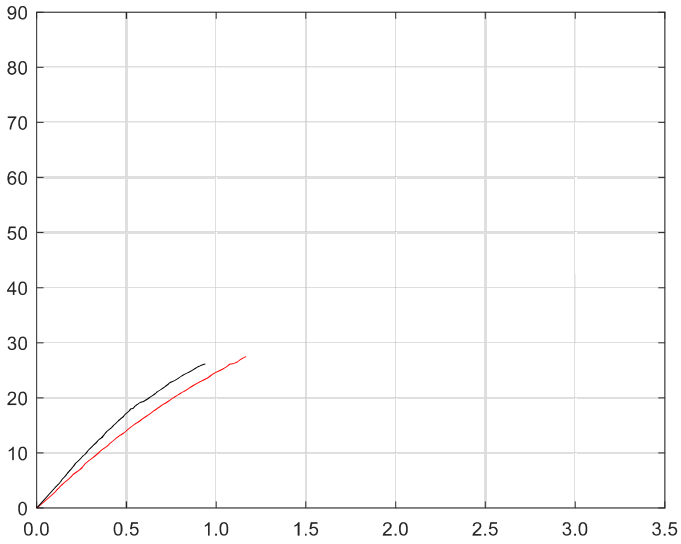

Figure 3.21: Stress versus strain curve for WF/PLA-TBP1.0 aligned in direction-3

3.4.2 Flexure test results for baseline WF/aPLA sets

Table 3.7 shows the flexural strength and flexural modulus of WF/aPLA baseline sets aligned in direction-1.

Table 3.7: Flexural material properties for WF/aPLA baseline sets aligned in direction-1

WF/aPLA d-1 Specimen Set	**Flexural Results**	
	Strength ($F1_f$) MPa *(SpecQty/CV)*	**Modulus ($E1_f$)** GPa *(SpecQty/CV)*
WF/aPLA-LBP1.5 *(as-printed)*	73.2 *(10/6.8%)*	4.59 *(10/4.6%)*
WF/aPLA-LBF1.6 *(machined)*	73.6 *(8/6.0%)*	4.99 *(8/7.4%)*

Figure 3.22 and Figure 3.23 show the stress versus strain plots for WF/aPLA-LBP1.5 and WF/aPLA-LBF1.6 specimen sets respectively.

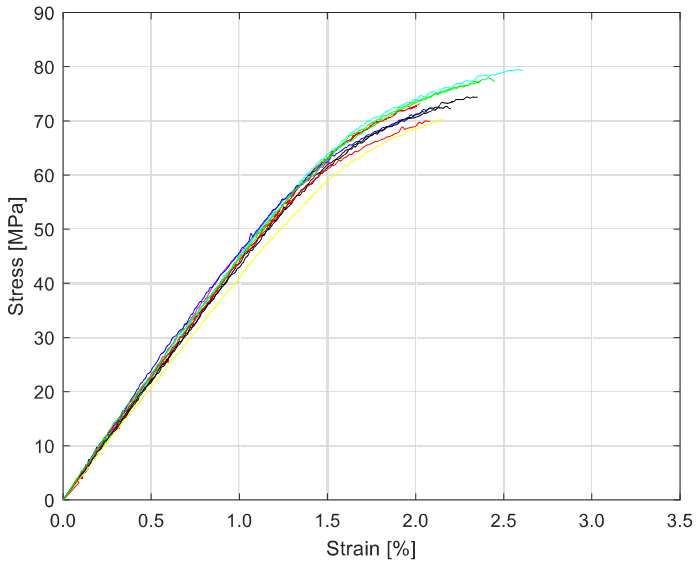

Figure 3.22: Stress versus strain curves for WF/aPLA-LBP1.5 aligned in direction-1

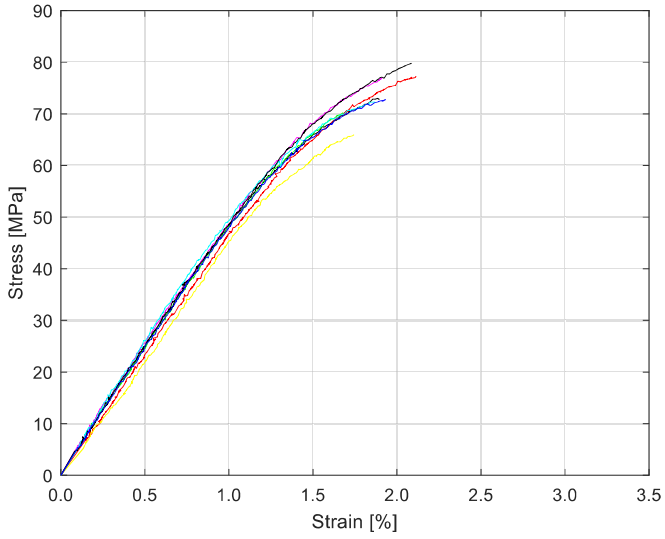

Figure 3.23: Stress versus strain curves for WF/aPLA-LBF1.6 aligned in direction-1

3.4.3 Flexure test results for baseline CF/ABS sets

Table 3.8 shows the flexural strength and flexural modulus results of CF/ABS as-printed set aligned in direction-1, while Figure 3.24 shows the stresses versus strain plots for that specimen set.

Table 3.8: Flexural material properties for CF/ABS baseline sets aligned in direction 1

WF/aPLA d-1 Specimen Set	**Flexural Results**	
	Strength ($F1_f$) MPa *(SpecQty/CV)*	**Modulus ($E1_f$)** GPa *(SpecQty/CV)*
CF/ABS-LBP1.5 *(as-printed)*	82.5 *(10/11%)*	6.95 *(10/15%)*

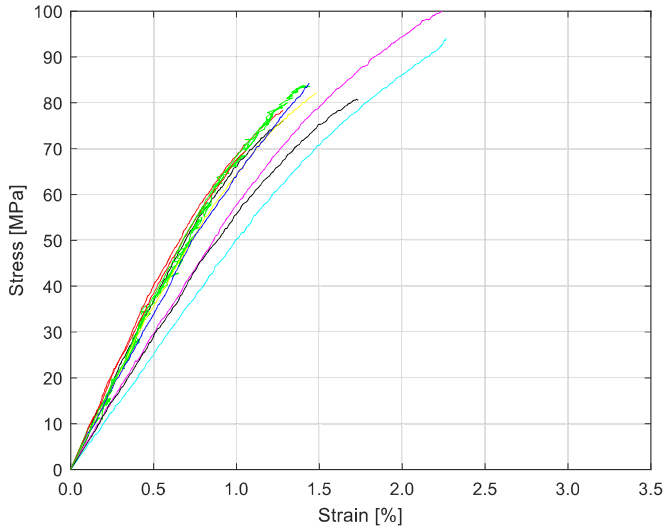

Figure 3.24: Stress versus strain curve for CF/ABS baseline as printed aligned in direction-1

3.4.4 Flexure test results for baseline as-printed sets

Table 3.9 shows flexural material properties for the three different large-scale 3D printed materials as-printed aligned in direction one.

Table 3.9: Flexural material properties for 3D printed materials baseline sets as-printed aligned in direction-1

As-printed Specimen Set	Flexural Results	
	Strength ($F1_f$) MPa *(SpecQty/CV)*	**Modulus ($E1_f$)** GPa *(SpecQty/CV)*
WF/PLA-LBP1.5	64.5 *(8/4.3%)*	4.2 *(10/8%)*
WF/aPLA-LBP1.5	73.2 *(10/6.8%)*	4.59 *(10/4.6%)*
CF/ABS-LBP1.5	82.5 *(10/11%)*	6.95 *(10/15%)*

3.5 Discussion of results

The purpose of the analysis is to determine if there is any difference in the flexural material properties of WF/PLA sets, when comparing sets with different width, surface finish, and direction in which the sets are aligned.

For WF/aPLA, the flexural material properties are compared for as-printed and machined specimens. In addition, flexural materials properties are compared between WF/PLA and WF/aPLA for as-printed and machined specimens.

An ANOVA t-test considering a p-value < 0.05 as statistically significant, was used to compare the flexural strength and modulus of the baseline sets mentioned before. The p-values are shown in Table 3.10 to Table 3.12 for WF/PLA, Table 3.13 for WF/aPLA and Table 3.14 and Table 3.15 for comparisons between WF/PLA and WF/aPLA.

3.5.1 Data analysis for WF/PLA specimens with a width of 1.0 in and 1.5 in aligned in direction-1

From Table 3.10, the p-value shows no difference in the flexural strength and flexural modulus of WF/PLA specimens with different widths.

Table 3.10: Data analysis for WF/PLA baseline sets of 1.5 in width and 1.0 in width aligned in direction-1

	Flexural Strength	Flexural Modulus
Sets	**p-value**	**p-value**
as-printed 1.5 – as-printed 1.0 in width	0.48	0.46

3.5.2 Data analysis for WF/PLA specimens as-printed and machined specimens aligned in direction-1

When comparing printed specimens with machined specimens of WF/PLA, Table 3.11 shows that the difference is statistically significant, meaning that machining influences flexural strength and modulus.

Table 3.11: Data analysis for WF/PLA baseline as-printed and machined aligned in direction-1

	Flexural Strength	Flexural Modulus
Sets	**p-value**	**p-value**
machined – as-printed	**2.65E-02**	**9.33E-05**

3.5.3 Data analysis for WF/PLA specimens aligned in direction-1 and 3

When comparing the as-printed set aligned in direction-1 and 3, from Table 3.12, the p-value shows that the difference in the flexural strength and flexural modulus is statistically significant, which means that these properties are different.

Table 3.12: Data analysis for WF/PLA baseline as-printed aligned in directions 1 and 3

	Flexural Strength	**Flexural Modulus**
Sets	**p-value**	**p-value**
as-printed direction-1 – as-printed direction-3	**7.93E-08**	**3.53E-03**

3.5.4 Data analysis for WF/aPLA as-printed and machined specimens aligned in direction-1

When comparing printed specimens with machined specimens for WF/aPLA, Table 3.13 shows that the difference is statistically significant only for the flexural modulus of elasticity, meaning that machining affects this material property.

Table 3.13: Data nalysis for WF/aPLA baseline as-printed and machined aligned in direction-1

	Flexural Strength	**Flexural Modulus**
Sets	**p-value**	**p-value**
machined – as-printed	0.43	**5.00E-03**

3.5.5 Data analysis between WF/PLA and WF/aPLA as-printed specimens aligned in direction-1

Table 3.14 shows that, the difference is statistically significant only when comparing WF/PLA and WF/aPLA. This means that the flexural strength and modulus differ for the two materials.

Table 3.14: Data Analysis between WF/PLA and WF/aPLA as-printed sets aligned in direction-1

As-printed Sets	Flexural Strength p-value	Flexural Modulus p-value
WF/PLA and WF/aPLA	**5.79E-03**	**6.00E-03**

3.5.6 Data analysis between WF/PLA and WF/aPLA machined specimens aligned in direction-1

When comparing WF/PLA and WF/aPLA, Table 3.15 shows no difference in machined specimens flexural modulus and flexural strength.

Table 3.15: Data Analysis between WF/PLA and WF/aPLA machined sets aligned in direction-1

Machined Sets	Flexural Strength p-value	Flexural Modulus p-value
WF/PLA and WF/aPLA	0.11	0.23

3.6 Conclusions

For WF/PLA, the flexural strength and flexural modulus were not different for specimens with different widths, which means that specimen width does not affect flexural material properties. When comparing WF/PLA as-printed and machined specimens, material properties were not the same, which means that machining impacts the flexural material properties.

The direction in which the specimens are aligned is relevant since different flexural material properties were obtained.

For WF/aPLA, the flexural strength is the only property that is the same when as-printed and machined specimens were compared.

CHAPTER 4

MOISTURE ABSORPTION

4.1 Introduction

The following chapter presents the results and findings from moisture absorption. The coefficient of moisture expansion was only evaluated for the bio-based materials (WF/PLA and WF/aPLA), and flexure tests for specimens under moisture absorption were only conducted for WF/aPLA and CF/ABS

4.2 Literature review

In the literature, Kariz et al. [42] describes that composite materials with wood flour, wooden particles in filaments caused clustering, clogging, and uneven flow through the nozzle, which caused more porous and non-solid/fused structures, which reduced mechanical properties. This might explain why the material is porous and presents voids.

Kamau-Devers et al. [43] observed swelling and cracking in WF/PLA specimens under moisture absorption. Trinh et al. [44] Observed swelling in the biocomposite and voids at the wood fiber-PLA interface.

Ayrilmid et al. [45] observed that water absorption of the specimens increased with increasing printing layer thickness while the thickness swelling decreased. The considered printing layers were 0.05 mm, 0.1 mm, 0.2 mm, and 0.3 mm.

When looking for wood plastic composites Lin et al. [46], Wang and Morrel [47], and Bledzki and Faruk [48] found that the size of wood particles affected the response WPC towards the water. Using larger particles in WPCs caused higher water absorption because the surface areas of large particles in contact with water were more significant on the composite surfaces.

Kim et al [49] studied the effect of moisture on WPC with 50% wood fibers in a conditioning chamber, achieving a range of 12-18% for the different materials used.

Moisture content and additional information from studies performed by authors in the literature for WF/PLA are illustrated in Table 4.1.

Table 4.1: Literature review for moisture content of WF/PLA

Author	**Material**	**Moisture Content (MC) (%)**	**Comments**
Kamau-Devers et al.	WF/PLA	5.98 (35°C)-12.43(47°C)	WF content 20%, disks of 2-inch diameter and 1/8-inch thickness, and Conditioned for 66 days
Kariz et al.	WF/PLA	0.7-3.1	WF content 20% and others, specimens of 80x12x4 mm, conditioned in climate chambers at 20°C with RH of 33, 65, and 87%, and conditioned for 16 days.
Ayrilmid et al.	WF/PLA	0.19-0.72	WF content 30%, specimen dimensions 100x15x4 mm, water temperature 20°C, and conditioned for 28 days.

Moisture content for WPC from studies performed by authors in the literature are illustrated in Table 4.2: Literature review for moisture content of WPC.

Table 4.2: Literature review for moisture content of WPC

Author	Material	Wood fibers content (%)	Method	Conditioning time (days)	Moisture Content (MC) (%)
Wang and Morrel	Trex® and Stranded® deck sections made of WPC	Not informed	Water immersion at 5°C and 25°C	215	11% and 16% respectively
Kim et al	Isostatic polypropylene and different wood species	50%	Conditioning chamber at 25°C and 100% RH.	51	12-18%

In the case of carbon fiber-reinforced polymers, Dzul-Cervantes et al. [50] found that a type of epoxy resin with CF as a reinforcement absorbs water linearly during the first ten days of the conditioning. After ten days of conditioning, the moisture absorption curves become asymptotic. Yu et al. [51] explain how composites can absorb water: water molecules diffuse into the epoxy matrix directly. Secondly, water flows along with the interface between carbon fiber and matrix due to capillarity effects, and thirdly, water can exist in the open area such as holes and microcracks. This is important when comparing the materials in this research work, considering holes and microcracks in each material.

Ferrell [52] investigated the effect of heat and moisture in CF/ABS, showing that conditioning temperature substantially influences the failure strain in multiple orientations. Also, moisture demonstrated an increase in variability and a reduction in tensile strength.

Haghighi-Yazdi et al. [53, 54] studied hygrothermal effects on polycarbonate (PC)/ABS, observing that for different conditions, the specimens reached a 0.41% of moisture equilibrium. Moisture content and additional information from studies performed by authors in the literature for carbon fiber-reinforced polymers are illustrated in Table 4.3.

Table 4.3: Literature review for moisture content (MC) for CF-reinforced polymers

Author	**Material**	**MC (%)**	**Comments**
Dzul-Cervantes et al.	Epoxy resin (ER), diglycidyl ether of bisphenol-A (DGEBA), Epon 828, and carbon fiber (CF) IM7	1.75	Temperature 25°C and relative humidity of 25% and 95%, after ten days, the moisture absorption rate decreased, becoming asymptotic after 30 days, and conditioned for 80 days.
Yu et al.	HexTow IM2C carbon fiber cloth in a 2-2 twill configuration/	1.4	Tap water at 80°C, and circulating water for 10, 20, 30, and 60 days.
Ferrell	CF/ABS	Not informed	CF content 15%

Table 4.3 continued

Haghighi-Yazdi et al.	Polycarbonate/acrylonitrile-butadiene-styrene (PC/ABS)	The equilibrium moisture content of 0.41%	Samples dimensions 64 x 13 x 3 mm, subjected to 5 different conditions: 65°C and 50% RH, 50°C and 93% RH, 65°C and 93% RH, 50°C and 50% RH, and lastly, stored at room temperature fully immersed in distilled water, conditioned until equilibrium, and conditioned for approximately 100 days
Haghighi-Yazdi et al.	Polycarbonate/acrylonitrile-butadiene-styrene (PC/ABS)	Not informed	Samples were subjected to different conditions: 50°C/50% RH, 50°C/ 93% RH, 50°C/fully immersed, 65°C/50% RH, 65°C/ 93% RH, 65°C/fully immersed, 80°C/50% RH, 80°C/ 75% RH, and 80°C/fully immersed.

For reference to the values obtained in this research work for the coefficient of moisture expansion (CME), Table 4.4 shows the values of CME for CF-reinforced composite materials.

Table 4.4: Values of coefficient of moisture expansion (CME) from the literature for CF-reinforced composite materials

Author	Material	CME	Comments
Poenninger and Defoort et al [55]	Unidirectional and bidirectional CF-reinforced polymers	3.10E-04 (bidirectional) 2.23E-03 (UD 90°) 5.25E-05 (UD 0°)	Evaluated for different fiber directions.
Chaid et al. [56]	Perlonmj stockinette white,	66.57E-06 52.9E-06	unidirectional laminate square plates with different lay-ups.
Pavankiran et al, 2007[57]	Unidirectional laminate made of CF-reinforced epoxy	1.92E-03	
Spacecraft structures and mechanical testing – Volume 1 [58]	CFRP (Carbon-reinforced polymers)	3.85E-05 (normal to fiber) 3.098E-03 (along the fiber)	Along the fiber direction and normal to the fiber direction, respectively

4.3 Moisture content

Two types of prismatic specimens were used for the moisture content testing: 1) specimens aligned in the direction 1, where moisture diffusion occurs primarily through the surfaces normal to directions 2 and 3; and 2) specimens aligned in the direction 3, where moisture diffusion occurs primarily through the surfaces normal to directions 1 and 2. These specimens are shown in Figure 4.1 and Figure 4.2.

The average moisture content measured for WF/PLA, WF/aPLA, and CF/ABS set are shown in Table 4.5 to Table 4.9.

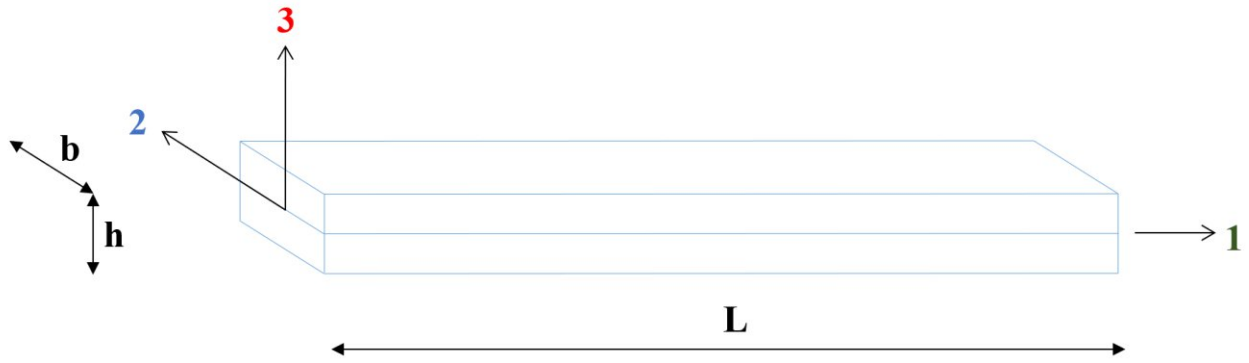

Figure 4.1: Prismatic specimen aligned in direction-1

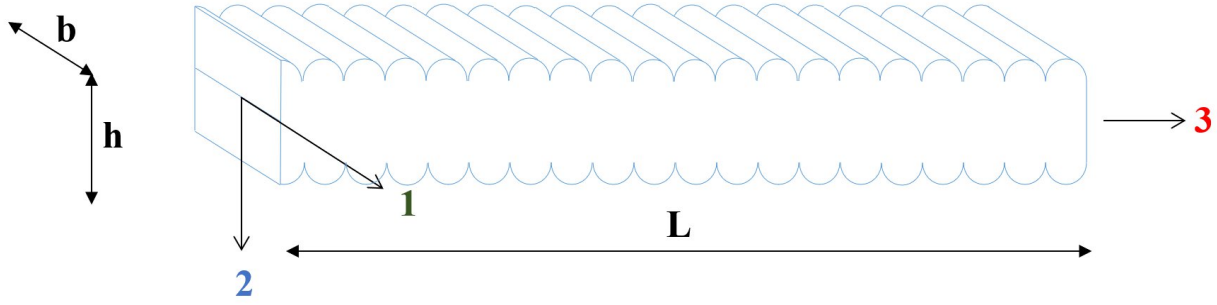

Figure 4.2: Prismatic specimen aligned in direction-3

Table 4.5: Average moisture content for WF/PLA sets aligned in direction-1

Set	Number of Specimens	Average moisture content (%)	Coefficient of variation (%)
WF/PLA-LMP1.0	6	8.34	2.01
WF/PLA-LMP1.5	10	7.74	4.08
WF/PLA-LMF1.6	8	8.45	7.54

Table 4.6: Average moisture content for WF/PLA set aligned in direction-3

Set	**Number of Specimens**	**Average moisture content (%)**	**Coefficient of variation (%)**
WF/PLA-TMP1.0	3	6.76	1.09

Table 4.7: Average moisture content for WF/aPLA set aligned in direction-1

Set	Number of Specimens	Average moisture content (%)	Coefficient of variation (%)
WF/aPLA-LMP1.5	6	9.23	0.72
WF/aPLA-LMF1.6	6	7.05	2.65

Table 4.8: Average moisture content for CF/ABS set aligned in direction-1

Set	**Number of Specimens**	**Average moisture content (%)**	**Coefficient of variation (%)**
CF/ABS-LMP1.5	6	1.35	7.63

Table 4.9: Average moisture for 3D printed materials as-printed aligned in direction-1

Set	Number of Specimens	Average moisture content (%)	Coefficient of variation (%)
WF/PLA-LMP1.5	10	7.74	4.08
WF/aPLA-LMP1.5	6	9.23	0.72
CF/ABS-LMP1.5	6	1.35	7.63

To see the variation of moisture over time, sorption curves were generated. Figure 4.3: Sorption curves for WF/PLA sets aligned in direction-1 to Figure 4.7: Sorption curves for WF/PLA, WF/aPLA, and CF/ABS as-printed sets aligned in direction-1 illustrate the sorption curves for WF/PLA sets aligned in direction-1 and 3 and for WF/aPLA and CF/ABS sets aligned in direction-3.

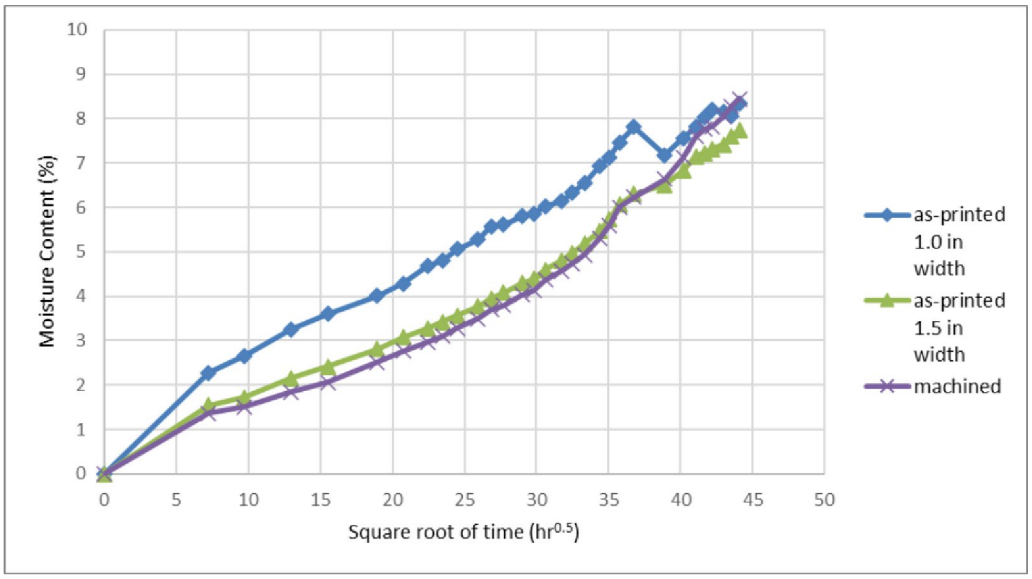

Figure 4.3: Sorption curves for WF/PLA sets aligned in direction-1

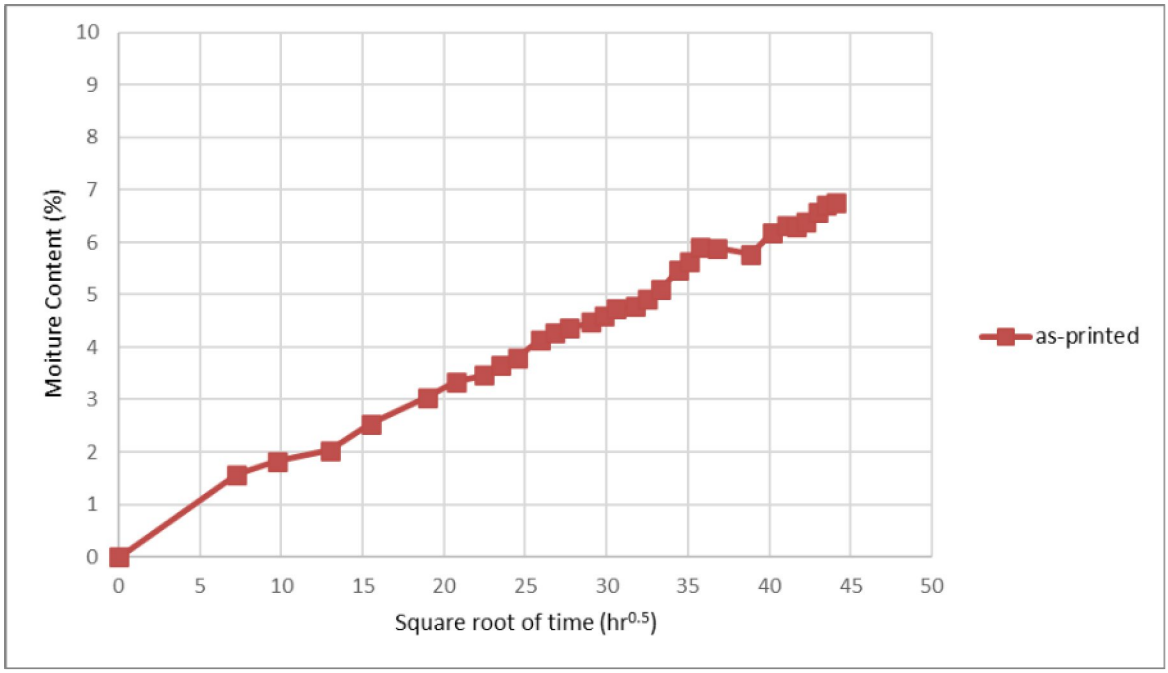

Figure 4.4: Sorption curve for WF/PLA set aligned in direction-3

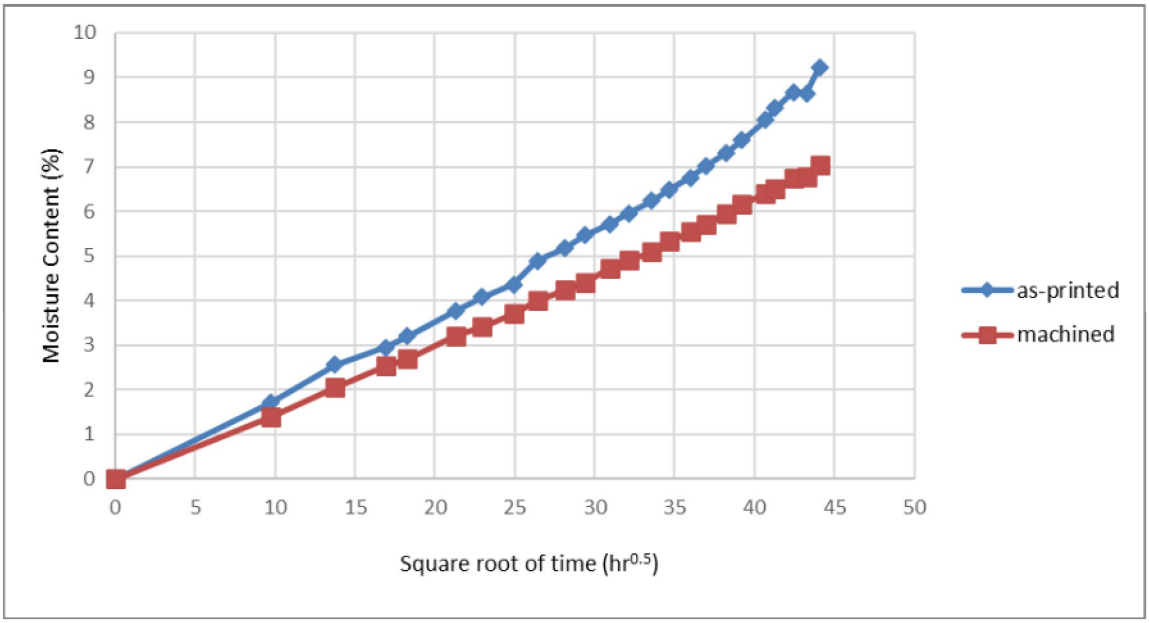

Figure 4.5: Sorption curves for WF/aPLA sets aligned in direction-1

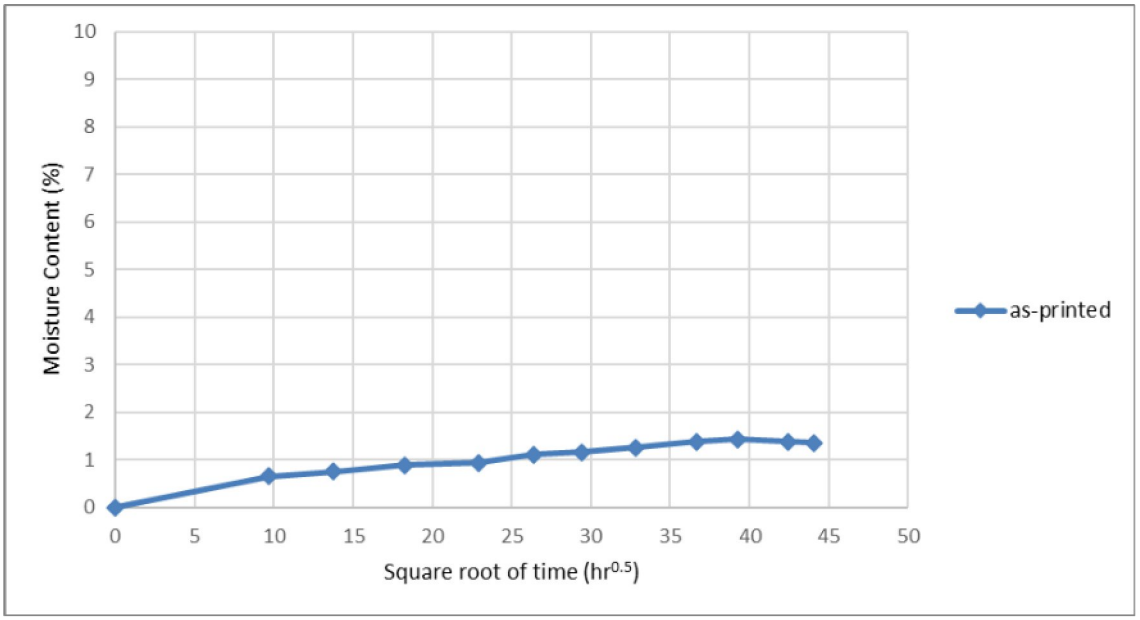

Figure 4.6: Sorption curve for CF/ABS set aligned in direction-1

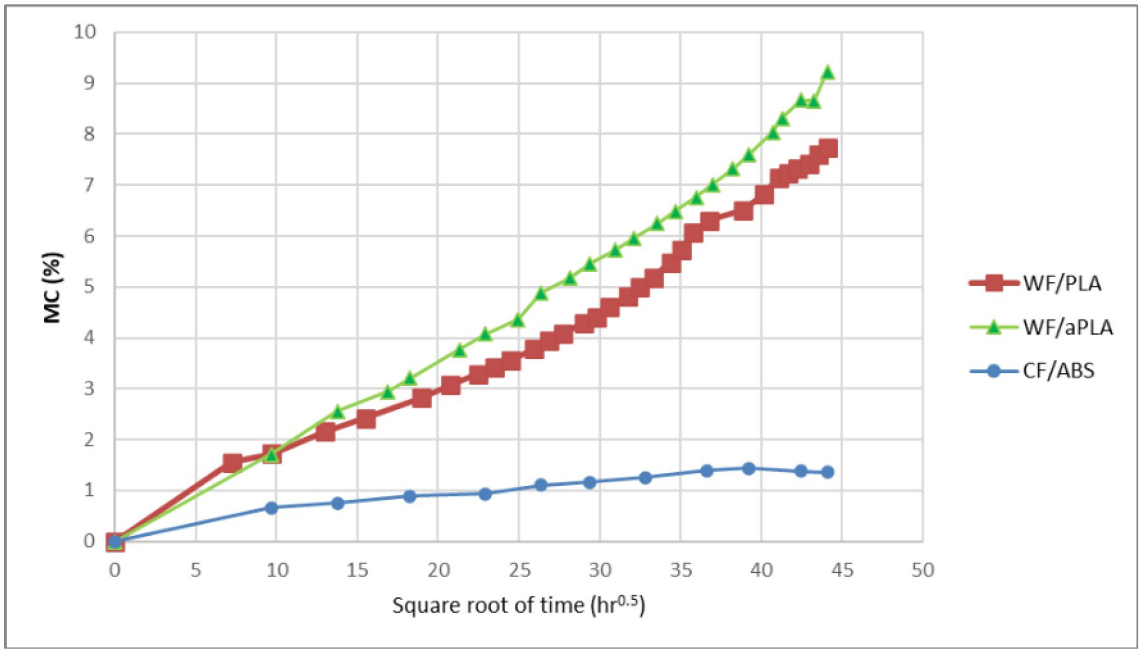

Figure 4.7: Sorption curves for WF/PLA, WF/aPLA, and CF/ABS as-printed sets aligned in direction-1

4.4 Coefficient of moisture expansion

According to [55, 56], the Coefficient of moisture expansion (CME) β is calculated using Equation (3).

$$\beta = \frac{\varepsilon_H}{M\ (\%)} \tag{3}$$

$$\varepsilon_H = \frac{\Delta l}{l_o} \tag{4}$$

Where:

ε_H	=	Moisture strain
Δl	=	Change in the dimension of width, height, or length, depending on the printing direction.
l_o	=	Initial dimension, width, height, or length depending on printing direction
β	=	Coefficient of moisture expansion for the composite material
$M\ (\%)$	=	Specimen moisture content in percentage

The coefficient of moisture expansion is only calculated for the bio-based materials (WF/PLA and WF/aPLA). For CF/ABS, moisture could not be measured accurately to obtain CME.

4.4.1 Coefficient of moisture expansion WF/PLA

This section presents the values of the coefficient of moisture expansion for the bio-based materials. Tables Table 4.10 to Table 4.12 show the values of the CME for WF/PLA sets aligned in direction-1, Table 4.13 show the values of the CME for WF/PLA set aligned in direction-3.

Table 4.10: Coefficient of moisture expansion for WF/PLA as printed with 1.5 in width, aligned in direction-1

Specimen	β_1	β_2	β_3
WF/PLA-LMP1.5 - 1	1.57E-03	2.61E-03	5.89E-03
WF/PLA-LMP1.5 - 2	1.67E-03	1.85E-03	5.79E-03
WF/PLA-LMP1.5 - 3	1.43E-03	2.28E-03	5.90E-03
WF/PLA-LMP1.5 - 4	1.54E-03	1.86E-03	5.69E-03
WF/PLA-LMP1.5 - 5	3.18E-03	9.94E-04	4.86E-03
WF/PLA-LMP1.5 - 6	2.33E-03	1.92E-03	4.87E-03
WF/PLA-LMP1.5 - 7	1.72E-03	1.57E-03	5.69E-03
WF/PLA-LMP1.5 - 8	3.20E-03	2.93E-03	5.50E-03
WF/PLA-LMP1.5 - 9	2.15E-03	2.05E-03	6.12E-03
WF/PLA-LMP1.5 - 10	2.39E-03	2.72E-03	5.38E-03
Average values	2.12E-03	2.08E-03	5.57E-03
CV (%)	31.07	27.87	7.64

Table 4.11: Coefficient of moisture expansion for WF/PLA as printed with 1.0 in width, aligned in direction-1

Specimen	β_1	β_2	β_3
WF/PLA-LMP1.0 - 1	5.86E-04	1.97E-03	5.18E-03
WF/PLA-LMP1.0 - 2	7.37E-04	1.97E-03	4.48E-03
WF/PLA-LMP1.0 - 3	7.04E-04	1.52E-03	4.88E-03
WF/PLA-LMP1.0 - 4	5.89E-04	6.33E-04	4.51E-03
WF/PLA-LMP1.0 - 5	5.35E-04	1.19E-03	5.24E-03
WF/PLA-LMP1.0 - 6	6.06E-04	2.19E-03	4.94E-03
Average values	6.26E-04	1.58E-03	4.87E-03
CV (%)	12.34	37.28	6.58

Table 4.12: Coefficient of moisture expansion for WF/PLA machined aligned in direction-1

Specimen	β_1	β_2	β_3
WF/PLA-LMF1.6 - 1	1.02E-03	2.32E-03	3.77E-03
WF/PLA-LMF1.6 - 2	1.12E-03	1.95E-03	3.97E-03
WF/PLA-LMF1.6 - 3	9.45E-04	1.87E-03	4.12E-03
WF/PLA-LMF1.6 - 4	1.00E-03	1.92E-03	3.38E-03
WF/PLA-LMF1.6 - 5	1.10E-03	2.01E-03	4.05E-03
WF/PLA-LMF1.6 - 6	1.08E-03	2.04E-03	3.21E-03
WF/PLA-LMF1.6 - 7	1.06E-03	2.61E-03	3.27E-03
WF/PLA-LMF1.6 - 8	1.13E-03	1.92E-03	4.02E-03
Average values	1.06E-03	2.08E-03	3.72E-03
CV (%)	6.07	12.25	10.20

Table 4.13: Coefficient of moisture expansion for WF/PLA as-printed aligned in direction-3

Specimen	β_1	β_2	β_3
WF/PLA-TMP1.0 - 1	1.02E-03	3.79E-03	2.41E-03
WF/PLA-TMP1.0 - 2	1.26E-03	2.98E-03	2.78E-03
WF/PLA-TMP1.0 - 3	1.55E-03	3.56E-03	2.72E-03
Average values	1.28E-03	3.44E-03	2.63E-03
CV (%)	20.93	12.12	7.49

4.4.2 Coefficient of moisture expansion WF/aPLA

Table 4.14 and Table 4.15 show the values of the CME for WF/aPLA sets aligned in direction-1.

Table 4.14: Coefficient of moisture expansion for WF/aPLA as-printed aligned in direction-1

Specimen	β_1	β_2	β_3
WF/aPLA-LMP1.5 - 1	1.70E-03	3.35E-03	5.39E-03
WF/aPLA-LMP1.5 - 2	1.81E-03	3.31E-03	5.57E-03
WF/aPLA-LMP1.5 - 3	1.70E-03	3.13E-03	6.24E-03
WF/aPLA-LMP1.5 - 4	1.65E-03	3.33E-03	5.43E-03
WF/aPLA-LMP1.5 - 5	1.93E-03	3.34E-03	5.24E-03
WF/aPLA-LMP1.5 - 6	2.18E-03	3.09E-03	5.62E-03
Average values	1.83E-03	3.26E-03	5.58E-03
CV (%)	10.86	3.58	6.23

Table 4.15: Coefficient of moisture expansion for WF/aPLA machined aligned in direction-1

Specimen	β_1	β_2	β_3
WF/aPLA-LMF1.6-1	1.61E-03	2.77E-03	9.12E-03
WF/aPLA-LMF1.6-2	1.59E-03	2.78E-03	1.00E-02
WF/aPLA-LMF1.6-3	1.71E-03	2.86E-03	9.86E-03
WF/aPLA-LMF1.6-4	1.25E-03	3.37E-03	9.22E-03
WF/aPLA-LMF1.6-5	1.99E-03	2.99E-03	1.08E-02
WF/aPLA-LMF1.6-6	1.61E-03	2.45E-03	1.00E-02
Average values	1.63E-03	2.87E-03	9.84E-03
CV (%)	14.59	10.56	6.29

4.5 Data Analysis Coefficient of Moisture Expansion

The purpose of the analysis is to determine if there is any difference in the coefficient of moisture expansion for WF/PLA sets, specifically what is compared is: coefficients within sets, and coefficients of sets with different width, surface finishing, and direction in which they are aligned.

For WF/aPLA what is compared is: coefficients within sets and coefficients of sets with different surface finishing. In addition coefficients of moisture expansion between materials compared for WF/PLA and WF/aPLA for as-printed and machined specimens.

ANOVA t-test considering a p-value < 0.05 as statistically significant, was used to compare the CME of the different sets. The p-values for WF/PLA the results are shown in TablesTable 4.10: Coefficient of moisture expansion for WF/PLA as printed with 1.5 in width, aligned in direction-

1to Table 4.21, for WF/aPLA the results are shown in Tables Table 4.22 toTable 4.24, and p-values between WF/PLA and WF/aPLA are shown in Tables Table 4.25 and Table 4.26

4.5.1 Data analysis of coefficient of moisture expansion for WF/PLA

Table 4.16 shows the p-value for WF/PLA as printed sets of 1.0 in and 1.5 in width aligned in direction-1; it can be de derived from this table that:

- For both sets, 1.0 in and 1.5 in width, the CME is different for the three directions analyzed.
- The set of 1.5 in width, contrary to the set of 1.0, presents an in-plane isotropy since the difference between β_1 vs. β_2 is not statistically significant.

Table 4.16: Data analysis for the coefficient of moisture expansion for WF/PLA as-printed sets aligned in direction-1.

Sets compared	**p-value**
as-printed 1.0 in width - 3 directions	**1.76E-11**
as-printed 1.0 in width β_1 vs. β_2	**0.010**
as-printed 1.0 in width β_1 vs. β_3	**1.68E-07**
as-printed 1.0 in width β_2 vs. β_3	0.097
as-printed 1.5 in width - 3 directions	**1.87E-14**
as-printed 1.5 in width β_1 vs. β_2	0.896
as-printed 1.5 in width β_1 vs. β_3	**3.80E-10**
as-printed 1.5 in width β_2 vs. β_3	**3.36E-11**

Table 4.17 shows the p-values for the coefficient of moisture expansion between WF/PLA as-printed of 1.0 in and 1.5 width sets aligned in direction-1.

4.5.1.1 Data analysis between WF/PLA specimens with a width of 1.0 and 1.5 in aligned in direction-1

From Table 4.17, it can be observed that the CME for direction-2 is the same, but for directions 1 and 3, the difference is statistically significant, which means that the CME is not the same for specimens with different widths.

Table 4.17: Data analysis for the coefficient of moisture expansion between WF/PLA as-printed of 1.0 in and 1.5 width sets aligned in direction-1.

Sets compared	p-value
β_1	**4.59E-05**
β_2	0.128
β_3	**2.68E-03**

4.5.1.2 Data analysis for WF/PLA machined specimens aligned in direction-1

Table 4.18 shows that when comparing the CME for all directions and between directions, the difference is statistically significant, meaning that machined specimens have different CME for each direction.

Table 4.18: Data analysis for the coefficient of moisture expansion for WF/PLA machined set aligned in direction-1.

Sets compared	p-value
machined - 3 directions	**3.59E-12**
machined β_1 vs β_2	**4.60E-06**
machined β_1 vs β_3	**1.21E-07**
machined β_2 vs β_3	**2.56E-07**

4.5.1.3 Data analysis between WF/PLA machined and as-printed specimens aligned in direction-1

From Table 4.19, it can be shown that machined and as-printed specimens only have the same coefficient for direction-2. For directions-1 and 3, the difference is statistically significant. Meaning that the CME is different if the specimen is as-printed or machined.

Table 4.19: Data analysis for the coefficient of moisture expansion for WF/PLA machined and as-printed sets aligned in direction -1.

Sets compared	p-value
β_1	**6.30E-04**
β_2	0.991
β_3	**4.75E-08**

4.5.1.4 Data analysis for WF/PLA as-printed specimens aligned in direction-3

Table 4.20 shows that as-printed specimens aligned in direction-3 the CME is different for each direction, except between direction-2 and 3.

Table 4.20: Data analysis for the coefficient of moisture expansion for WF/PLA as-printed set aligned in direction-3.

Sets compared	p-value
as-printed - 3 directions	**3.92E-04**
as-printed β_1 vs. β_2	**3.03E-03**
as-printed β_1 vs. β_3	**2.83E-03**
as-printed β_2 vs. β_3	0.060

4.5.1.5 Data analysis between WF/PLA as-printed specimens aligned in direction-1 and 3

Table 4.21 shows that when comparing the CME for all directions, the difference is statistically significant. This means the CME is different when the specimens are aligned in directions 1 and 3.

Table 4.21: Data analysis for the coefficient of moisture expansion between WF/PLA as-printed sets aligned in directions 1 and 3

Sets compared	p-value
β_1	**9.76E-03**
β_2	**7.62E-03**
β_3	**1.72E-07**

4.5.2 Data analysis of coefficient of moisture expansion for WF/aPLA

4.5.2.1 Data analysis for WF/aPLA as-printed specimens aligned in direction-1

Table 4.22 shows that when comparing the CME for all directions and between directions, the difference is statistically significant, meaning that WF/aPLA as-printed specimens have different CME for each direction.

Table 4.22: Data analysis for the coefficient of moisture expansion for WF/aPLA as-printed set aligned in direction-1.

Sets compared	p-value
as-printed – 3 directions	**9.95E-11**
as-printed β_1 vs. β_2	**3.25E-07**
as-printed β_1 vs. β_3	**1.51E-08**
as-printed β_2 vs. β_3	**3.88E-06**

4.5.2.2 Data analysis for WF/aPLA machined specimens aligned in direction-1

Table 4.23 shows that when comparing the CME for all directions and between directions, the difference is statistically significant, meaning that WF/aPLA machined specimens have different CME for each direction.

Table 4.23: Data analysis for the coefficient of moisture expansion for WF/aPLA machined set aligned in direction-1.

Sets compared	p-value
machined - 3 directions	**9.23E-13**
machined β_1 vs. β_2	**1.80E-05**
machined β_1 vs. β_3	**3.41E-08**
machined β_2 vs. β_3	**2.73E-08**

4.5.2.3 Data analysis between WF/aPLA machined and as-printed specimens aligned in direction-1

From Table 4.24, it can be derived that machined and as-printed specimens only have the same coefficient for direction-1. For directions 2 and 3, the difference is statistically significant. Meaning that the CME is different if the specimen is as-printed or machined.

Table 4.24: Data analysis for the coefficient of moisture expansion between WF/aPLA as-printed and machined set aligned in direction-1.

Sets compared	**p-value**
as-printed vs. machined β_1	0.136
as-printed vs. machined β_2	**2.46E-02**
as-printed vs. machined β_3	**5.31E-07**

4.5.3 Data analysis of coefficient of moisture expasion between materials

4.5.3.1 Data analysis between WF/PLA and WF/aPLA as-printed sets aligned in direction-1

From Table 4.25, when comparing the CME for as-printed specimens of WF/PLA and WF/aPLA, two out of three of the coefficients have no significant difference, with only the CME in direction-2 now being the same.

Table 4.25: Data analysis for the coefficient of moisture expansion between WF/PLA and WF/aPLA as-printed sets aligned in direction-1.

Sets compared	p-value
as-printed β_1	0.227
as-printed β_2	**9.16E-05**
as-printed β_3	0.939

4.5.3.2 Data analysis between WF/PLA and WF/aPLA machined sets aligned in direction-1

From Table 4.26, the CME is different for all directions when comparing the CME for machined specimens of WF/PLA and WF/aPLA.

Table 4.26: Data analysis for the coefficient of moisture expansion between WF/PLA and WF/aPLA machined sets aligned in direction-1.

Sets compared	p-value
machined β_1	**1.62E-03**
machined β_2	**4.67E-04**
machined β_3	**3.43E-08**

4.5.4 Discussion of results for the coefficient of moisture expansion

The values obtained for the coefficient of moisture expansion were not the same when comparing specimens with different width and as-printed and machined. Further investigation is needed to set testing parameters so the CME is not dependent on the width and surface finishing of the materials.

Values from as-printed specimens with a width of 1.5 in aligned in direction-1 were selected for WF/PLA and WF/aPLA since the values are more conservative and these types of specimens are more representative of printed parts.

4.6 Flexure test results for sets under moisture absorption

The following sections provide the results for WF/aPLA and CF/ABS flexural properties under moisture absorption.

4.6.1 Flexure test results for WF/aPLA sets under moisture absorption

Table 4.27 shows the flexural strength and flexural modulus of WF/aPLA sets subjected to moisture absorption aligned in direction-1.

Table 4.27: Flexural material properties for WF/aPLA sets under moisture absorption aligned in direction-1

WF/aPLA d-1 Specimen Set	**Flexural Results**	
	Strength ($F1_f$) MPa *(SpecQty/CV)*	**Modulus ($E1_f$)** GPa *(SpecQty/CV)*
WF/aPLA-LMP1.5 *(as-printed)*	19.4 *(6/4.6%)*	2.34 *(6/15%)*
WF/aPLA-LMF1.6 *(machined)*	36.8 *(6/9.9%)*	2.86 *(6/3.4%)*

Figure 4.8 and Figure 4.9 show the stress versus strain plots for WF/aPLA-LMP1.5, WF/aPLA-LMF1.6 specimen sets, respectively.

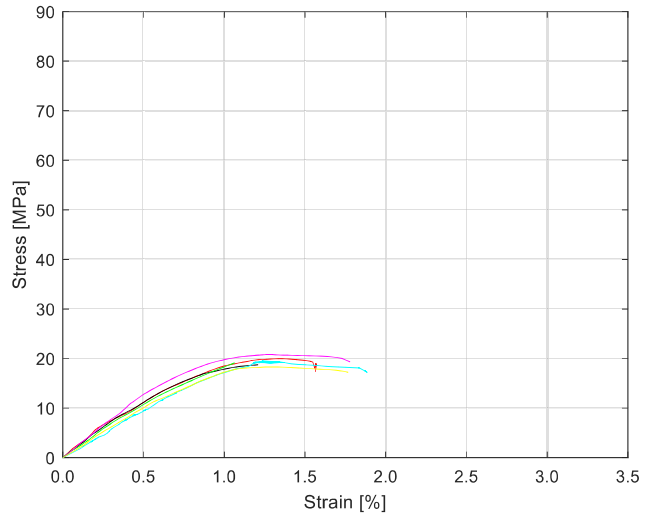

Figure 4.8: Stress versus strain curve for WF/aPLA-LMP1.5 aligned in direction-1.

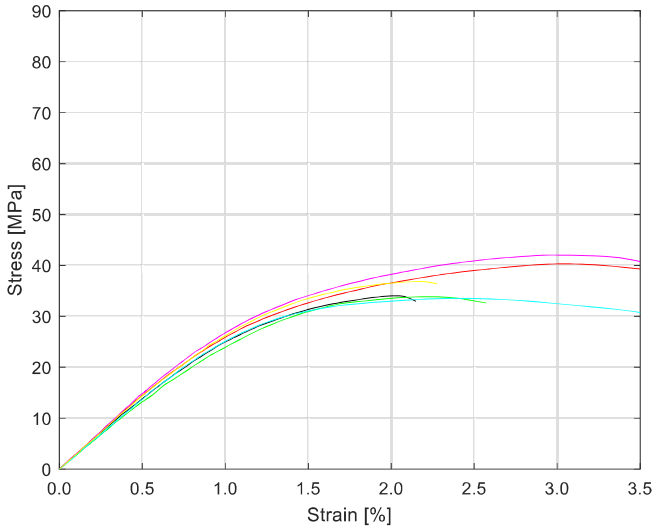

Figure 4.9: Stress versus strain curve for WF/aPLA-LMF1.6 aligned in direction-1.

4.6.2 Flexure test results for CF/ABS sets under moisture absorption

Table 4.28: Flexural material properties for CF/ABS sets under moisture absorption aligned in direction-1 shows the flexural strength and flexural modulus of CF/ABS set subjected to moisture absorption aligned in direction-1.

Table 4.28: Flexural material properties for CF/ABS sets under moisture absorption aligned in direction-1

CF/ABS d-1 Specimen Set	Flexural Results	
	Strength ($F1_f$) MPa *(SpecQty/CV)*	**Modulus ($E1_f$)** GPa *(SpecQty/CV)*
CF/ABS-LMP1.5 *(as-printed)*	42.12 *(6/8.9%)*	5.74 *(6/12%)*

Figure 4.10: Stress versus strain curve for CF/ABS as printed under moisture absorption, aligned in direction-1. show the stress versus strain plots for CF/ABS specimen set.

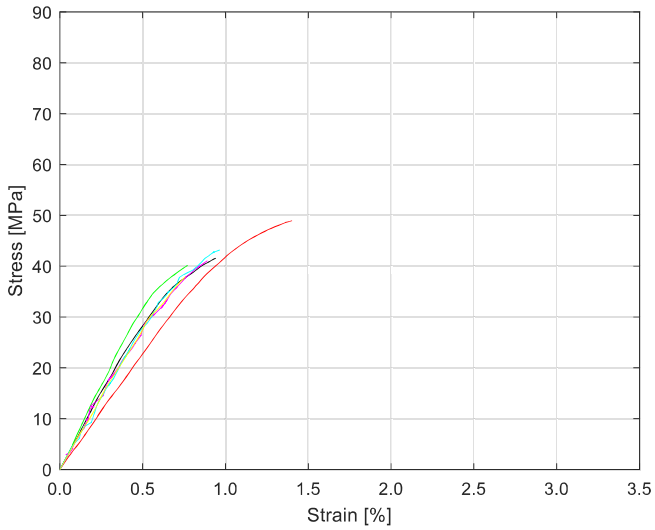

Figure 4.10: Stress versus strain curve for CF/ABS as printed under moisture absorption, aligned in direction-1.

4.6.3 Data Analysis for sets under moisture absorption

The purpose of the analysis is to determine if there is any difference in the flexural material properties of WF/aPLA and CF/ABS subjected to moisture absorption.

ANOVA t-test considering a p-value < 0.05 as statistically significant, was used to compare the flexural strength and modulus between baseline sets and those under moisture absorption. Table 4.29: Results comparison of moisture absorption to baseline for WF/aPLA aligned in direction-1 and Table 4.30 show the p-values obtained for WF/aPLA CF/ABS respectively.

Table 4.29: Results comparison of moisture absorption to baseline for WF/aPLA aligned in direction-1

	Baseline MPa *(SpecQty/CV)*	**Moisture** GPa *(SpecQty/CV)*	**Reduction** %	**p-value**
	Flexural Strength Results ($F1_f$)			
WF/aPLA-LP1.5	73.2 *(10/6.8%)*	19.4 *(6/4.7%)*	73	**1.57E-13**
WF/aPLA-LP1.6	73.6 *(8/6.0%)*	36.8 *(6/9.9%)*	50	**5.92E-10**
	Flexural Modulus Results ($E1_f$)			
WF/aPLA-LP1.5	4.59 *(10/4.6%)*	2.34 *(6/15%)*	49	**8.57E-11**
WF/aPLA-LP1.6	4.99 *(8/7.4%)*	2.86 *(6/3.4%)*	43	**5.22E-09**

The results indicate:

- Moisture absorption will impact WF/aPLA, affecting flexural strength and modulus.
- For WF/aPLA as a printed set, the difference with the baseline set is statistically significant, with a reduction of 73% for flexural strength and a 49% reduction for flexural modulus of elasticity.
- For WF/aPLA machined set, the difference with the baseline set is statistically significant, with a reduction of 50% for flexural strength and a 43% reduction for flexural modulus of elasticity.

Table 4.30: Results comparison of moisture absorption to baseline for CF/ABS aligned in direction-1

	Baseline MPa *(SpecQty/CV)*	**Moisture** GPa *(SpecQty/CV)*	**Reduction** %	**p-value**
	Flexural Strength Results ($F1_f$)			
CF/ABS-LP1.5	82.5 *(10/11%)*	42.1 *(6/8.9%)*	49	**4.28E-08**
	Flexural Modulus Results ($E1_f$)			
CF/ABS-LP1.5	6.95 *(10/15%)*	5.74 *(6/12%)*	18	**0.011**

- Moisture absorption will impact CF/ABS, affecting flexural strength and modulus.
- For CF/ABS as a printed set, the difference with the baseline set is statistically significant, with a reduction of 49% for flexural strength and an 18% reduction for flexural modulus of elasticity.

4.7 Conclusions

CF/ABS is the material that has the lowest moisture content compared to WF/PLA and WF/aPLA. When comparing as-printed sets, CF/ABS has an average moisture content of 1.35%, versus WF/PLA and WF/aPLA, with an average moisture content of 7.74% and 9.23%, respectively.

In the case of WF/PLA, width, directions, and surface finishing impact the moisture content. When comparing machined samples with as-printed, machined specimens had a 10% higher moisture content. It is essential to mention that this experiment was conducted for 81 days.
In the case of WF/aPLA, specimen surface finishing impacts the moisture content. Contrary to WF/PLA, when comparing as-printed specimens with machined specimens, as-printed samples had a 24% higher moisture content.

For the coefficient of moisture expansion, WF/PLA as-printed specimens are transversally isotropic, while machined ones are not. If both types of sets are compared, only direction two can be considered to have the same CME. The CME for WF/PLA also depends on the direction in which the specimens were aligned with specimens aligned in directions 1 and 3 is different.

WF/aPLA, as-printed and machined, are not transversally isotropic, showing a CME for each direction to be different if both types of sets are compared, only direction-1 can be considered to have the same CME.

When WF/PLA and WF/aPLA sets are compared, if both are as-printed, only the CME for direction-2 is not the same. In the case of machined specimens, the CME is different for all directions.

Moisture absorption has a negative impact on the flexural properties of large-scale 3D printed materials. From the flexural test, as-printed sets of WF/aPLA have a decrease of 73% in flexural strength and a decrease of 49% in its flexural modulus. In the case of machined specimens, the decrease is 50% and 43%, respectively. As-printed CF/ABS set has a decrease of 49% in its flexural strength and a reduction of 18% in its flexural modulus.

CHAPTER 5

FREEZE-THAW CYCLING

5.1 Introduction

The following chapter presents the results and findings from freeze-thaw cycling. Flexure tests for specimens under this environmental conditioning were conducted for WF/PLA, WF/aPLA, and CF/ABS.

5.2 Literature review for freeze-thaw cycling

Friedrich et al. [59] made a recompilation of studies on wood plastic composite materials under freeze-thaw cycling. Table 5.1 shows the findings from these studies, different authors, methods used, and quantification of impact on mechanical properties.

Table 5.1: Freeze-thaw conditionings from literature for WPCs [59]

References	Formulation (%)	Production Method	Condition Method
Adhikary et al.,	50-Pine 50-Plastics	Injection-molded	Cycles: Water soaking until equilibrium; 1 d freezing; 1 d thawing. In total, twelve cycles.
Pilarski/Matuana	25/38/50-Wood 72/62/50-PVC Incl.5-Additives	Extruded	Cycles: Water soaking until equilibrium; 1 d freezing; 1 d thawing. In total, twelve cycles.

Table 5.1 continued

Wang et al.,	50-Rice Hull 50-PE (*PE)*	Extruded	Cycles: Water soaking for 2.5 d; 1 freezing; 1 d thawing. In total, six cycles.
Tamakar/Lopez	46-Pine 54-PP incl. 13-Additives	Extruded	Cycles: Water soaking for 20 d; 1 freezing; 1 d thawing. In total, four cycles.

Table 5.3 and Table 5.4 show the results from the literature obtained in decrease in modulus of rupture (MOR) and Young's modulus (MOE).

Table 5.2: Freeze-thaw conditionings from literature for WPCs – Changes in mechanical properties [59]

Reference	**days**	**MOR baseline (MPa)**	**MOR, weathered (MPa)**	**MOR Decrease (%)**	**MOE, Baseline (GPa)**	**MOE, weathered (GPa)**	**MOE Decrease (%)**
Adhikary et al.,	12	14.4-39.6	10.1-32.3	9.00-29.9	1.34-2.34	0.81-1.36	16.4-66.5
Pilarski/Matuana	12	36.6-46.4	26.8-43.7	2.2-15.2	2.04-3.38	1.68-2.63	10.0-29.8
Wang et al.,	6	13.6	12.9	5.5	1610	940	41.6
Tamrakar/Lopez-Anido	4	22.5	21.4	8.0	3700	2000	46.0

Table 5.3: Additional literature review for freeze-thaw cycling of WPCs

References	Material	Methods	MOR/MOE Loses	Comments
Pilarski and Matuana [60]	WPC with HDPE	15 cycles of water submersion, freezing, and thawing.	49% (MOE) and 21% (MOR), 37% (MOE) and 5% (MOR).	50% wood flour, loses were significant compared to control samples and use 15 instead of 5 cycles.
Turku et al. [61]	WPC composites extruded from recycled plastic.	3 cycles of water immersion, freezing, and thawing.	Flexural properties 2-26%, Modulus 2-30%.	Wood flour content is not specified, the Swell of wood particles leads to stresses in the matrix and microcracking
Pilarski and Matuana [62]	WPC with rigid PVC Matrix.	5 Cycles of water submersion, freezing, and thawing.	3.5% for flexural strength.	46% wood flour content and losses were less than 25% compared to previous studies.

In the case of carbon fiber reinforced polymers, Mohamed et al. [63] found that tensile testing on ABS reveals a clear difference between the performance of FDM materials with exposure to freeze-thaw conditions. Tensile strength and strain-at-peak load are substantially reduced from the baseline with freeze-thaw exposures, independent of the angle at which the coupons were tested.

Table 5.4: Freeze-thaw cycling results from the literature for ABS

References	Material	Methods	MOR/MOE Loses	Comments
Mohamed et al.	ABS	300 cycles, minimum 14 days at 22°C and 50% relative humidity	0° samples decrease by 24% in strength and 90° and 45° decrease of 19.5% and 20.1%	All samples were immersed in a 5% saline solution during freeze-thaw cycling.

5.3 flexure test results for specimens under freeze-thaw cycling

The following sections provide the results for flexural properties for WF/PLA, WF/aPLA, and CF/ABS under freeze-thaw cycling.

5.3.1 Flexure test results for freeze-thaw cycling on WF/PLA sets

Table 5.5 shows the flexural strength and flexural modulus of WF/PLA sets subjected to freeze-thaw cycling aligned in direction-1.

Table 5.5: Flexural material properties for WF/PLA freeze-thaw cycling sets aligned in direction-1

WF/PLA d-1 Specimen Set	**Flexural Results**	
	Strength ($F1_f$) MPa *(SpecQty/CV)*	**Modulus ($E1_f$)** GPa *(SpecQty/CV)*
WF/PLA-LFP1.5 *(as-printed)*	64.1 *(7/3.8%)*	3.64 *(7/9.7%)*
WF/PLA-LFP1.0 *(as-printed)*	55.4 *(1)*	3.75 *(6/6.2%)*
WF/PLA-LFF1.6 *(machined)*	68.6 *(5/7.1%)*	2.83 *(5/14%)*

Table 5.6 shows the flexural strength and flexural modulus of WF/PLA sets subjected to freeze-thaw cycling aligned in direction-3.

Table 5.6: Flexural material properties for WF/PLA freeze-thaw cycling sets aligned in direction-3

WF/PLA d-3 Specimen Set	**Flexural Results**	
	Strength ($F3_f$) MPa *(SpecQty)*	**Modulus ($E3_f$)** GPa *(SpecQty)*
WF/PLA-TFP1.5 *(as-printed)*	27.2 *(3)*	3.23 *(3)*

Figure 5.1 to Figure 5.4 show the stress versus strain plots for WF/PLA-LFP1.5, WF/PLA-LFP1.0, WF/PLA-LFF1.6, and WF/PLA-TFP1.0 specimen sets, respectively.

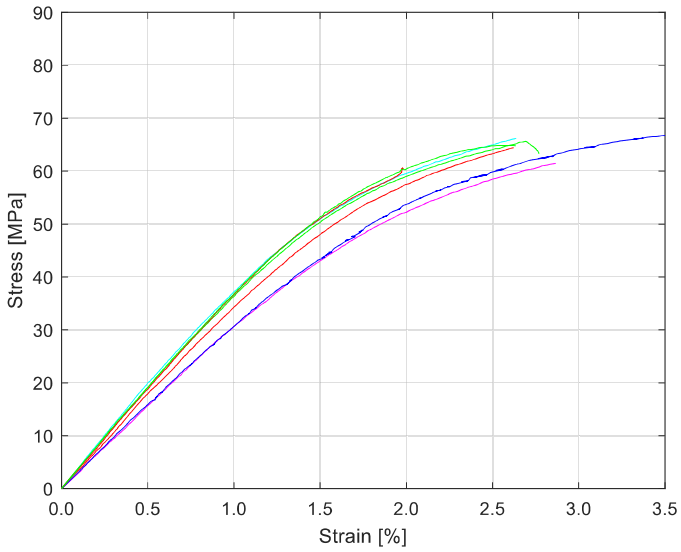

Figure 5.1: Stress versus strain curves for WF/PLA-LFP1.5 aligned in direction-1.

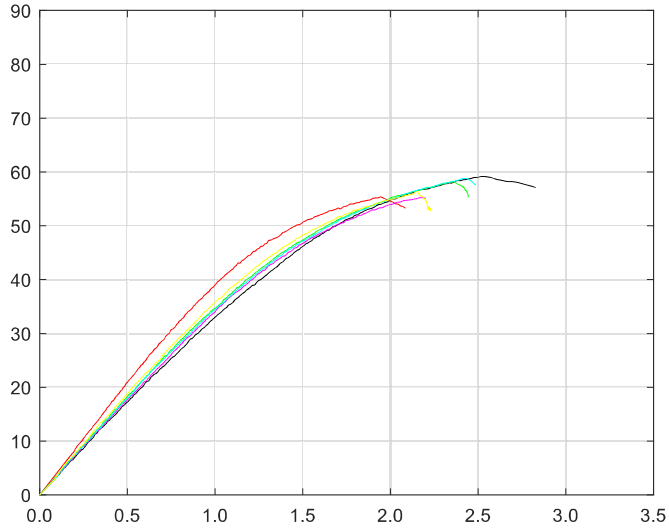

Figure 5.2: Stress versus strain curves for WF/PLA-LFP1.0 aligned in direction-1.

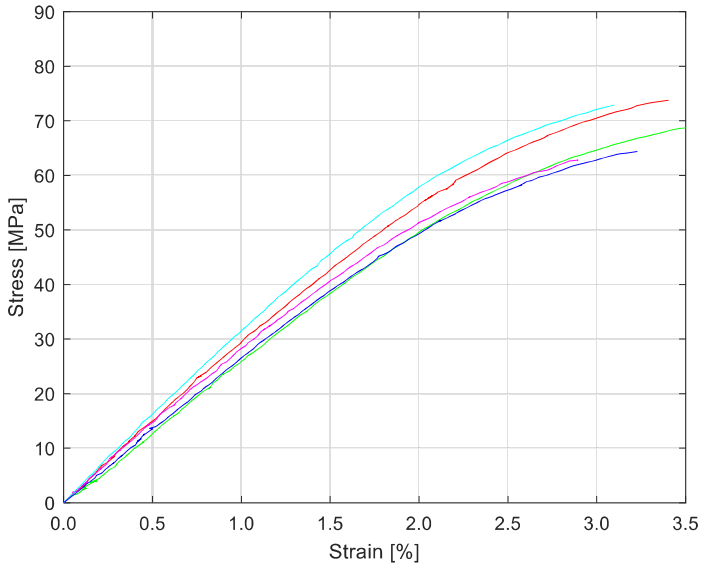

Figure 5.3: Stress versus strain curveS for WF/PLA-LFF1.6 aligned in direction-1.

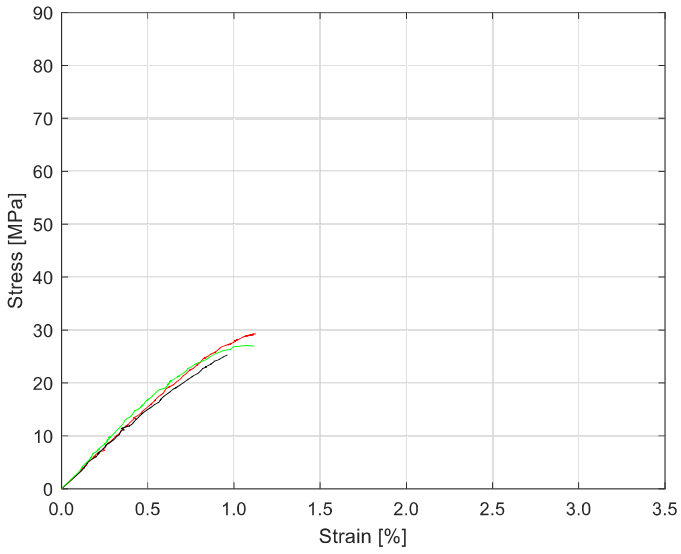

Figure 5.4: Stress versus strain curves for WF/PLA-TFP1.0 aligned in direction-3.

5.3.2 Flexure test results for freeze-thaw cycling on WF/aPLA sets

Table 5.7 shows the flexural strength and flexural modulus of WF/aPLA sets subjected to freeze-thaw cycling aligned in direction-1.

Table 5.7: Flexural material properties for WF/aPLA freeze-thaw cycling sets aligned in direction-1

WF/aPLA d-1 Specimen Set	**Flexural Results**	
	Strength ($F1_f$) MPa *(SpecQty/CV)*	**Modulus ($E1_f$)** GPa *(SpecQty/CV)*
WF/aPLA-LFP1.5 *(as-printed)*	71.9 *(10/4.3%)*	4.33 *(10/4.9%)*
WF/aPLA-LFF1.6 *(machined)*	83.4 *(4/8.9%)*	5.09 *(4/4.2%)*

Figure 5.5 and Figure 5.6 show the stress versus strain plots for WF/aPLA-LFP1.5 and WF/PLA-LFF1.6 specimen sets respectively.

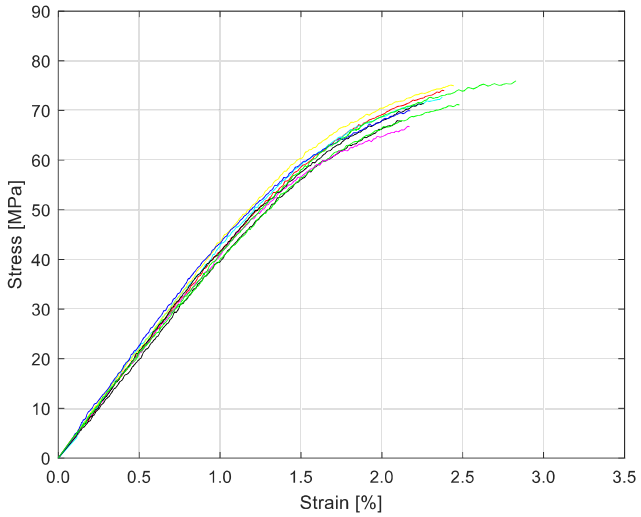

Figure 5.5: Stress versus strain curves for WF/aPLA-LFP1.5 aligned in direction-1.

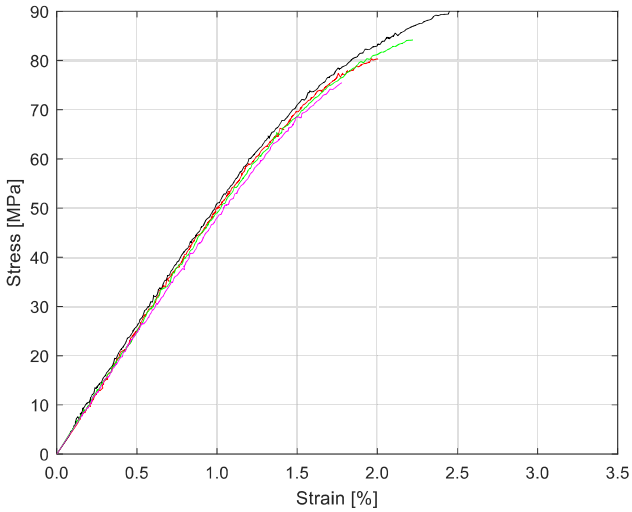

Figure 5.6: Stress versus strain curves for WF/aPLA-LFF1.6 aligned in direction-1.

5.3.3 Flexure test results for freeze-thaw cycling on CF/ABS sets

Table 5.8: Flexural material properties for CF/ABS freeze-thaw cycling sets aligned in direction-1 shows the flexural strength and flexural modulus of CF/ABS sets subjected to freeze-thaw cycling aligned in direction-1.

Table 5.8: Flexural material properties for CF/ABS freeze-thaw cycling sets aligned in direction-1

CF/ABS d-1 Specimen Set	**Flexural Results**	
	Strength ($F1_f$) MPa *(SpecQty/CV)*	**Modulus ($E1_f$)** GPa *(SpecQty/CV)*
CF/ABS-LFP1.5 *(as-printed)*	83.9 *(6/9.4%)*	6.83 *(6/16%)*

Figure 5.7 shows the stress versus strain plots for CF/ABS-LFP1.5 specimen set.

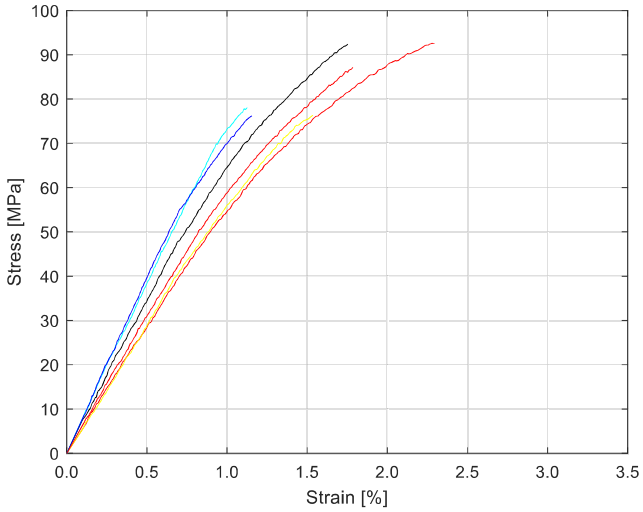

Figure 5.7: Stress versus strain curves for CF/ABS-LFP1.5 aligned in direction-1.

5.3.4 Data analysis for freeze-thaw cycling sets

ANOVA t-test considering a p-value < 0.05 as statistically significant, was used to compare the flexural strength and flexural modulus between baseline sets and those under freeze-thaw cycling. The p-values for WF/PLA are shown in Tables Table 5.9 and Table 5.10, for WF/aPLA in Table 5.11, and for CF/ABS Table 5.12.

Table 5.9: Data Analysis for WF/PLA aligned in direction-1 set under freeze-thaw cycling

	Baseline MPa *(SpecQty/CV)*	**Freeze-thaw** GPa *(SpecQty/CV)*	**Reduction** %	**p-value**
	Flexural Strength Results ($F1_f$)			
WF/PLA-LP1.5	64.5 *(8/4.3%)*	64.1 *(7/3.8%)*	<1	0.40
WF/PLA-LP1.0	64.4 *(3)*	55.4 *(1)*	-	-
WF/PLA-LP1.6	77.2 *(6/8.1%)*	68.6 *(5/7.1%)*	11	**0.017**
	Flexural Modulus Results ($E1_f$)			
WF/PLA-LP1.5	4.2 *(10/8%)*	3.64 *(7/9.7%)*	14	**1.49E-03**
WF/PLA-LP1.0	4.27 *(4)*	3.75 *(6/6.2%)*	12	**0.013**
WF/PLA-LP1.6	5.15 *(6/7.2%)*	2.83 *(5/14%)*	45	**1.89E-06**

Table 5.10: Data Analysis for WF/PLA aligned in direction-3 sets under freeze-thaw cycling

	Baseline MPa *(SpecQty)*	**Freeze-thaw** GPa *(SpecQty)*	**Reduction** %	**p-value**
	Flexural Strength Results ($F1_f$)			
WF/PLA-TP1.0	26.9 *(10)*	27.2 *(6)*	-	0.42
	Flexural Modulus Results ($E1_f$)			
WF/PLA-TP1.0	3.30 *(10)*	3.23 *(6)*	2	0.41

Table 5.11: Data Analysis for WF/aPLA aligned in direction-1 set under freeze-thaw cycling

	Baseline MPa *(SpecQty/CV)*	**Freeze-thaw** GPa *(SpecQty/CV)*	**Reduction** %	**p-value**
	Flexural Strength Results ($F1_f$)			
WF/aPLA-LP1.5	73.2 *(10/6.8%)*	71.9 *(10/4.3%)*	2	0.25
WF/aPLA-LP1.6	73.6 *(8/6.0%)*	83.4 *(4/8.9%)*	-	**7.79E-03**
	Flexural Modulus Results ($E1_f$)			
WF/aPLA-LP1.5	4.59 *(10/4.6%)*	4.33 *(10/4.9%)*	6	**0.007**
WF/aPLA-LP1.6	4.99 *(8/7.4%)*	5.09 *(4/4.2%)*	-	0.33

Table 5.12: Data Analysis for CF/ABS aligned in direction-1 set under freeze-thaw cycling

	Baseline MPa *(SpecQty/CV)*	**Freeze-thaw** GPa *(SpecQty/CV)*	**Reduction** %	**p-value**
	Flexural Strength Results ($F1_f$)			
CF/ABS-LP1.5	82.5 *(10/11%)*	83.9 *(6/9.4%)*	-	0.106
	Flexural Modulus Results ($E1_f$)			
CF/ABS-LP1.5	6.95 *(10/15%)*	6.83 *(6/16%)*	2	0.336

The results indicate:

- Freeze-thaw cycling decreases the flexural strength and modulus of WF/PLA material aligned in direction-1 for flexural strength and modulus. It does not affect the material aligned in direction-3.
- Freeze-thaw cycling does not affect flexural strength of WF/aPLA, but it does affect flexural modulus.
- Freeze-thaw cycling does not affect flexural strength and modulus of CF/ABS.

- For WF/PLA as-printed sets with 1.5 and 1.0 in width aligned in direction-1, the difference with baseline specimens is statistically significant, with a reduction of 14% and 12%, respectively, for the flexural modulus of elasticity.
- For WF/PLA machined set aligned in direction-1, the difference with the baseline set is statistically significant, with a reduction of 11% for flexural strength and a 45% reduction for flexural modulus of elasticity.

5.4 Conclusions

Freeze-thaw cycling has a negative impact on the flexural properties of large-scale 3D printed materials made of WF/PLA aligned in direction-1. It did not affect the material when it is aligned in direction-3. For as-printed specimens, there is a 14% and 12% reduction in the flexural modulus for samples with 1.0 in and 1.5 in width, respectively. If the sets are machined, there is a reduction of 11% for flexural strength and a 45% reduction for flexural modulus of elasticity. Freeze-thaw cycling did not affect the flexural properties of materials made of WF/aPLA and CF/ABS.

For WF/aPLA, freeze-thaw cycling affects the flexural modulus, with a reduction of 6%. CF/ABS is not affected by three cycles, this material should be subjected to more freeze-thaw cycles.

CHAPTER 6

SIMULATED WEATHERING BASED ON UV AND CONDENSATIONS CYCLES

6.1 Introduction

The following chapter presents the results for simulated weathering based on UV and condensation cycles for CF/ABS specimens.

6.2 Environmental conditioning results

The following section presents the results obtained from measurements of surface roughness and contact angle in machined specimens and observations on as-printed specimens. The comparison was between baseline and exposed specimens and between exposure hours.

6.2.1 Surface roughness machined specimens

Due to the dimension of the specimens, surface roughness was only measured perpendicular to the beads, as shown in Figure 6.1: Motion of the device and beads direction considered for CF/ABS specimens.. The device couldn't be placed to measure surface roughness parallel to the beads.

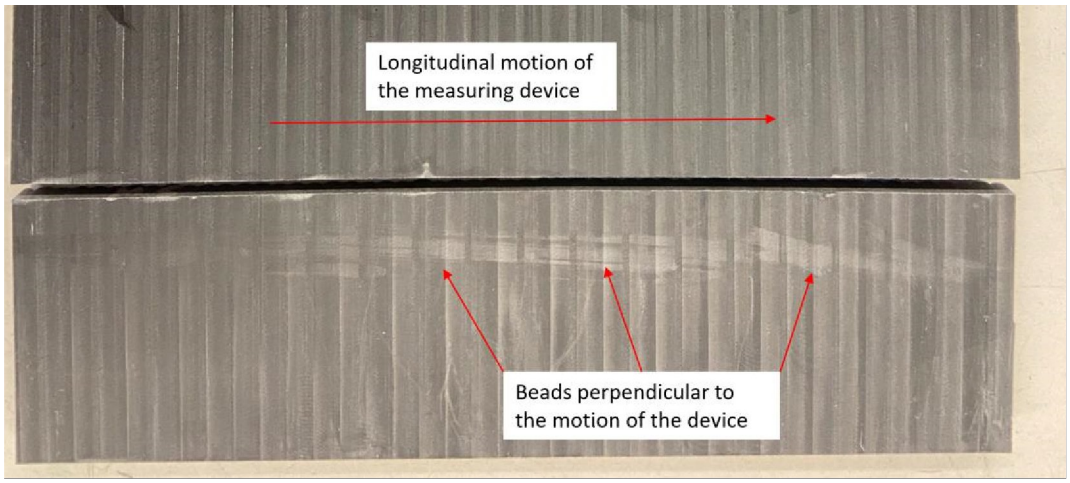

Figure 6.1: Motion of the device and beads direction considered for CF/ABS specimens.

Table 6.1 shows the surface roughness for baseline specimens at each exposure time. The increase in surface roughness is illustrated in Figure 6.2.

Table 6.1: Surface Roughness for CF/ABS machined specimens

Specimen	**Surface Roughness 0 h of exposure**	**Surface Roughness 500 h of exposure**	**Surface Roughness 957 h of exposure**	**Surface Roughness 2000 h of exposure**
Average (μm)	0.92	1.93	2.78	3.61
Standard deviation (μm)	0.14	0.15	0.11	0.07
CV (%)	15.69	7.72	3.85	1.98

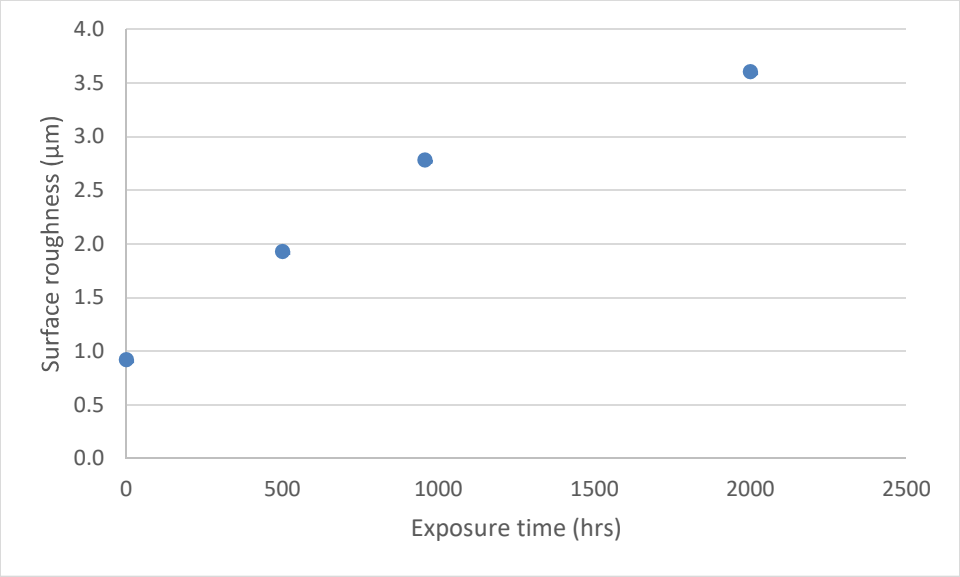

Figure 6.2: Surface Roughness for machines specimens at different exposures times

After each exposure, the material presented discoloration. It can be attributed to the ABS part of the composite material. Davis et al. [64] studied the influence of UV exposure on ABS chemical properties and microstructure. It was observed as yellow-brown discoloration after a simulated weather time of two weeks. The discoloration was localized at the specimen surface, with fading and slight yellowing. This is shown in Figure 6.3 for 500 h exposure, Figure 6.4 for 957 h exposure, and Figure 6.5 for 2000 h exposure.

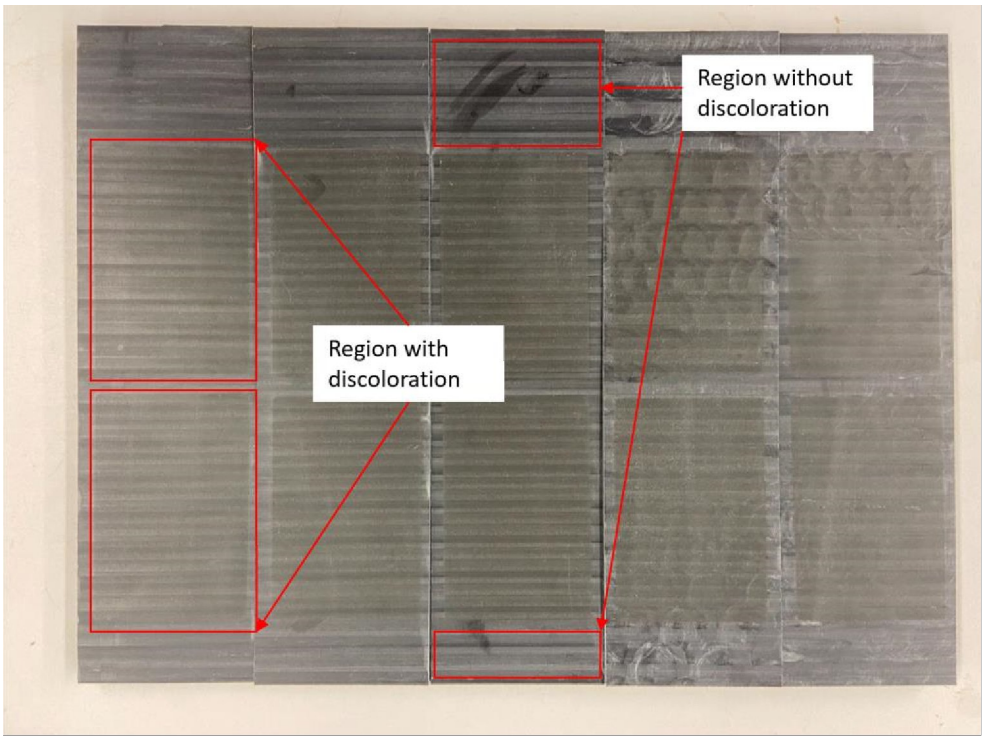

Figure 6.3: Machined specimens after 500 h of exposure.

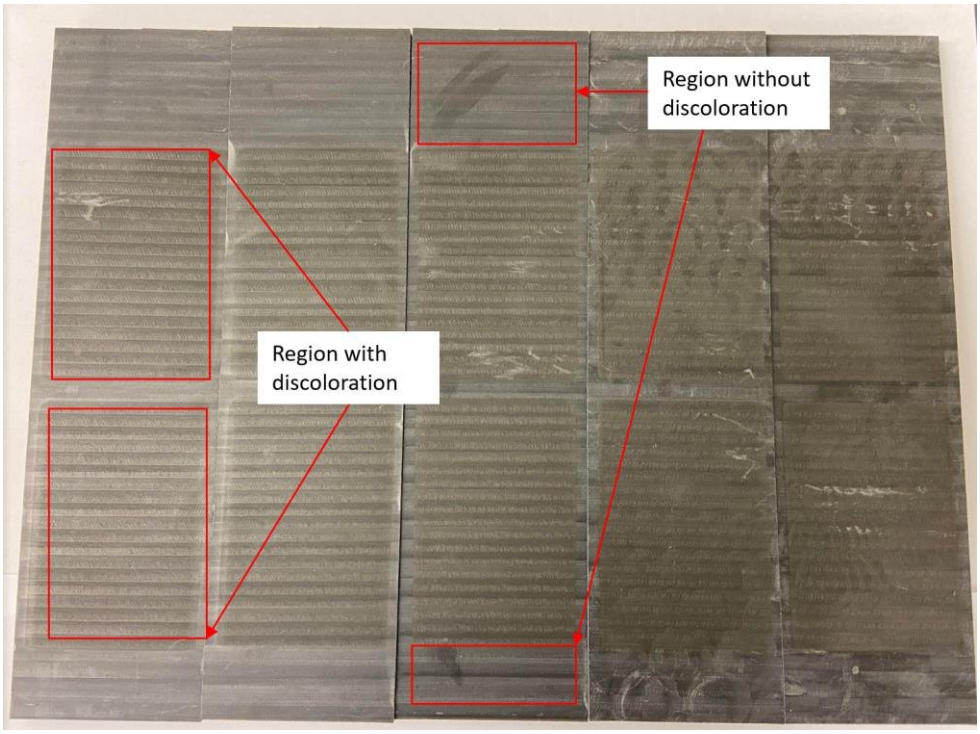

Figure 6.4: Machined specimens after 957 h of exposure

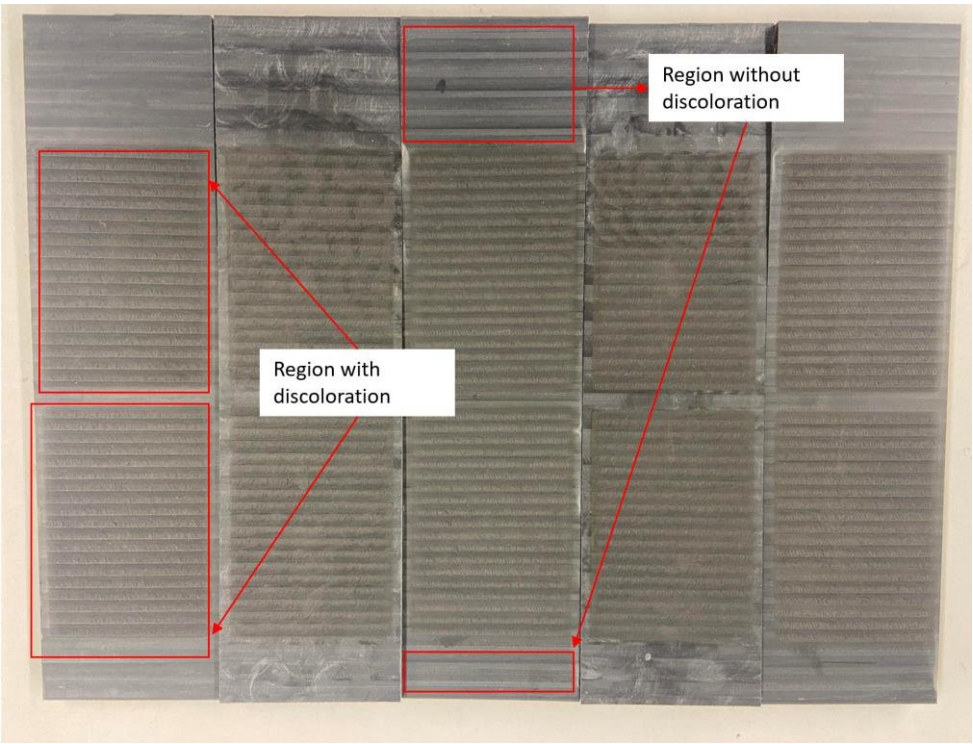

Figure 6.5: Machined specimens after 2000 h of exposure

6.2.2 Contact angle machined specimens

Contact angle measurements for each exposure time are shown in Table 6.2.

Table 6.2: Contact Angle measurement 0 h exposure

		Contact Angle		Surface free energy
Exposure time	**Specimen**	**Water**	**diiodo-methane**	**Total**
Baseline	Average	82.26 °	47.85 °	39.29 mN/m
specimens – 0h	CV (%)	6.22	10.18	4.67
500 h	Average	54.69 °	47.55 °	53.06 mN/m
	CV (%)	15.14	14.40	8.12

Table 6.2 continued

957 h	Average	53.47 °	29.42 °	58.64 mN/m
	CV (%)	6.20	12.74	4.28
2000 h	Average	71.57 °	24.40 °	51.29 mN/m
	CV (%)	4.53	32.12	4.35

*mN = 0.001 N

The variation in contact angle for water and diiodo-methane can be seen in Figure 6.6. Contact angle in the water from 0 h to 500 h of exposure is reduced by 35%, then it remains constant from 500 h to 965 h, and at last, it increases by 34% in the last interval from 957 h to 2000 h. In the case of diido-methane, the contact angles remain constant from 0 h to 500 h, then decrease by 38% from 500 h to 965 h, and at last, it keeps decreasing in the last inverval by 17% from 957 h to 2000 hrs.

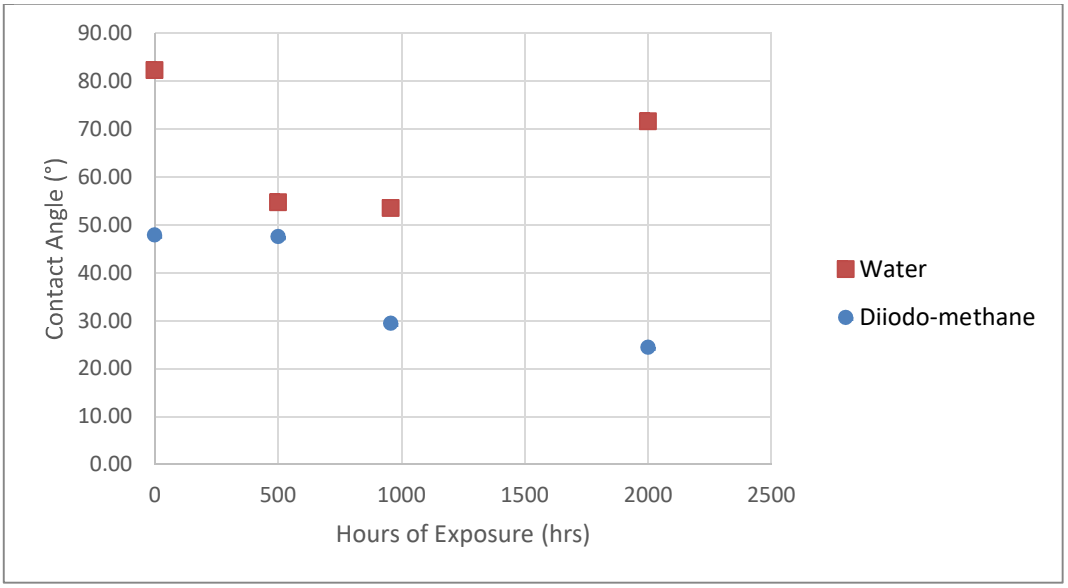

Figure 6.6: Contact angle for water and diiodo-methane in CF/ABS specimens.

6.2.3 Observations for as-printed specimens

Due to the nature of as-printed specimens, it was not possible to measure surface roughness and contact angle. It was only possible to make visual observations.

After exposure for 500 h, it was noted that the material presented discoloration. This discoloration increased for 957 h and 2000h of exposure. Figure 6.7, Figure 6.8, and Figure 6.9 show as-printed specimens at different exposure times of 500 h, 957h, and 2000h.

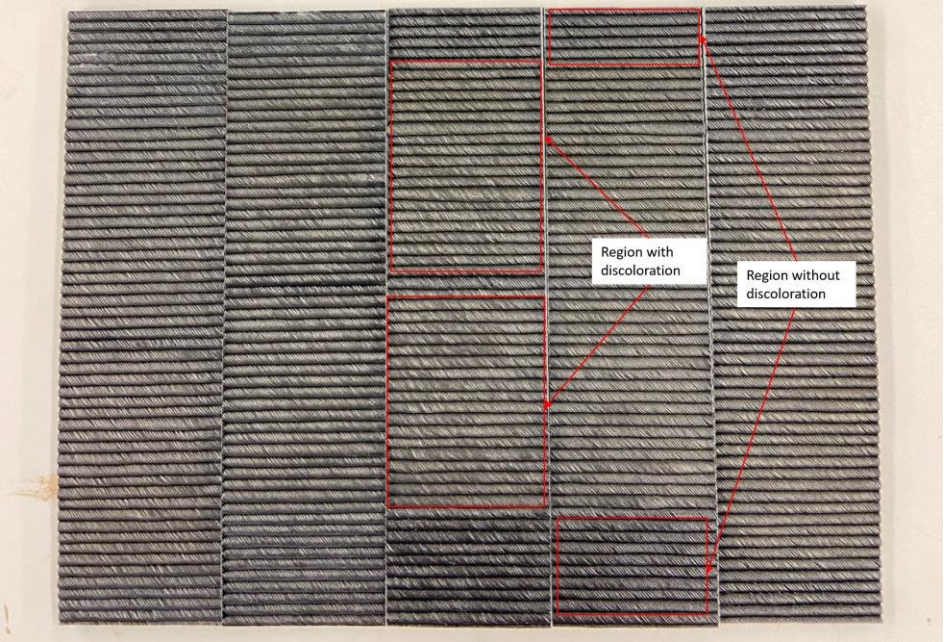

Figure 6.7: As-printed specimens after 500 h of exposure.

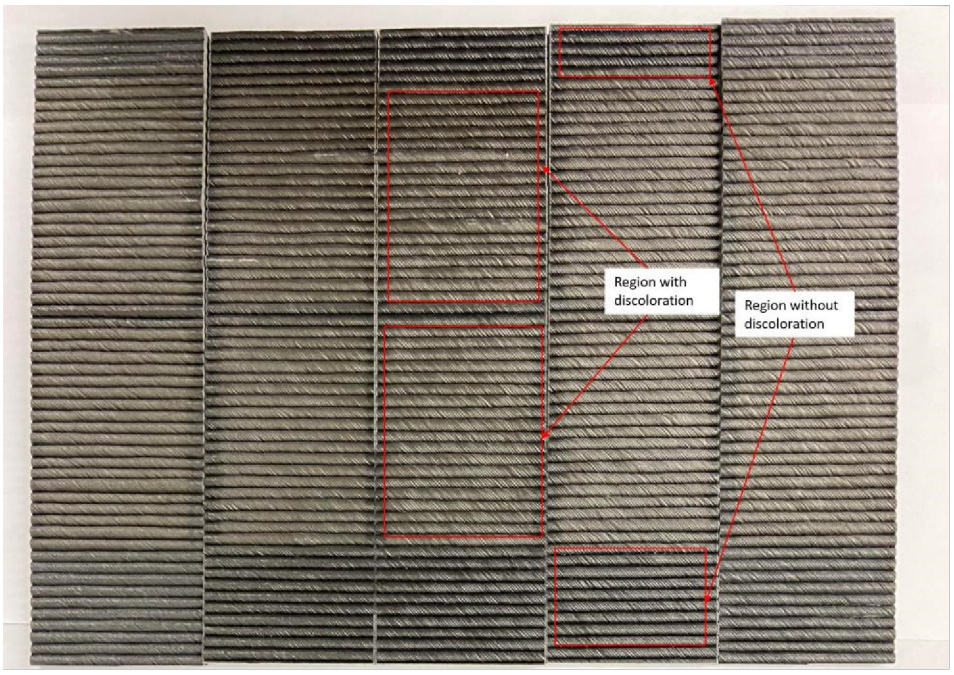

Figure 6.8: As-printed specimens after 957 h of exposure.

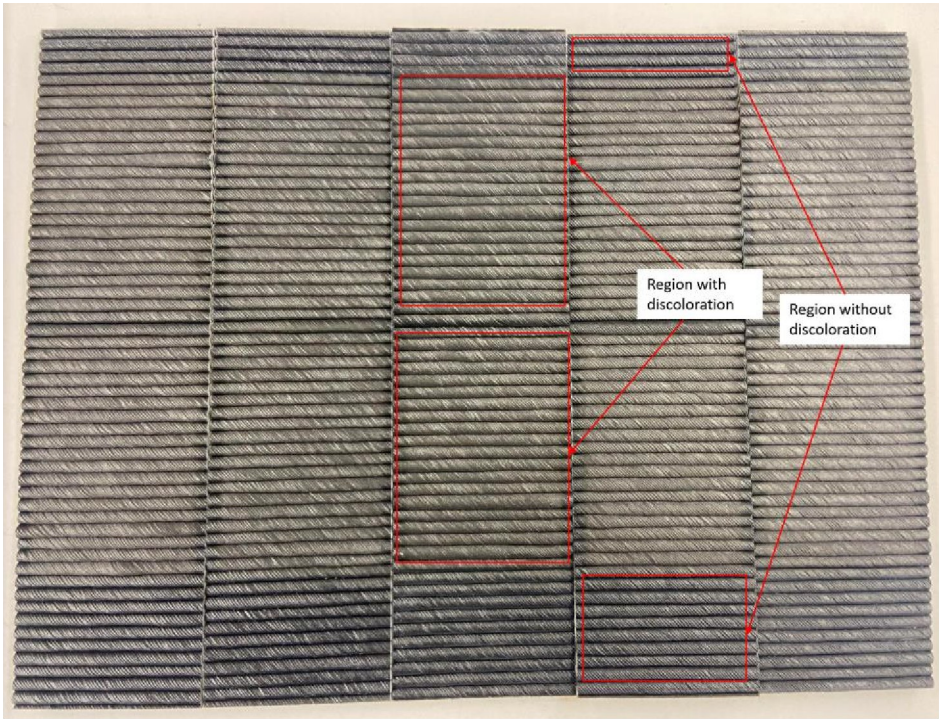

Figure 6.9: As-printed specimens after 2000 h of exposure.

6.3 Data analysis for surface roughness on machined specimens

ANOVA t-test considering a p-value < 0.05 as statistically significant was used to compare the data sets from baseline specimens to exposed specimens. Table 6.3 shows the p-values obtained for the data sets compared.

Table 6.3: Anova t-test p-values for surface roughness data

	baseline and 500 h	**baseline and 957 h**	**500 h and 957 h**	**baseline and 2000 h**	**500 h and 2000 h**	**957 h and 2000 h**
p-value	1.04E-05	3.08E-08	1.44E-05	7.08E-10	1.30E-06	3.56E-08

The data analysis shows a significant difference in surface roughness between every data set compared. It is essential to notice that the highest surface roughness increase happen during the first 500 h of exposure, with an increase of 110%. Table 6.4 shows the percentage increase in surface roughness.

Table 6.4: Increase in surface roughness for sets at different exposure times

Exposure	**% Increase in Surface Roughness**
from 0 h to 500 h	110
from 500 h to 957h	44
from 957 h to 2000 h	30

6.4 Data analysis for contact angle on machined specimens

ANOVA t-test considering a p-value < 0.05 as statistically significant, was used to compare the data sets from baseline specimens to exposed specimens. Table 6.5 shows the p-values obtained for the data sets compared.

Table 6.5: Anova t-test p-values for contact angle data

Exposures	Water	Diiodo-methane
Baseline and 500 h	4.72E-04	0.94
Baseline and 957 h	1.30E-05	3.24E-04
500 h and 957 h	0.79	1.65E-03
Baseline and 2000h	7.74E-03	9.52E-04
500 h and 2000 h	5.25E-03	2.14E-03
957 h and 2000 h	5.22E-05	0.28

6.5 Conclusions

The durability of the CF/ABS material to simulated exterior weather was evaluated by exposure to multiple cycles of UV light radiation and condensation. The exposure effect was assessed through surface roughness and contact angle measurements, and by visual inspection.

After initial exposure (500 hrs.), the material shows a significant increase in surface roughness. For longer exposures, there is a slower rate of increase in surface roughness.

In the contact angle measurements, it was observed that after 2000 hours for both polar and non-polar liquids considered, the material had a significant reduction in contact angle, which implies that the material had increased the affinitity to both liquids.

Machined and as-printed specimens showed discoloration after exposure, which increased over time.

Based on the measurements and observations, a protective coating should be considered for exterior exposure.

CHAPTER 7

PROPERTY RETENTION FACTORS

Property retention factors are defined as factors that account for the remaining material properties, in this case, for the remaining flexural strength and flexural modulus of the materials after environmental exposure. These factors were calculated as the ratio between the characteristic values of baseline set and sets under a environmental conditioning.
The following sections introduce the nomenclature used, the standards, and how the factors are calculated.

7.1 Nomenclature used for property retention factors

The nomenclature used for property retention factors is the following: C_S^i and C_E^i, where the subscripts "S" means that is used for flexural strength and "E" that is used for flexural modulus. Superscript "i" represents what exposure the factor is being used. This superscript "i" can be "M" for moisture absorption or "F" for freeze-thaw cycling. Table 7.1 summarizes the property retention factors used in this chapter and their meaning.

Table 7.1: Property retention factors definition

Factor	Definition
C_S^F	Property retention factor for flexural strength for 3D-printed materials under freeze-thaw cycling
C_E^F	Property retention factor for flexural modulus for 3D-printed materials under freeze-thaw cycling
C_S^M	Property retention factor for flexural strength for 3D-printed materials under moisture absorption
C_E^M	Property retention factor for flexural modulus for 3D-printed materials under moisture absorption

7.2 ASTM standard D7290 description

Characteristic values were calculated according to ASTM Standard D7290-06 [65]. This standard was used since it is specific for evaluating material property characteristic values for polymeric composites for civil engineering structural applications. The characteristic values are a statistically-based material property representing the 80% lower confidence bound on the 5th-percentile value of a specified population. This value accounts for statistical uncertainty due to the finite sample size. According to the standard, the 80% confidence bound, and 5th percentile levels were selected so that composite material characteristics values will produce resistance factors for Load and Resistance Factor Design like those for other civil engineering materials.

7.3 Material property distribution

Following the standard procedure, first, it is necessary to detect outlier values on the data sets. Only one set was found to have an outlier, but after investigating, it was determined that the outlier remained in the data set since it was found that there was no cause to remove it.
The material property value probability distribution function is assumed to follow the two-parameter Weibull distribution in this standard practice. This distribution is applied to an as-printed set that showed a significant reduction in their flexural strength and flexural modulus according to Chapters 4 and 5. These materials are WF/PLA under freeze-thaw cycling and WF/aPLA and CF/ABS under moisture absorption.

It is possible to fit a Weibull distribution to the data using the following MATLAB functions:

- pd = fitdist(x,'wbl'), fits a Weibull distribution to the data x.
- y = pdf (pd, x_values), gives the probability density function as a function of values on the independent variable x.
- histogram (x, n,'Normalization','pdf') gives the normalized histogram for the data in x with an n number of bins.

Figure 7.1 to Figure 7.10 show the normalized histogram and the Weibull function fit for the flexural Strength and Modulus of the as-printed sets mentioned.

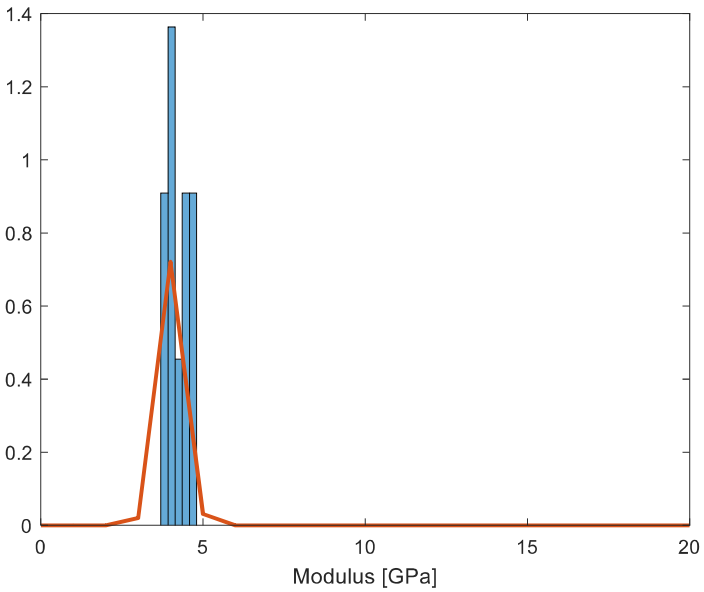

Figure 7.1: Normalized histogram and Weibull function for flexural modulus of as-printed set of WF/PLA baseline aligned in direction-1

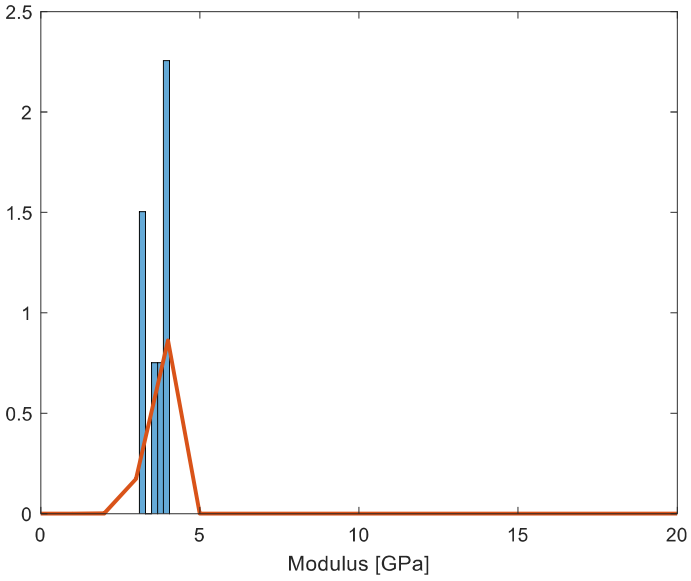

Figure 7.2: Normalized histogram and Weibull function for flexural modulus of as-printed set of WF/PLA under freeze-thaw cycling aligned in direction-1

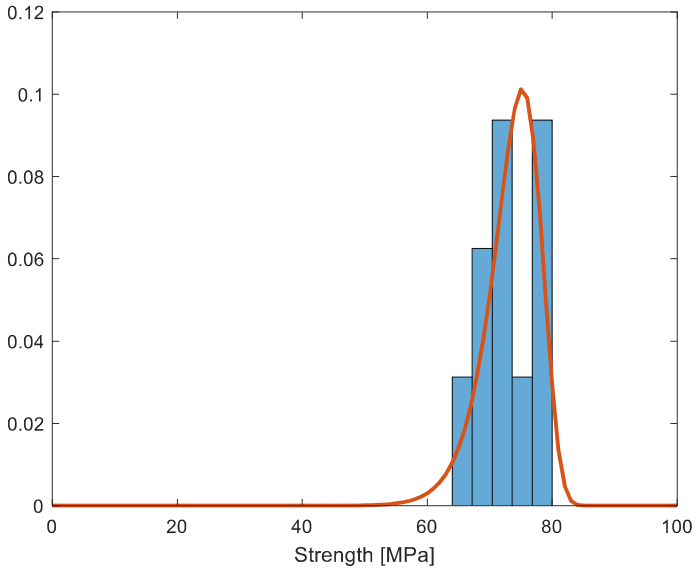

Figure 7.3: Normalized histogram and Weibull function for flexural strength of as-printed set of CF/ABS baseline aligned in direction-1

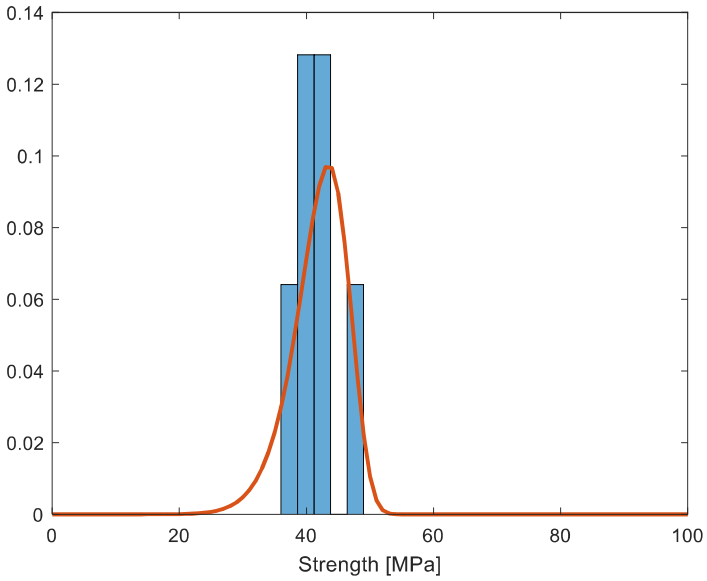

Figure 7.4: Normalized histogram and Weibull function for flexural strength of as-printed set of CF/ABS under moisture absorption aligned in direction-1

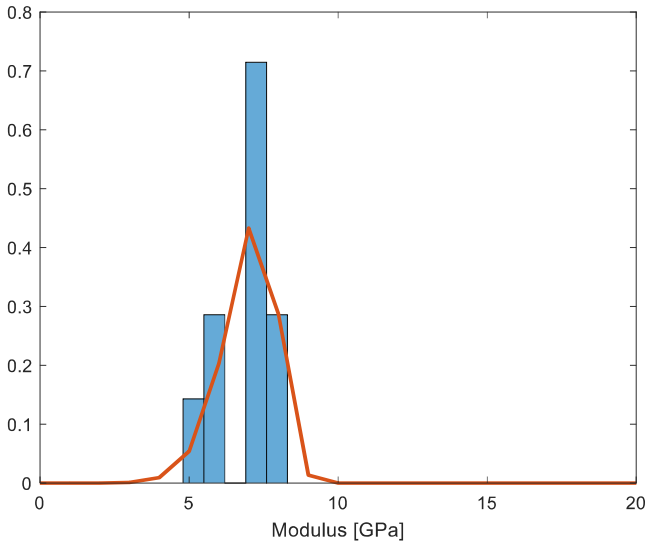

Figure 7.5: Normalized histogram and Weibull function for flexural modulus of an as-printed set of CF/ABS baseline aligned in direction-1

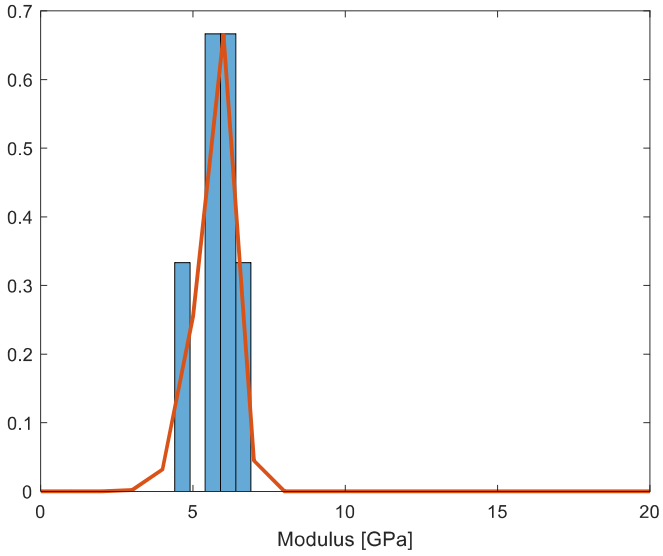

Figure 7.6: Normalized histogram and Weibull function for flexural modulus of an as-printed set of CF/ABS under moisture absorption aligned in direction-1

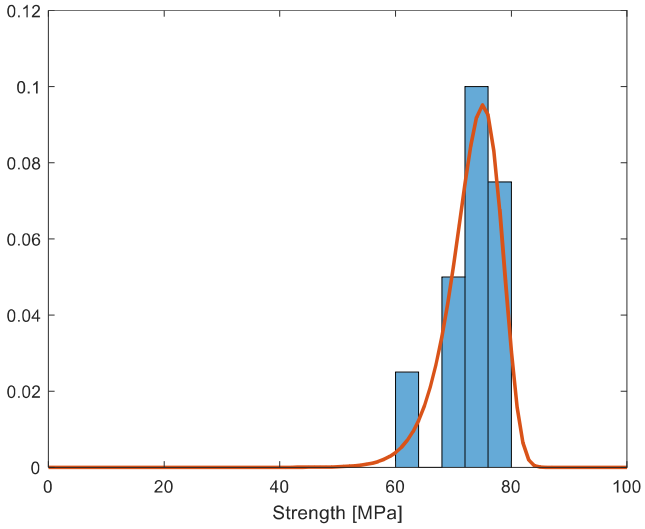

Figure 7.7: Normalized histogram and Weibull function for flexural strength of as-printed set of WF/aPLA baseline aligned in direction-1

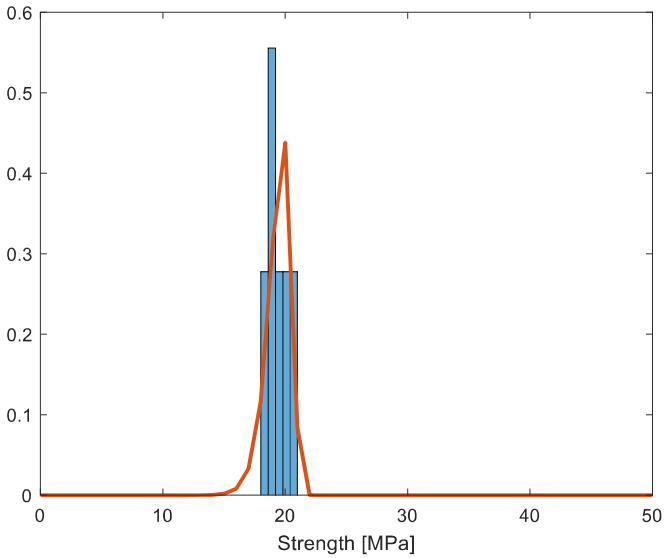

Figure 7.8: Normalized histogram and Weibull function for flexural strength of as-printed set of WF/aPLA under moisture absorption aligned in direction-1

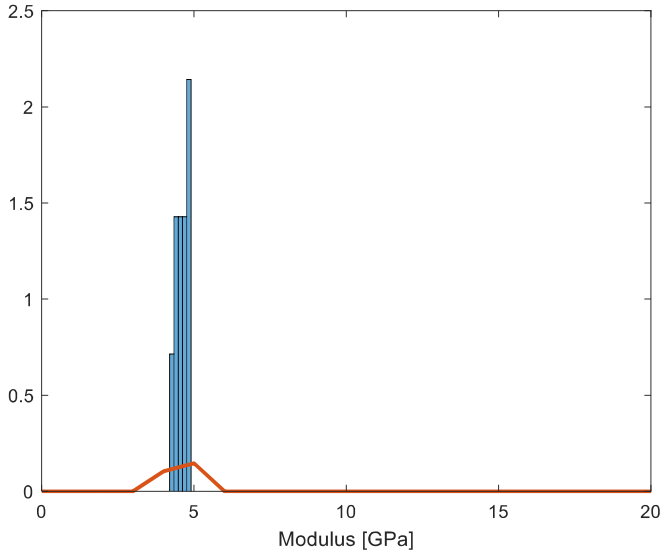

Figure 7.9: Normalized histogram and Weibull function for flexural modulus of an as-printed set of WF/aPLA baseline aligned in direction-1

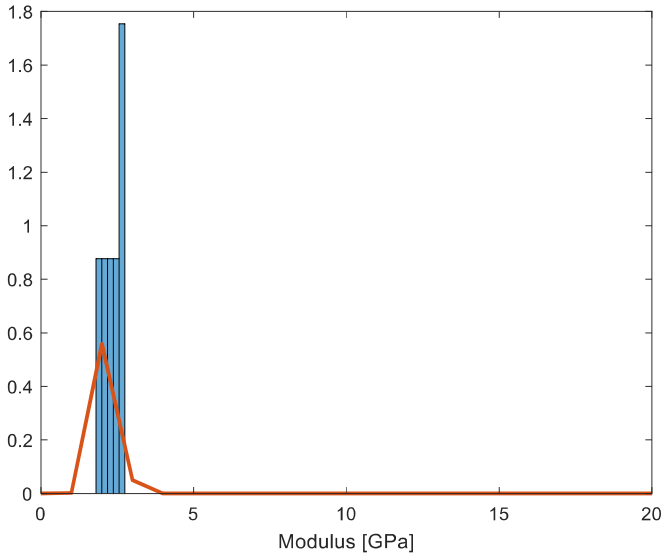

Figure 7.10: Normalized histogram and Weibull function for flexural modulus of an as-printed set of WF/aPLA under moisture absorption aligned in direction-1

7.4 Characteristic values

The characteristic values were calculated according to Equation 6. It depends on the nominal value and data confidence factor. The factor and equations used are defined as follows:

$$x_{char} = \Omega\, x_{0.05} \tag{5}$$

$$x_{0.05} = \hat{\alpha}[0.0513]^{\frac{1}{\hat{\beta}}} \tag{6}$$

Where:

x_{char}	=	Characteristic value
Ω	=	Data confidence factor, calculated according to TABLE 1 from ASTM standard D7290
$x_{0.05}$	=	Nominal value
$\hat{\beta}$	=	Maximum likelihood estimates of the Weibull shape parameter
$\hat{\alpha}$	=	Maximum likelihood estimates of the Weibull scale parameter

MATLAB function wblfit(x) computes the (Maximum likelihood estimates) MLEs of the Weibull shape parameter β and shape parameter α. Also, using function mle(x,'distribution','wbl'), MLE can be obtained.

Table 7.2 to Table 7.6 summarize the number of specimens, MLEs, nominal values, data confidence factor, and characteristic value for baseline and under moisture absorption specimens.

Table 7.2: Summary table for flexural modulus characteristic values for baseline and under freeze-thaw cycling sets of as-printed WF/PLA aligned in direction-1.

Set	**n**	**COV (%)**	$\widehat{\boldsymbol{\alpha}}$	$\widehat{\boldsymbol{\beta}}$	$\boldsymbol{x_{0.05}}$ **(GPa)**	**Ω**	$\boldsymbol{x_{char}}$ **(GPa)**
Baseline	10	8.56	4.39	14.3	3.57	0.914	3.26
Moisture absorption	7	8.73	3.78	14.0	3.06	0.893	2.73

Table 7.3: Summary table for flexural strength characteristic values for baseline and under moisture absorption sets of as-printed CF/ABS aligned in direction-1.

Set	**n**	**COV (%)**	$\widehat{\boldsymbol{\alpha}}$	$\widehat{\boldsymbol{\beta}}$	$\boldsymbol{x_{0.05}}$ **(MPa)**	**Ω**	$\boldsymbol{x_{char}}$ **(MPa)**
Baseline	10	5.98	75.4	20.8	65.4	0.940	61.4
Moisture absorption	6	10.5	43.8	11.6	33.9	0.871	29.5

Table 7.4: Summary table for flexural modulus characteristic values for baseline and under moisture absorption sets of as-printed CF/ABS aligned in direction-1.

Set	**n**	**COV (%)**	$\widehat{\boldsymbol{\alpha}}$	$\widehat{\boldsymbol{\beta}}$	$\boldsymbol{x_{0.05}}$ **(MPa)**	**Ω**	$\boldsymbol{x_{char}}$ **(MPa)**
Baseline	10	13.3	7.36	8.99	5.29	0.866	4.58
Moisture absorption	6	11.1	6.01	10.85	4.57	0.864	3.95

Table 7.5: Summary table for flexural strength characteristic values for baseline and under moisture absorption sets of as-printed WF/aPLA aligned in direction-1.

Set	n	COV (%)	$\hat{\alpha}$	$\hat{\beta}$	$x_{0.05}$ (MPa)	Ω	x_{char} (MPa)
Baseline	10	6.36	75.3	19.5	64.6	0.936	60.5
Moisture absorption	6	5.12	19.8	24.4	17.6	0.938	16.5

Table 7.6: Summary table for flexural modulus characteristic values for baseline and under moisture absorption sets of as-printed WF/aPLA aligned in direction-1.

Set	n	COV (%)	$\hat{\alpha}$	$\hat{\beta}$	$x_{0.05}$ (MPa)	Ω	x_{char} (MPa)
Baseline	10	4.83	4.69	25.86	4.18	0.950	3.97
Moisture absorption	6	13.0	2.48	9.25	1.80	0.836	1.50

7.5 Property retention factors calculation

This section presents property retention factors for large-scale 3D printed as-printed sets under freeze-thaw cycling and moisture absorption. As mentioned, the property retention factor were calculated as the ratio between the characteristic values of environmentally conditioned sets and baseline sets for each condition.

Table 7.7: Property retention factors for as-printed materials under freeze-thaw cycling

Material	C_S^F	C_E^F
WF/PLA	1.00*	0.84

*This property retention factor equals 1.00 since the difference between the flexural Strength of baseline specimens and the ones under freeze-thaw is not statistically significant.

Table 7.8: Property retention factors for as-printed materials under moisture absorption

Material	C_S^M	C_E^M
WF/aPLA	0.27	0.38
CF/ABS	0.48	0.86

7.6 Conclusions

Property retention factors were calculated for the materials that showed a statistically significant difference compared to baseline specimens when exposed to moisture absorption and freeze-thaw cycling.

The WF/PLA material subjected to freeze-thaw cycling retained 100% of its flexural strength and 84% of its flexural modulus. The WF/aPLA material subjected to moisture absorption retained 27% of its flexural strength and 38% of its flexural modulus. The CF/ABSmaterial subjected to moisture absorption retained 48% of its flexural strength and 93% of its flexural modulus.

These retention factors are only for this the sets of conditioning routines presented in this research work.

CHAPTER 8

FINITE ELEMENT ANALYSIS OF HIGHWAY CULVERT DIFFUSER

8.1 Geometry of the diffuser

The diffuser is divided into four segments of 45 in. in length, and each part has a variable diameter that goes from 33.7 in. in the joint to 67.6 in. in the outlet. When the segments are connected, the total length of the diffuser is 180 in. Figure 8.1 shows the segments, top and side view of the highway culvert diffuser. Figure 8.2 shows the assembled pieces of diffuser.

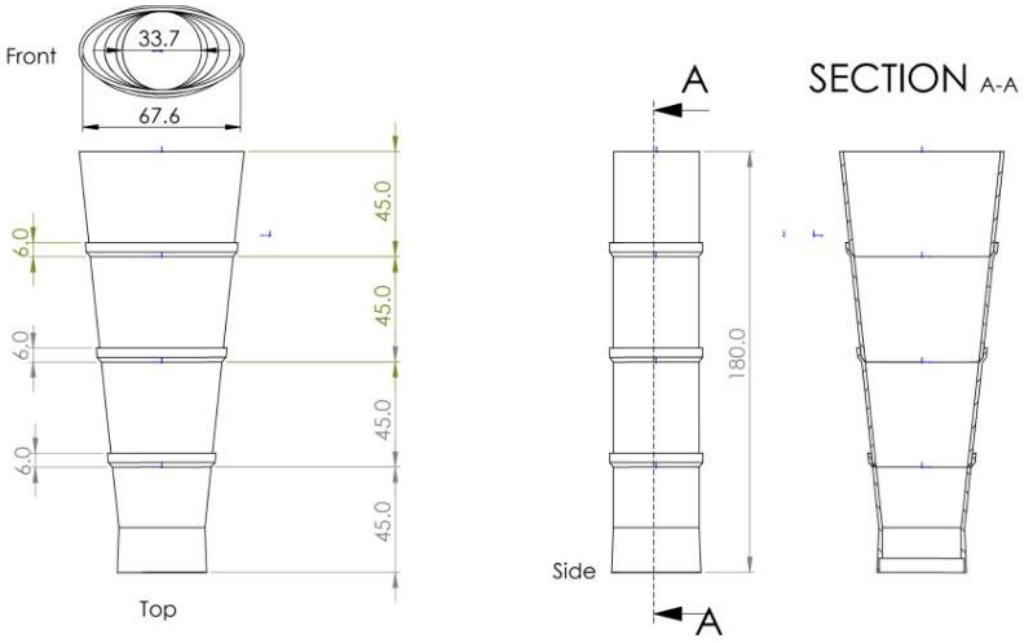

Figure 8.1: Geometry of the highway culvert diffuser

Figure 8.2: Assembled large-scale 3D printed highway culvert diffuser.

As a simplification, the part connected to the pre-existent highway culvert was considered with a constant diameter of 33.7 in. in an extension of 19.2 in. At this length, the pre-existent culvert is inserted six inches in this segment and glued with adhesive, as shown in Figure 8.3. Those six inches are not considered for modeling.

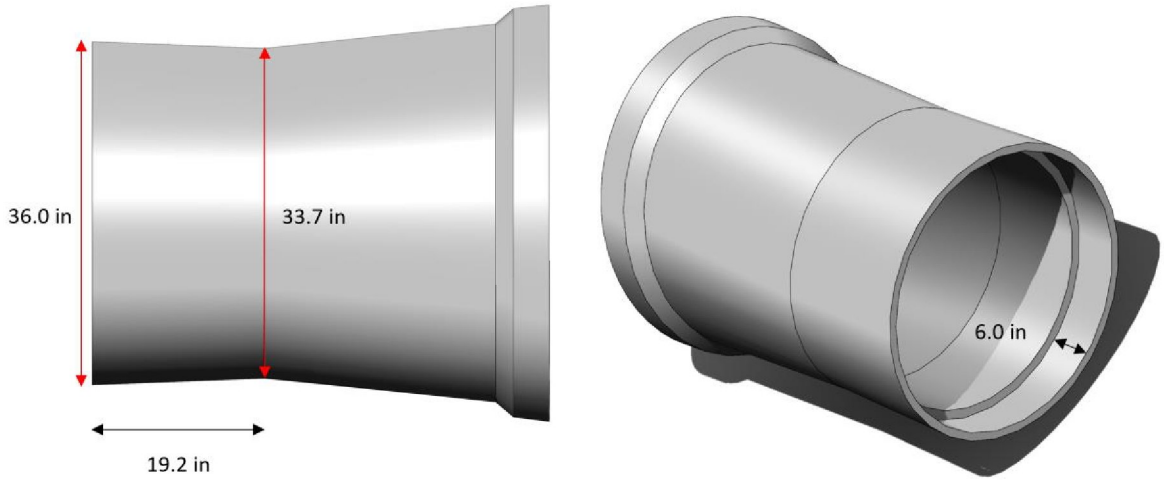

Figure 8.3: Section of the diffuser connected to the pre-existent culvert.

8.2 Finite element model

The finite element model represents the buried diffuser that needs to withstand loads from the backfill and self-weight.

8.2.1 Material properties

Material properties for CF/ABS were considered according to the research work of Bhandari et al. [66] and Schweizer et al. [67].

For parts at the desktop scale, strength in 1-3 and 2-3 planes have comparable values. Since no data was available in literature for large-scale 3D printed parts, the shear strengths in 1-3 and 2-3 plane were based on results of a small scale 3D printing study [66]. Table 8.1 shows the material properties used for the 3D model.

Table 8.1: Materials properties for CF/ABS used for the highway culvert diffuser Abaqus model.

Material property	Value
Tensile Modulus direction-1 (GPa)	4.89
Tensile Modulus directions 2 and 3 (GPa)	2.45
Poisson ratio 1-2 and 2-3	0.18
Poisson ratio 1-3	0.36
Shear modulus 1-2, 1-3, and 2-3 (GPa)*	0.80
Tensile Strength direction-1 (MPa)	40.5
Tensile Strength directions 2 and 3 (MPa)	19.7
Shear Strength in directions 1-3 and 1-2 (MPa)	20.0*

*Properties obtained for specimens manufactured using small-scale desktop 3D printers [66].

8.2.2 Modeling

For simplicity, the model of the diffuser is considered as a whole section, which differs from the original geometry that is divided in four sections. The parts are connected with adhesive, the connected parts or joints will develop stress concentrations, the model presented will not suffer from stress conectrations . Stress concentration on the joints is not of interest for this research work, the intent of the model is to obtain ratios of stress/buckling and applied load for the baseline and the environmentally exposed highway culver differ.

The section used for the modeling corresponds to a shell/ continuum shell composite material with symmetric layers; each layer has a 0.75 in. thickness and the same angular orientation. The elements correspond to S4R, a 4-node doubly curved thin or thick shell, with reduced integration, hourglass control and finite membrane strains. Figure 8.4 and Figure 8.5 show the 3D model of the diffuser and global directions of the shell composite.

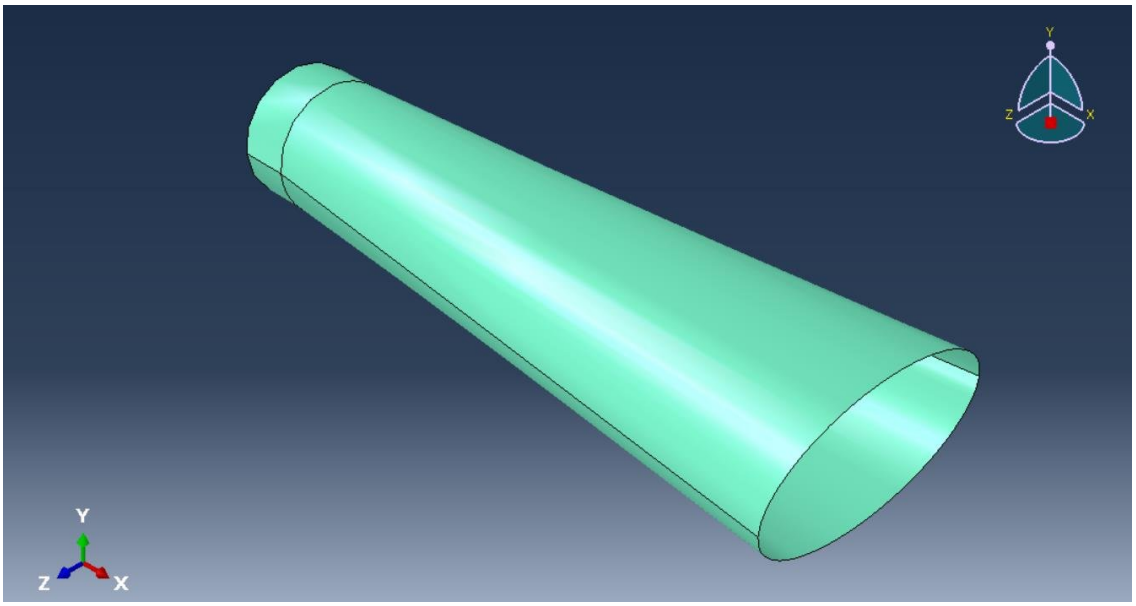

Figure 8.4: 3D model of the highway culvert diffuser

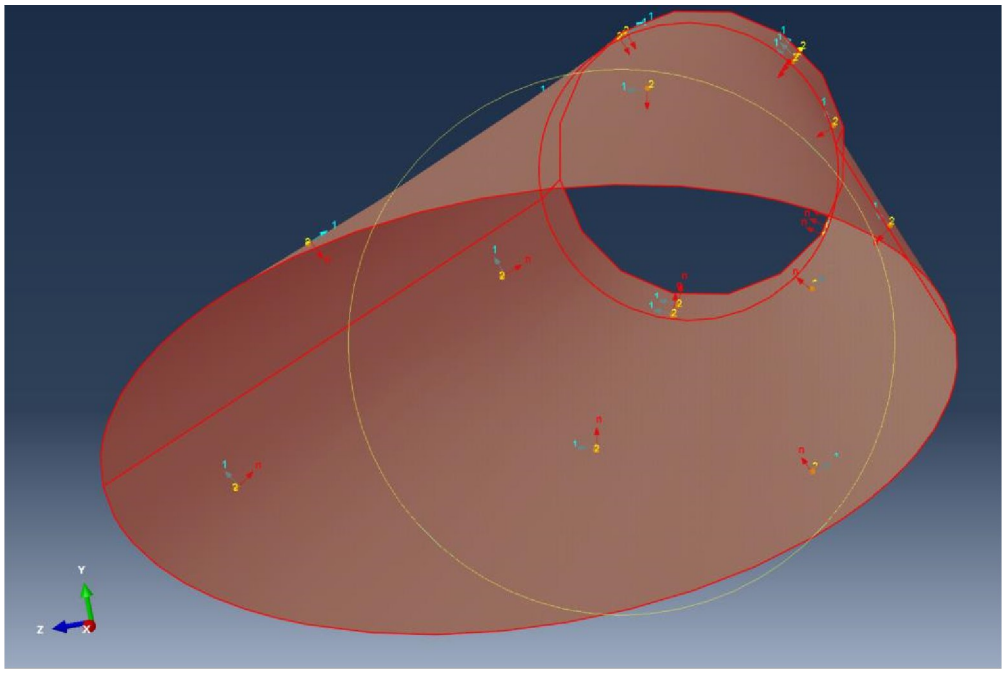

Figure 8.5: Local orientation of the model

8.2.3 Boundary conditions

The joint of the existing liner with the diffuser was modeled as fixed, meaning that displacements and rotations in each global direction are 0. The bottom part of the whole diffuser was restricted to moving vertically, meaning that displacement in global direction Y is 0, as shown in Figure 8.6.

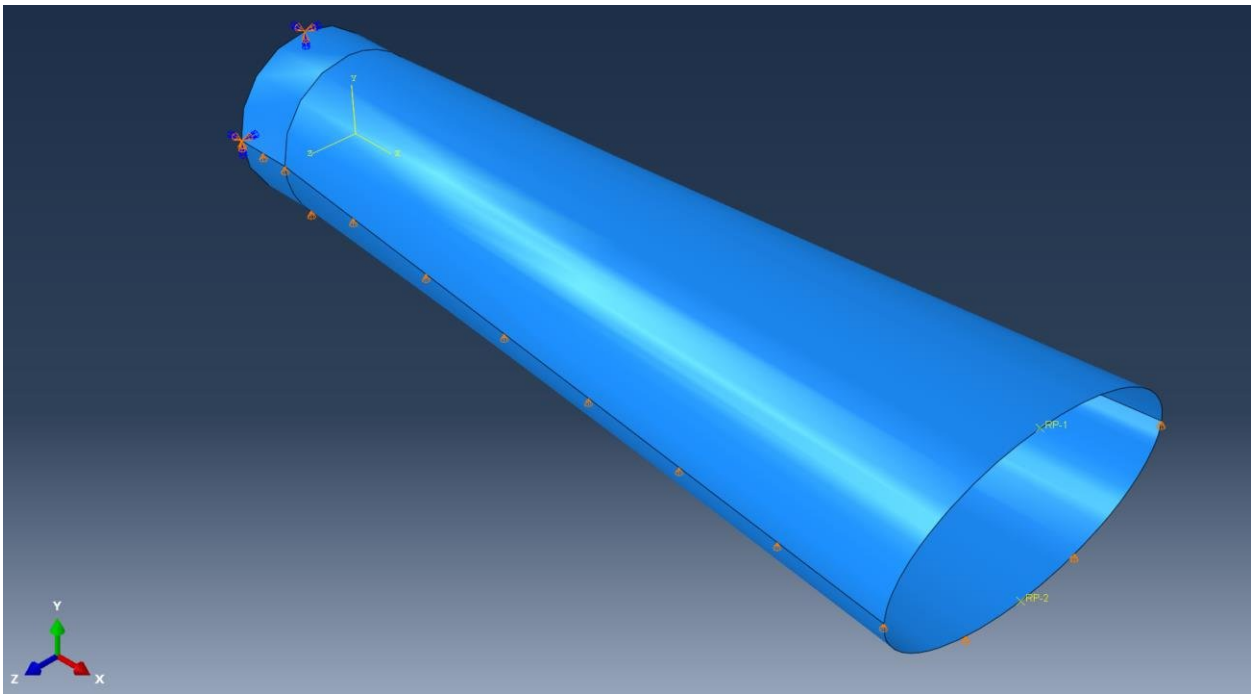

Figure 8.6: Boundary conditions and loads of the Highway culvert Diffuser Model.

8.2.4 Loads

The following section presents the loads applied on the highway culvert diffuser. The loads considered were the weight of the soil on the diffuser top surface and the diffuser self-weight, as shown in Figure 8.7 and Figure 8.8.

8.2.4.1 Soil pressure calculation and self-weight

The height of the embankment is 4.0 m. over the joint between the liner and the diffuser. The embankment slopes at 2:1 towards the diffuser outlet. This consideration was conservative since the diffuser outlet might not be covered with soil.

Considering a soil density of 1.8 ton/m^3, a gravity of 9.81 m/s^2, and a height of 1 m, the total pressure on the top surface equals 17.7 kN/m^2. The total load at the joint and at the end of the diffuser are shown in Table 8.2.

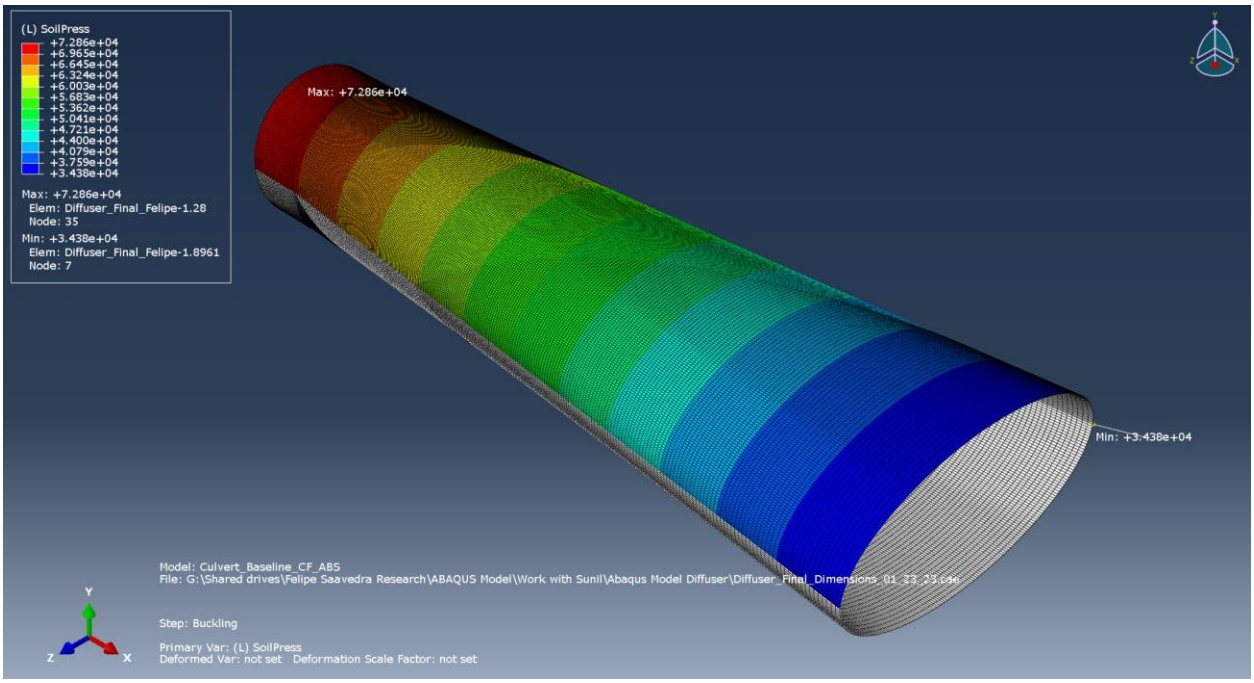

Figure 8.7: Soil pressure on the top of the diffuser.

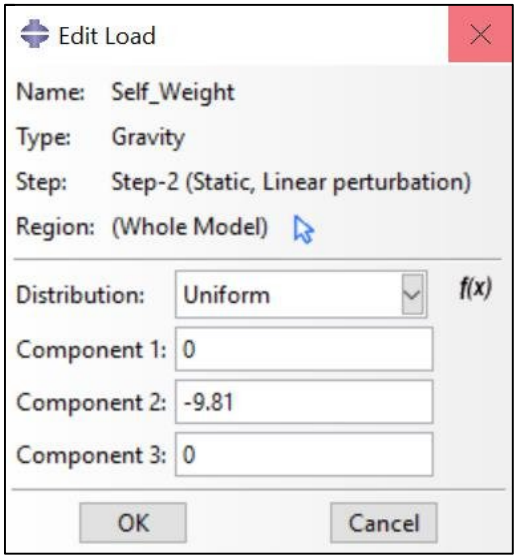

Figure 8.8: Self-weight load.

Table 8.2: Soil pressure values

Point	height of soil (m)	Soil pressure (kN/m2)
Joint	3.96	72.9
End of diffuser	1.68	34.4

8.2.4.2 Buckling Loads

The software calculates buckling loads internally, considering self-weight and soil pressure.

8.2.5 Mesh convergence study

For the mesh convergence study, three models were considered. These models had 23,520, 45,920, and 934,400 elements, respectively. It was found that it converges for 93,440 elements. Table 8.3 shows the values for S11 and eigenvalues for mode one for each model. The model

with 93440 elements was selected for modeling. Variation of S11 and eigenvalues are shown in Figure 8.9 and Figure 8.10.

Table 8.3: Values of Stresses and eigenvalues for each model in the convergence study

Model	Elements	Nodes	S11 C (MPa)	Eigenvalue Mode 1
1	23520	23680	8.94	8.77
2	45920	46144	9.25	8.76
3	93440	93760	9.58	8.75

*C = Compression stress.

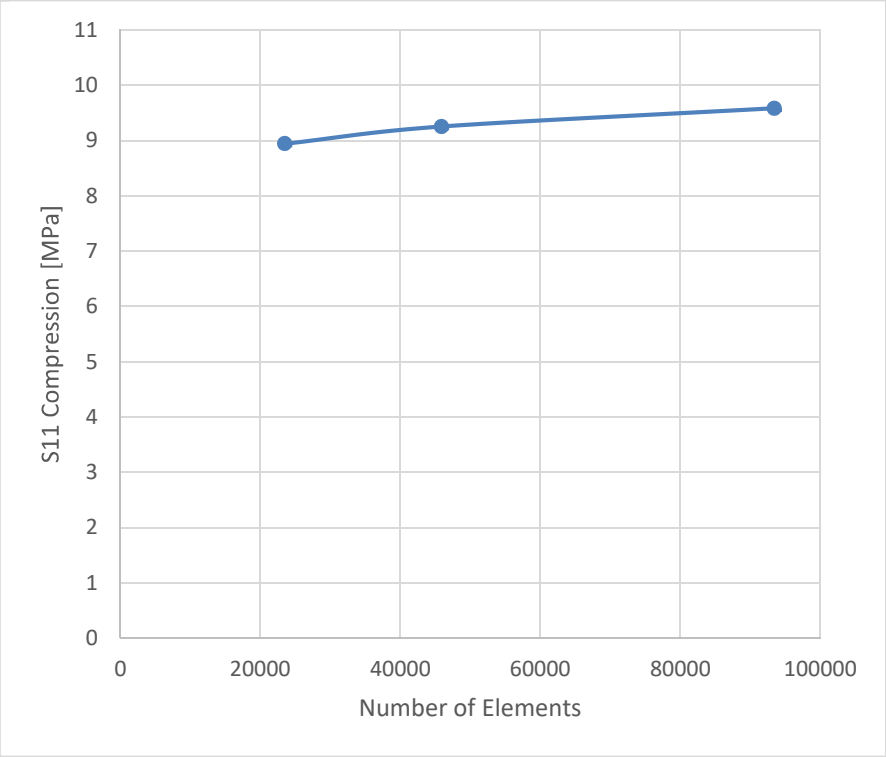

Figure 8.9: S11 stress v/s number of elements for convergence study

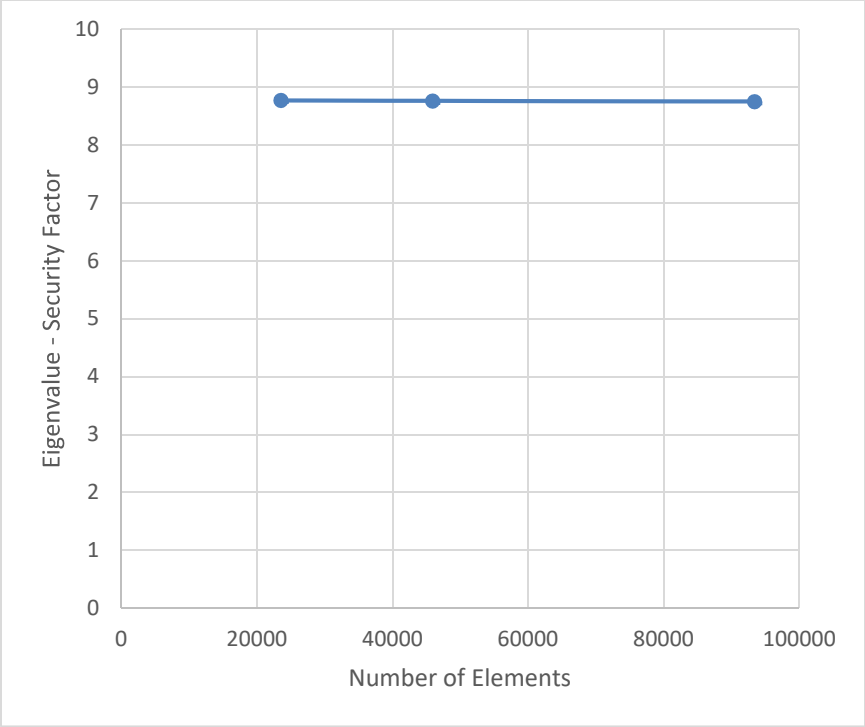

Figure 8.10: Eigenvalue mode one v/s number of elements for convergence study

8.3 Results

8.3.1 Stress results for the culvert

The stresses in the highway culvert diffuser due to self-weight and soil pressure and ratios between applied loads and strength are shown in Table 8.4 and Table 8.5. Figure 8.11, Figure 8.12, and Figure 8.13 show the maximum stress values for S11, S22, and S12 and its location.

Table 8.4: Compression and Tension stress on the diffuser due to self-weight and soil pressure

Stress	Compression (MPa)	Applied load / Strength	Tension (MPa)	Applied load / Strength
S11	9.38	0.23	6.44	0.16
S22	0.77	0.04	0.61	0.03

Table 8.5: Shear stress on the diffuser due to self-weight and soil pressure

Stress	S12 Shear (MPa)	Applied load / Strength
S12	0.32	0.02

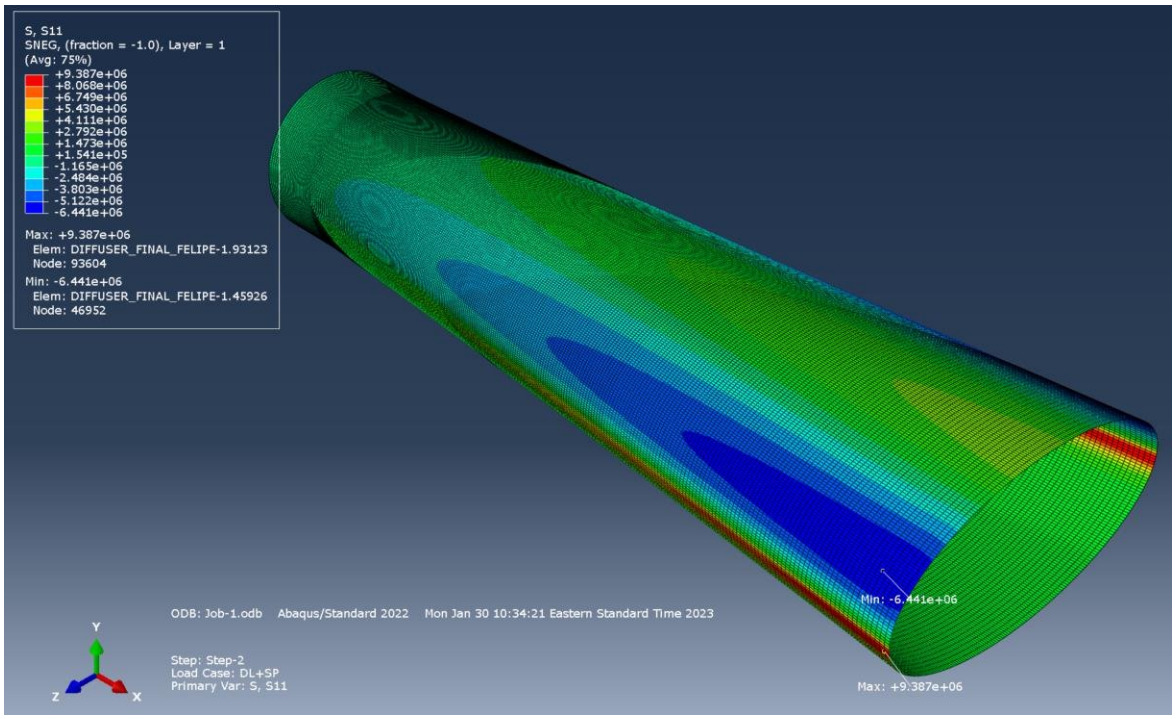

Figure 8.11: S11 stresses on the diffuser model due to self-weight and soil pressure

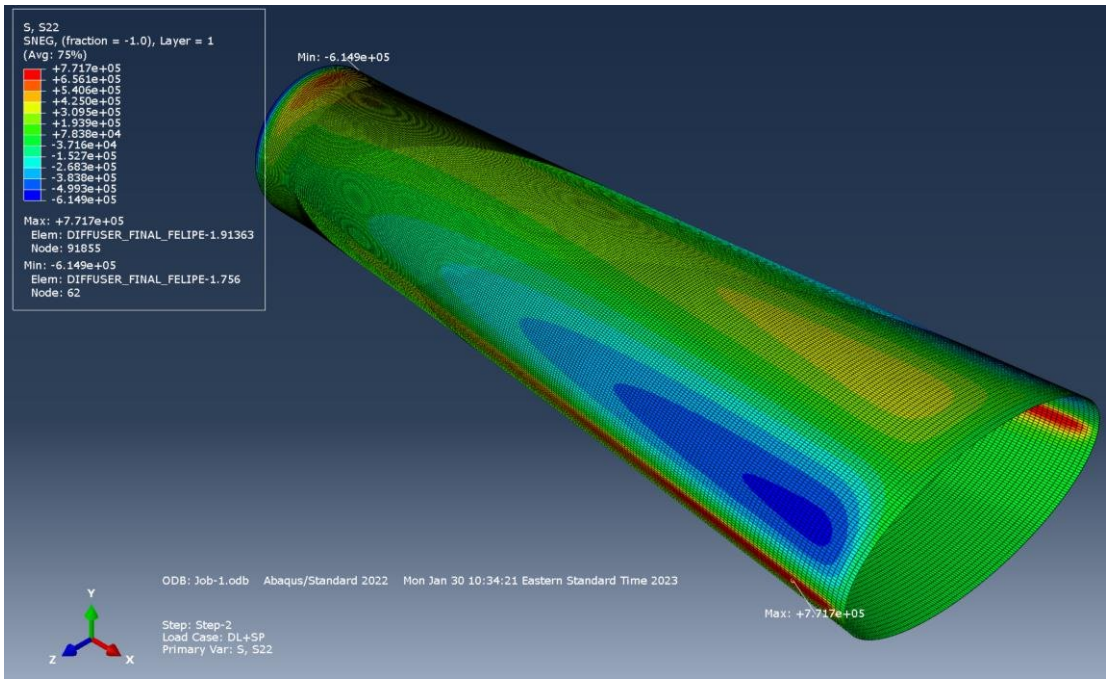

Figure 8.12: S22 stresses on the diffuser model due to self-weight and soil pressure

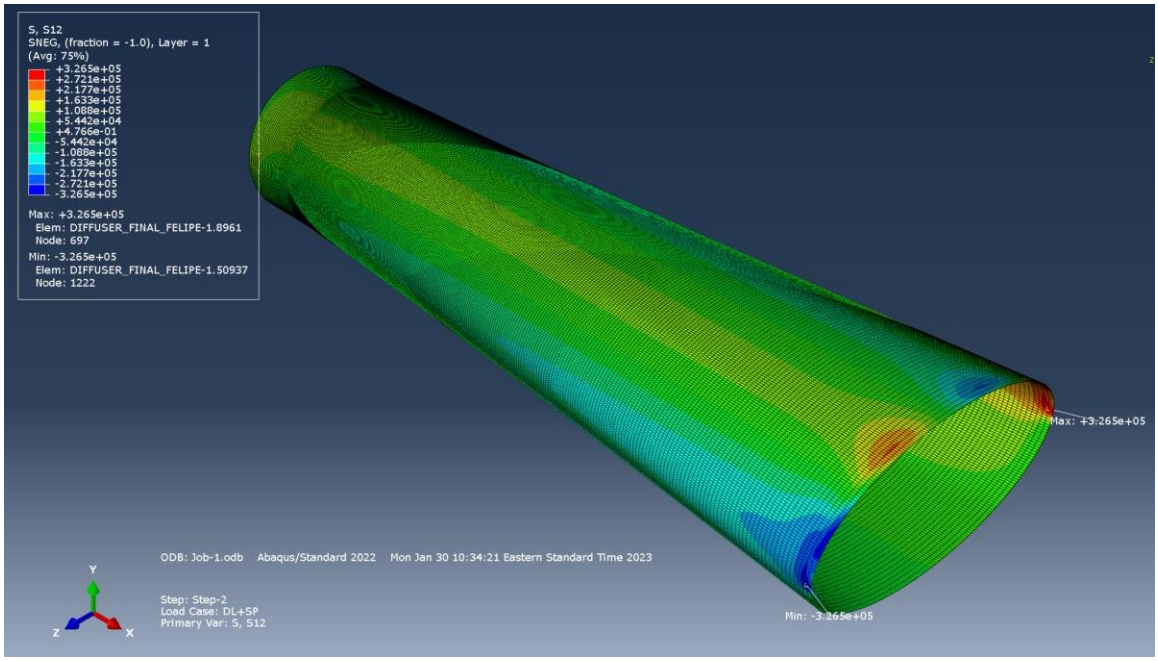

Figure 8.13: S12 stresses on the diffuser model

8.3.2 Stress result in culverts being environmentally exposed to moisture

From Chapter 7, material property retention factors were obtained, with a factor of 0.48 for flexural strength and 0.86 for flexural modulus for CF/ABS exposed to moisture. A new model was created considering a reduced modulus for directions 1 and 2, considering the reduced flexural strength, the ratios between applied loads and reduced strength are shown in Table 8.6.

Table 8.6: Compression and Tension stress on the diffuser

Stress	Compression (MPa)	Applied load / Strength	Tension (MPa)	Applied load / Strength
S11	9.42	0.49	6.44	0.33
S22	0.77	0.08	0.62	0.07

8.3.3 Buckling analysis

Buckling analysis was conducted for three models, the first with baseline material properties, the second one considering only one layer for the structure of the diffuser, and the third with the property retention factors applied for moisture absorption. Table 8.7 shows the eigenvalues, which are the safety factors for the loads that the model has.

Table 8.7: Values of safety factor for buckling for the three models.

Mode	Eigenvalues for baseline model	Eigenvalues for one layer model	Eigenvalues for environmentally exposed model
1	11.9	1.63	10.3
2	15.5	2.07	13.4
3	22.4	3.31	19.8
4	22.9	3.39	20.0
5	30.2	4.56	26.7
6	31.5	4.83	27.8
7	34.3	5.14	30.1
8	38.5	5.44	34.2
9	39.1	6.25	34.3
10	39.6	6.30	34.8

8.3.3.1 Buckling analysis of two layers

This analysis considers a composite material with two layers (1.5 in thickness in total) oriented in the same direction. Eigenvalues are values that represent the ratio between buckling load and applied loads. Table 8.7 shows the eigenvalues for each mode.

8.3.3.2 Buckling analysis of one layer

This analysis considers only one layer (0.75 in thickness). Eigenvalues are values of safety factors for the loads that the model has. Table 8.7 shows the eigenvalues for each mode.

8.3.3.3 Buckling analysis for culverts environmentally exposed to moisture

This analysis considers a composite material with two layers (1.5 in thickness in total) oriented in the same direction. Eigenvalues are values ratios between applied loads and strength. Table 8.7 shows the eigenvalues for each mode.

8.4 Discussion of results

From the results presented in previous sections:

- The selected mesh is suitable for the model of the highway culvert diffuser; the number of elements converges when checking values for stresses and eigenvalues.
- The highest ratios of strength/ buckling loads and applied loads are equal to equal to 0.23 for S11; this means that the culvert is designed on the safer side, which can be checked with the buckling analysis (for two layers), obtaining a ratio of buckling load and applied loads of factor of 11.9 for mode 1.
- Buckling analysis for one layer shows that the ratio between the buckling load and applied load for mode one is 1.63; this is not on the conservative side and shows why it was better to use two layers for the diffuser.
- The highest ratios of strength/ buckling loads and applied loads for the culvert environmentally exposed to moisture are equal to 0.49. This means the culvert is designed on the safer side, even after moisture exposure. This can be checked with the buckling analysis, obtaining a security factor of 10.3 for mode 1.

8.5 Conclusions

The ratios of applied load/buckling load for the model with the property retention factors applied are double of the ones with baseline material properties. These ratios are lower than 1, showing that the diffuser was design on the safer side and it can withstand service loads even after it is exposed to moisture.

The FE models are a valuable tool for calculating ratios of strength/buckling loads for the diffuser and can be used for any geometry and loading.

CHAPTER 9

CONCLUSIONS AND RECOMMENDATIONS

9.1 Material properties of materials MANUFACTURED BY LARGE SCALE 3D PRINTING

For WF/PLA, the flexural strength and flexural modulus were not different for specimens with different widths, which means that specimen width does not affect flexural material properties. When comparing WF/PLA as-printed and machined specimens, material properties were not the same, which means that machining impacts the flexural material properties.

The direction in which the specimens are aligned is relevant since different flexural material properties were obtained.

For WF/aPLA, the flexural strength is the only property that is the same when as-printed and machined specimens were compared.

9.2 Environmental conditioning

CF/ABS is the material that has the lowest moisture content compared to WF/PLA and WF/aPLA. When comparing as-printed sets, CF/ABS has an average moisture content of 1.35%, versus WF/PLA and WF/aPLA, with an average moisture content of 7.74% and 9.23%, respectively.

In the case of WF/PLA, width, directions, and surface finishing impact the moisture content. When comparing machined samples with as-printed, machined specimens had a 10% higher moisture content. It is essential to mention that this experiment was conducted for 81 days, and that a longer perior could produce different results.

In the case of WF/aPLA, specimen surface finishing impacts the moisture content. Contrary to WF/PLA, when comparing as-printed specimens with machined specimens, as-printed samples had a 24% higher moisture content.

For the coefficient of moisture expansion, WF/PLA as-printed specimens are transversally isotropic, while machined ones are not. If both types of sets are compared, only direction-2 can be considered to have the same CME. The CME for WF/PLA also depends on the direction in which the specimens were aligned, with specimens aligned in directions-1 and 3 being different.

WF/aPLA, as-printed and machined, are not transversally isotropic, showing a CME for each direction to be different if both types of sets are compared, only direction 1 can be considered to have the same CME.

When WF/PLA and WF/aPLA sets are compared, if both are as-printed, only the CME for direction-2 is not the same. In the case of machined specimens, the CME is different for all directions.

Moisture absorption has a negative impact on the flexural properties of large-scale 3D printed materials. From the flexural test, as-printed sets of WF/aPLA have a decrease of 73% in flexural strength and a decrease of 49% in its flexural modulus. In the case of machined specimens, the decrease is 50% and 43%, respectively. As-printed CF/ABS set has a decrease of 49% in its flexural strength and a reduction of 18% in its flexural modulus.

Freeze-thaw cycling has a negative impact on the flexural properties of large-scale 3D printed materials made of WF/PLA aligned in direction-1. It did not affect the material when it is aligned in direction-3. For as-printed specimens, there is a 14% and 12% reduction in the flexural modulus for samples with 1.0 in and 1.5 in width, respectively. If the sets are machined, there is a reduction of 11% for flexural strength and a 45% reduction for flexural modulus of elasticity. Freeze-thaw cycling did not affect the flexural properties of materials made of WF/aPLA and CF/ABS.

For WF/aPLA, freeze-thaw cycling affects the flexural modulus, with a reduction of 6%. CF/ABS is not affected by three cycles, this material should be subjected to more freeze-thaw cycles.

The durability of the CF/ABS material to simulated exterior weather was evaluated by exposure to multiple cycles of UV light radiation and condensation. The exposure effect was assessed through surface roughness and contact angle measurements, and by visual inspection. After initial exposure (500 hrs.), the material shows a significant increase in surface roughness. For longer exposures, there is a slower rate of increase in surface roughness.

In the contact angle measurements, it was observed that after 2000 hours for both polar and non-polar liquids considered, the material had a significant reduction in contact angle, which implies that the material had increased the affinitity to both liquids.

Machined and as-printed specimens showed discoloration after exposure, which increased over time.

Based on the measurements and observations, a protective coating should be considered for exterior exposure.

9.3 Property retention factors

Property retention factors were calculated for the materials that showed a statistically significant difference compared to baseline specimens when exposed to moisture absorption and freeze-thaw cycling.

The WF/PLA material subjected to freeze-thaw cycling retained 100% of its flexural strength and 84% of its flexural modulus. The WF/aPLA material subjected to moisture absorption retained 27% of its flexural strength and 38% of its flexural modulus. The CF/ABS material subjected to moisture absorption retained 48% of its flexural strength and 93% of its flexural modulus.

These retention factors are only for this the sets of conditioning routines presented in this research work.

9.4 Finite element modeling for highway culvert diffuser

The selected mesh is suitable for the model of the highway culvert diffuser; the number of elements converges when checking values for stresses and eigenvalues.

The ratios of strength/buckling for the model with the property retention factors applied are the double of the ones with baseline material properties. This ratios are lower than 1, showing that the diffuser was design on the safer side and it can withstand service loads even after it is exposed to moisture.

REFERENCES

1. Talagani, F., et al., *Numerical Simulation of Big Area Additive Manufacturing (3D Printing) of a Full Size Car.* Sampe Journal, 2015. **51**: p. 27.

2. ISO/ASTM, ISO/ASTM 52900:2021 Standard Terminology for Additive Manufacturing - General Principles - Terminology 2015.

3. Wimpenny, L.J.K.P.M.P.D.I., 3D Printing and Additive Manufacturing Technologies. 2019.

4. Spoerk, M., C. Holzer, and J. Gonzalez-Gutierrez, Material extrusion-based additive manufacturing of polypropylene: A review on how to improve dimensional inaccuracy and warpage. Journal of Applied Polymer Science, 2020. 137(12): p. 48545.

5. Gebhardt, A., Understanding Additive Manufacturing. 2011.

6. Gibson, I.R., D. W.; Stucker, B., Additive ManufacturingTechnologies: 3D Printing, Rapid Prototyping, and DirectDigital Manufacturing. 2021.

7. Labonnote, N., et al., Additive construction: State-of-the-art, challenges and opportunities. Automation in Construction, 2016. 72: p. 347-366.

8. Cantor, K.M. and P. Watts, 12 - Plastics Processing, in Applied Plastics Engineering Handbook, M. Kutz, Editor. 2011, William Andrew Publishing: Oxford. p. 195-203.

9. Kafle, A., et al., 3D/4D Printing of Polymers: Fused Deposition Modelling (FDM), Selective Laser Sintering (SLS), and Stereolithography (SLA). Polymers, 2021. 13(18): p. 3101.

10. Bhandari, S., et al., Large-scale extrusion-based 3D printing for highway culvert rehabilitation. 2021.

11. Bhandari, S., R. Lopez-Anido, and J. Anderson, Large Scale 3D Printed Thermoplastic Composite Forms for Precast Concrete Structures. 2020.

12. Bhandari, S., Lopez-Anido, R.A., Saavedra Rojas, F.A., LeBihan Alan, Design and Manufacture of Precast Concrete Formworks Using Polymer Extrusion-Based Large-Scale Additive Manufacturing and Postprocessing. 2022.

13. Bhandari, S. and D.F. Erb Jr, OVERVIEW OF THERMOPLASTIC COMPOSITES IN BRIDGE APPLICATIONS.

14. Advanced Structures and Composite Center (ASCC), U.o.M., Biohome3D, Biobased additively manufactured home. 2022.

15. Jipa, A. and B. Dillenburger, 3D Printed Formwork for Concrete: State-of-the-Art, Opportunities, Challenges, and Applications. 3D Printing and Additive Manufacturing, 2022. 9: p. 107.

16. Peters, B., Additive formwork: 3D printed flexible formwork. 2014.

17. Doka. New construction of the Sächsische Aufbaubank (SAB) Leipzig, Germany. 2019; Available from: https://www.doka.com/en/references/europe/saechsische-aufbaubank.

18. Najafi, M. and D.V. Bhattachar, Development of a culvert inventory and inspection framework for asset management of road structures. Journal of King Saud University - Science, 2011. 23(3): p. 243-254.

19. Salem, O., B. Salman, and M. Najafi, Culvert Asset Management Practices and Deterioration Modeling. Transportation Research Record, 2012. 2285(1): p. 1-7.

20. Liedtka, C., Life Cycle Analysis and Implications of 3D Printed Bio-Based Homes, A Preliminary Study, in Honor College. 2022, University of Maine.

21. Tofail, S., et al., Additive manufacturing: Scientific and technological challenges, market uptake and opportunities. Materials Today, 2017. 21.

22. Lee, J.-Y., J. An, and C.K. Chua, Fundamentals and applications of 3D printing for novel materials. Applied Materials Today, 2017. 7: p. 120-133.

23. Gao, W., et al., The status, challenges, and future of additive manufacturing in engineering. Computer-Aided Design, 2015. 69: p. 65-89.

24. Shah, J., et al., Large-scale 3D printers for additive manufacturing: design considerations and challenges. The International Journal of Advanced Manufacturing Technology, 2019. 104: p. 1-15.

25. Bull, C.Y.a.J., Durability of Materials and Structures in Building and Civil Engineering. 2006, Dunbeath, Scotland: Whittles Publishing.

26. Karbhari, V., et al., Durability Gap Analysis for Fiber-Reinforced Polymer Composites in Civil Infrastructure. Journal of Composites for Construction - J COMPOS CONSTR, 2003. 7.

27. Nelson, W.B., Accelerated Testing: Statistical Models, Test Plans, and Data Analysis. 2004. 624.

28. (AASHTO), A.A.o.S.H.a.T.O., Guide Specification for Design of Bonded FRP Systems for Repair and Strengthening of Concrete Bridges Elements. 2012.

29. Engineers, A.S.o.C., ASCE/SEI 74-23 Standard, Load and Resistance Factor Design (LRFD) for Pultruded Fiber Reinforced Polymer (FRP) Structures, ASCE Press, Reston, VA, 2023. 2023.

30. Gardner, D.J., Y. Han, and L. Wang, Wood–Plastic Composite Technology. Current Forestry Reports, 2015. 1(3): p. 139-150.

31. Stark, N.M. and D.J. Gardner, 7 - Outdoor durability of wood–polymer composites, in Wood–Polymer Composites, K.O. Niska and M. Sain, Editors. 2008, Woodhead Publishing. p. 142-165.

32. Gardner, D.J. and A. Bozo, Ten-year field study of wood plastic composites in Santiago, Chile: biological, mechanical and physical property performance. Maderas. Ciencia y tecnología, 2018. 20: p. 257-266.

33. Grassi, G., S. Lupica Spagnolo, and I. Paoletti, Fabrication and durability testing of a 3D printed façade for desert climates. Additive Manufacturing, 2019. 28: p. 439-444.

34. International, A., ASTM D4762-18 Standard Guide for Testing Polymer Matrix Composite Materials. 2018. p. 25.

35. Lafhaj, Z. and Z. Dakhli, Performance Indicators of Printed Construction Materials: a Durability-Based Approach. Buildings, 2019. 9(4): p. 97.

36. International, A., D7264/D7264M - 21 Standard Test Method for Flexural Properties of Polymer Matrix Composite Materials. 2021. p. 10.

37. international, A., D5229/D5229M - 20 - Standard Test Method for Moisture Absorption Properties and Equilibrium Conditioning of Polymer Matrix Composite Materials. 2020. p. 20.

38. International, A., D7031 - 11 - Standard Guide for Evaluating Mechanical and Physical Properties of Wood-Plastic Composite Products. 2019.

39. International, A., ASTM G154 - 16 Standard Practice for Operating Fluorescent Ultraviolet (UV) Lamp Apparatus for Exposure of Nonmetallic Materials. 2016. p. 11.

40. International, A., ASTM D6272 - 17 Standard Test Method for Flexural Properties of Unreinforced and Reinforced Plastics and Electrical Insulating Materials by Four-Point Bending. 2017. p. 9.

41. International, A., ASTM D790 - 17 Standard Test Methods for Flexural Properties of Unreinforced and Reinforced Plastics and Electrical Insulating Materials. 2017. p. 12.

42. Kariz, M., M. Sernek, and M. Kuzman, Effect of humidity on 3D-printed specimens from wood-pla filaments. Wood Research, 2018. 63: p. 917-922.

43. Kamau-Devers, K., Z. Kortum, and S.A. Miller, Hydrothermal aging of bio-based poly(lactic acid) (PLA) wood polymer composites: Studies on sorption behavior, morphology, and heat conductance. Construction and Building Materials, 2019. 214: p. 290-302.

44. Trinh, B.M., E.O. Ogunsona, and T.H. Mekonnen, Thin-structured and compostable wood fiber-polymer biocomposites: Fabrication and performance evaluation. Composites Part A: Applied Science and Manufacturing, 2021. 140: p. 106150.

45. Ayrilmis, N., et al., Effect of printing layer thickness on water absorption and mechanical properties of 3D-printed wood/PLA composite materials. International Journal of Advanced Manufacturing Technology, 2020.

46. Lin, Q., X. Zhou, and G. Dai, Effect of hydrothermal environment on moisture absorption and mechanical properties of wood flour–filled polypropylene composites. Journal of Applied Polymer Science, 2002. 85(14): p. 2824-2832.

47. Wang, W. and J.J. Morrell, Water sorption characteristics of two wood-plastic composites. 2004: Forest Products Society.

48. Bledzki, A.K. and O. Faruk, Creep and impact properties of wood fibre–polypropylene composites: influence of temperature and moisture content. Composites Science and Technology, 2004. 64(5): p. 693-700.

49. Kim, J.-W., D. Harper, and A. Taylor, Effect of wood species on water sorption and durability of wood-plastic composites. Wood and Fiber Science, 2008. 40: p. 519-531.

50. Dzul-Cervantes, M.A.A., et al., Effect of moisture content and carbon fiber surface treatments on the interfacial shear strength of a thermoplastic-modified epoxy resin composites. Journal of Materials Research and Technology, 2020. 9(6): p. 15739-15749.

51. Yu, B., et al., Interfacial and Glass Transition Properties of Surface-Treated Carbon Fiber Reinforced Polymer Composites under Hygrothermal Conditions. Engineered Science, 2018. 2: p. 67-73.

52. Ferrel, W.H., Processing-Structure-Performance Relationships in Fused Filament Fabricated Fiber Reinforced ABS for Material Qualification. 2020, The University of Tennesee, Knoxville. p. 202.

53. Haghighi-Yazdi, M., J.K.Y. Tang, and P. Lee-Sullivan, Moisture uptake of a polycarbonate blend exposed to hygrothermal aging. Polymer Degradation and Stability, 2011. 96(10): p. 1858-1865.

54. Haghighi-Yazdi, M., P. Lee-Sullivan, and A. Moallemi, Specific heat capacity of polycarbonate/acrylonitrile–butadiene–styrene (PC/ABS) blend after hygrothermal aging. Journal of Thermal Analysis and Calorimetry, 2017. 130.

55. Poenninger, A. and B. Defoort, Determination of the coefficient of moisture expansion (CME). 2003.

56. Chaid, J., F. Abdulla, and I. Jalil, CALCULATION OF MOISTURE EXPANSION COEFFICIENT OF THE ABOVE KNEE PROSTHETIC SOCKET LAMINATION MATERIALS. Journal of Engineering and Sustainable Development, 2016. Vol. 20,, September 2016: p. 189-196.

57. Vaddadi, P., T. Nakamura, and R.P. Singh, Inverse Analysis to Determine Hygrothermal Properties in Fiber Reinforced Composites. Journal of Composite Materials, 2006. 41(3): p. 309-334.

58. Burke, W., Spacecraft Structures and Mechanical Testing, volume 1. NASA STI/Recon Technical Report N, 1991. 93: p. 15718.

59. Friedrich, D. and A. Luible, Investigations on ageing of wood-plastic composites for outdoor applications: A meta-analysis using empiric data derived from diverse weathering trials. Construction and Building Materials, 2016. 124: p. 1142-1152.

60. Pilarski, J.M. and L.M. Matuana, Durability of wood flour-plastic composites exposed to accelerated freeze–thaw cycling. II. High density polyethylene matrix. Journal of Applied Polymer Science, 2006. 100(1): p. 35-39.

61. Turku, I., T. Kärki, and A. Puurtinen, Durability of wood plastic composites manufactured from recycled plastic. Heliyon, 2018. 4(3): p. e00559.

62. Pilarski, J.M. and L.M. Matuana, Durability of wood flour-plastic composites exposed to accelerated freeze–thaw cycling. Part I. Rigid PVC matrix. Journal of Vinyl and Additive Technology, 2005. 11(1): p. 1-8.

63. Darwish, O.M., Effect of Saline Immersion and Freeze-Thaw Cycles on Performance of Fused Deposition Modelling (FDM) Materials. 2019, University of Dayton.

64. Davis, P., B.E. Tiganis, and L.S. Burn, The effect of photo-oxidative degradation on fracture in ABS pipe resins. Polymer Degradation and Stability, 2004. 84(2): p. 233-242.

65. International, A., ASTM D7290-06 Standard Practice for Evaluating Material Property Characteristic Values for Polymeric Composites for Civil Engineering Structural Applications. 2022. p. 4.

66. Bhandari, S., et al., Elasto-Plastic Finite Element Modeling of Short Carbon Fiber Reinforced 3D Printed Acrylonitrile Butadiene Styrene Composites. JOM, 2020. 72(1): p. 475-484.

67. Schweizer, K.M., Bhandari, S., Lopez-Anido, R.A., and Wang, L., Recycling Large-Scale 3D Printed Polymer Composite Precast Concrete Forms, in CICE 2023, 11th International Conference on FRP Composites in Civil Engineering. 2023: Rio de Janeiro, Brazil.

BIOGRAPHY OF THE AUTHOR

Felipe Saavedra was born in Chile. He grew up in different cities in Chile, including Concepción and Chillán. He graduated from Colegio Técnico Profesional Darío Salas, Chillán, Chile in 2011. He attended Universidad de Concepción in Chile from 2012 to 2018. He graduated with a bachelor's degree in Civil Engineering in 2018. He started working in 2018 in Chile as a project engineer. He did this for almost three years until covid happened. He had to decide if he wanted to move to the capital of Chile to take the next step in his career as an engineer or to go back to school to get this M.S He wisely decided to pursue the M.S. He started his graduate studies at the University of Maine in the spring of 2021. He is a candidate for the Master of Science degree in Civil Engineering from the University of Maine in May 2023.